(2)

Edward L. Ginzton Laboratory
Stanford University
Stanford, California 94305

FINAL TECHNICAL REPORT
TO THE
AIR FORCE OFFICE OF SCIENTIFIC RESEARCH
FOR
A PROGRAM OF RESEARCH
IN

NEW LIGHT SOURCES AND CONCEPTS FOR ELECTRO-OPTIC SAMPLING

Contract F49620-92-J-0099

Principal Investigator

David M. Bloom
Associate Professor of Electrical Engineering

Original contains color plates: All DTIC reproductions will be in black and white

March, 1994

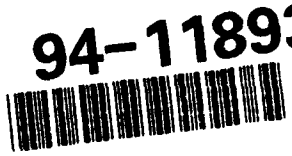

REPORT DOCUMENTATION PAGE

Form Approved
OMB No. 0704-0188

1. AGENCY USE ONLY (Leave blank)	2. REPORT DATE	3. REPORT TYPE AND DATES COVERED
	Mar 94	Final Technical Report 1Jan92-31Dec93

4. TITLE AND SUBTITLE
New Light Sources and Concepts for Electro-Optic Sampling

5. FUNDING NUMBERS

F49620-92-J
0099

6. AUTHOR(S)
David M. Bloom

7. PERFORMING ORGANIZATION NAME(S) AND ADDRESS(ES)
Edward L. Ginzton Laboratory
W. W. Hansen Laboratories of Physics
Stanford University
Stanford, CA 94305-4028

8. PERFORMING ORGANIZATION REPORT NUMBER
~~F49620-92-J-0099~~
AFOSR-TR- 94 0236

9. SPONSORING/MONITORING AGENCY NAME(S) AND ADDRESS(ES)
Department of the Air Force
Air Force Office of Scientific Research (AFSC)
Bolling Air Force Base, DC 20332-6448

10. SPONSORING/MONITORING AGENCY REPORT NUMBER
2301 AS

11. SUPPLEMENTARY NOTES

12a. DISTRIBUTION/AVAILABILITY STATEMENT
Unlimited
Approved for public release; distribution unlimited.

12b. DISTRIBUTION CODE

13. ABSTRACT (Maximum 200 words)

Research to improve electro-optic sampling led to the development of several high performance optical phase modulators. These phase modulators serve as a 'time-lens' in a series of experiments on temporal optical systems. These systems are used to generate, manipulate and measure optical pulses. Significant results have been shown in three areas. First is active optical pulse compression, where 55 ps 1.064 μm pulses were compressed to 1.7 ps. Notably, laser timing jitter is reduced in this process. Second, temporal imaging demonstrated the ability to magnify the time axis of an optical pulse, stretching a short pulse into a longer replica. This tool has application in pulse shape measurement and optical signal processing. Finally, a new method of optical pulse shape measurement was demonstrated with 3 ps time resolution, excellent power sensitivity and relative system simplicity. These experiments have opened up the field of temporal optics.

14. SUBJECT TERMS	15. NUMBER OF PAGES
Electro-optic sampling	12
	16. PRICE CODE

17. SECURITY CLASSIFICATION OF REPORT	18. SECURITY CLASSIFICATION OF THIS PAGE	19. SECURITY CLASSIFICATION OF ABSTRACT	20. LIMITATION OF ABSTRACT
Unclassified	Unclassified	Unclassified	Unlimited

GENERAL INSTRUCTIONS FOR COMPLETING SF 298

The Report Documentation Page (RDP) is used in announcing and cataloging reports. It is important that this information be consistent with the rest of the report, particularly the cover and title page. Instructions for filling in each block of the form follow. It is important to *stay within the lines* to meet *optical scanning requirements*.

Block 1. Agency Use Only *(Leave blank)*.

Block 2. Report Date. Full publication date including day, month, and year, if available (e.g. 1 Jan 88). Must cite at least the year.

Block 3. Type of Report and Dates Covered. State whether report is interim, final, etc. If applicable, enter inclusive report dates (e.g. 10 Jun 87 - 30 Jun 88).

Block 4. Title and Subtitle. A title is taken from the part of the report that provides the most meaningful and complete information. When a report is prepared in more than one volume, repeat the primary title, add volume number, and include subtitle for the specific volume. On classified documents enter the title classification in parentheses.

Block 5. Funding Numbers. To include contract and grant numbers; may include program element number(s), project number(s), task number(s), and work unit number(s). Use the following labels:

C	- Contract	PR	- Project
G	- Grant	TA	- Task
PE	- Program Element	WU	- Work Unit Accession No.

Block 6. Author(s). Name(s) of person(s) responsible for writing the report, performing the research, or credited with the content of the report. If editor or compiler, this should follow the name(s).

Block 7. Performing Organization Name(s) and Address(es). Self-explanatory.

Block 8. Performing Organization Report Number. Enter the unique alphanumeric report number(s) assigned by the organization performing the report.

Block 9. Sponsoring/Monitoring Agency Name(s) and Address(es). Self-explanatory.

Block 10. Sponsoring/Monitoring Agency Report Number. *(If known)*

Block 11. Supplementary Notes. Enter information not included elsewhere such as: Prepared in cooperation with...; Trans. of...; To be published in.... When a report is revised, include a statement whether the new report supersedes or supplements the older report.

Block 12a. Distribution/Availability Statement. Denotes public availability or limitations. Cite any availability to the public. Enter additional limitations or special markings in all capitals (e.g. NOFORN, REL, ITAR).

- **DOD** - See DoDD 5230.24, "Distribution Statements on Technical Documents."
- **DOE** - See authorities.
- **NASA** - See Handbook NHB 2200.2.
- **NTIS** - Leave blank.

Block 12b. Distribution Code.

- **DOD** - Leave blank.
- **DOE** - Enter DOE distribution categories from the Standard Distribution for Unclassified Scientific and Technical Reports.
- **NASA** - Leave blank.
- **NTIS** - Leave blank.

Block 13. Abstract. Include a brief *(Maximum 200 words)* factual summary of the most significant information contained in the report.

Block 14. Subject Terms. Keywords or phrases identifying major subjects in the report.

Block 15. Number of Pages. Enter the total number of pages.

Block 16. Price Code. Enter appropriate price code *(NTIS only)*.

Blocks 17. - 19. Security Classifications. Self-explanatory. Enter U.S. Security Classification in accordance with U.S. Security Regulations (i.e., UNCLASSIFIED). If form contains classified information, stamp classification on the top and bottom of the page.

Block 20. Limitation of Abstract. This block must be completed to assign a limitation to the abstract. Enter either UL (unlimited) or SAR (same as report). An entry in this block is necessary if the abstract is to be limited. If blank, the abstract is assumed to be unlimited.

DISCLAIMER NOTICE

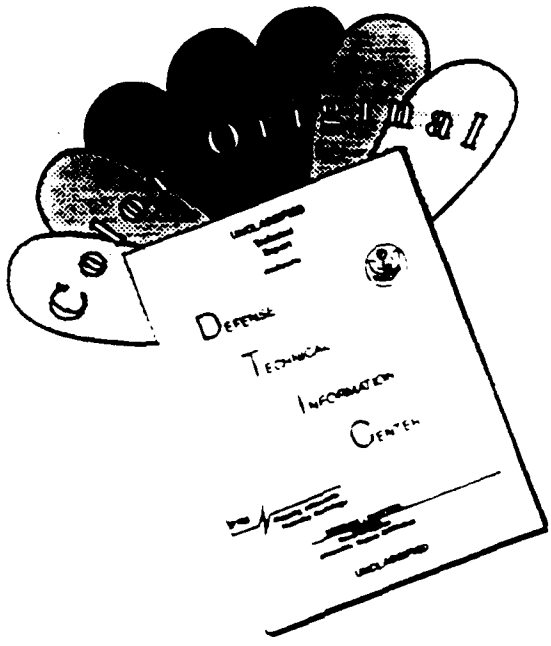

THIS DOCUMENT IS BEST QUALITY AVAILABLE. THE COPY FURNISHED TO DTIC CONTAINED A SIGNIFICANT NUMBER OF COLOR PAGES WHICH DO NOT REPRODUCE LEGIBLY ON BLACK AND WHITE MICROFICHE.

1. Objectives

The research objectives for this contract were divided into two areas: improvements to electro-optic sampling, and development of an optical analog to the microwave synthesizer

1.1 Synthesized optical source

The optical analog to the microwave synthesizer is an optical source whose wavelength can be tuned and locked to a stable wavelength reference. The goal was to build an optical source tunable over 100 GHz with kilohertz linewidth using a new laser technology and high speed photodiode / electrical samplers previously developed in our group.

1.2 Improvements to electro-optic testing

These were pursued in two directions: 1) New approaches for electro-optic sampling based on erbium doped fiber amplifiers and 2) New optical sources. The new approach to electro-optic sampling was an idea to increase the commercial viability of this IC test technique, which has mainly been a laboratory tool. The recent development of practical optical amplifiers initially appeared to allow changes in measurement system topology which would replace an inconvenient modelocked laser source with an economic and practical laser diode. The effort in new optical sources capitalized on expertise in optical modulators to build compact, high performance, modelocked lasers.

2. Status of Research Effort

Summary

Impressive research gains have been made in the field of temporal optics. This emerging field explores new methods to generate, manipulate and measure optical pulses. This work grew from Objective 1.2, Improvements to Electro-optic Sampling with New Optical Sources. High performance optical phase modulators allowed us to experimentally open up this field, and has produced two Ph.D. theses, a CLEO postdeadline paper, and stimulated a lot of interest in the field including a column in Scientific America, May 1993. One thesis describing the optical phase modulator used as a 'time-lens' in these experiments and the first experiments in active pulse compression or temporal focusing was included as an appendix in the Interim Technical report filed for this contract. The second thesis

describes three additional and interesting experiments using this time-lens is included as an appendix in this report.

The important experimental results demonstrated to date include 1) active pulse compression of 55 ps pulses to 1.7 ps. The active compression or temporal focusing process reduces the timing jitter on the input pulses more than a factor of 5. This property is important in electro-optic sampling where timing jitter degrades time resolution. 2) Temporal imaging of optical pulses with time reversal. This experiment has shown the ability to magnify a portion of the time axis by -4X which means that an output pulse is a slowed, time-reversed, replica of the input. This has application in optical signal processing and pulse shape measurement. 3) Time-to-frequency conversion has been introduced as a new pulse shape measurement technique combining picosecond time resolution with excellent power sensitivity.

2.1 Synthesized optical source

Work on the optical synthesized source concentrated on the development of surface emitting lasers (SEL). These are key components because of their ability to smoothly tune wavelength, unlike distributed feedback lasers, which undergo mode hops when tuning. This research did not meet the goal because of difficulties in obtaining adequate surface emitting lasers. The other key technologies needed to make this system, high speed photodiodes and electrical samplers have been developed by the group in companion research and could be used when the appropriate laser technology is mature.

2.2 Improvements to electro-optic testing.

This research has produced some breakthrough results, mainly from our work on new optical sources which led to the development of high performance optical phase modulators. One of the phase modulators has been used to perform the pioneering experiments in the new field of temporal optics. This contract has supported interesting and useful research in optical pulse generation, manipulation and manipulation. More modest results have been achieved in the field of electro-optic testing.

2.2.1 The new approach to electro-optic testing

Summary: This work explored the possibilities of using fast electronics in tandem with erbium doped optical amplifiers to build an electro-optic sampling system without a pulsed laser, the component which limits the commercial application of electro-optic circuit

testing. This work showed that the new approach is fundamentally flawed and is not appropriate.

In order to build a more commercially practical electro-optic testing system, a new technique was pursued. This technique is a 'slow optics - fast electronics' approach which was designed to take advantage of the group expertise in high speed electrical sampling circuits. In the traditional 'fast optics- slow electronics' electro-optic sampling system, short optical pulses and a slow photodetector are used to measure the GaAs circuit waveforms using equivalent time sampling. The drawback to this system is the complex laser needed to generate the short pulses. In the new approach, a simple, commercially available CW laser diode is used to probe the circuit under test. The laser is modulated directly by the circuit waveform, and the modulation is detected by a fast photodiode and electrical receiver. The advantage of this system is that it is less complex, and all components are commercially available. It was seen as a way of making electro-optic testing commercially feasible.

To test this idea, we built an electro-optic testing system around the laser diode and fast electrical receiver using an HP 71400 Lightwave Signal Analyzer. This is a fast photodiode followed by an electrical amplifier and electrical spectrum analyzer. An erbium doped fiber optical amplifier precedes this electrical receiver. This amplifier was built and has greater than 30 dB of gain with good noise performance. The electrical spectrum analyzer receiver measures the magnitude of the frequency domain of the circuit under test. Such an receiver is characterized by a small electrical filter, so that the received noise level is minimized. The system performed as expected, with a bandwidth of 22 GHz, limited by the photodetector and electrical spectrum analyzer.

The more interesting type of system is one which measures the time domain of the circuit waveform. This system is equivalent to a high impedance voltage probe and sampling oscilloscope used to measure internal node voltage waveforms. To build such a system, we used a sampling oscilloscope as the electrical receiver. The fundamental problem with this type of system, and the flaw which prevented our system from working as originally hoped, is the increased receiver noise level in the sampling electrical receiver. The sampling receiver has an equivalent noise bandwidth which is many times larger than the noise bandwidth of the spectrum analyzer. This increased noise level overwhelms the received signal.

Our work has lead us to the conclusion that the sampling process should be done with optics, rather than electronics. This means that pulsed lasers must be used to get the high time resolution, rather than sampling the received electrical signal. While both techniques rely on mixing between the sampling pulses and circuit waveforms, there is a

distinct advantage to doing this mixing in the optical domain. In the electrical sampling approach, the circuit waveform is imprinted on the CW laser beam. The sampling is done after the light has been detected; the photocurrent has an AC component proportional to the circuit voltage. The electrical sampling pulses turn a sampling bridge on and off to downconvert the frequency of the high speed fluctuations to a lower frequency. The key is that the sampling bridge is passive: the sampling diodes are either conducting or not. When the are conducting, the RF line is connected to the IF output. The IF voltage is always less than or equal to the RF voltage, and IF power is proportional to the amount of time the diode switch is closed. The longer the switch is closed, the closer the IF power approaches the RF power. However, to get high time resolution, the switch should be closed for a short amount of time. So time resolution comes at the expense of low power transfer to the IF port. Since there is always noise in the IF, the signal to noise ratio decreases for short time resolution. The erbium doped fiber amplifier preceding the photodiode and electrical receiver also adds broadband noise which is sampled down to the IF port to further reduce the signal to noise ratio.

The story is different when the sampling is done in the optical domain. This is the traditional 'fast optics-slow electronics' approach to electro-optic testing which uses a pulsed laser source to get high time resolution. The AC component of the detected photocurrent is proportional to the average optical power and is independent of the pulse duration or repetition rate. Therefore, time resolution and signal to noise ratio are independent and sensitive, high time resolution results are possible.

We conclude that in electro-optic testing systems, high time resolution measurements should be made by sampling with pulsed laser sources, rather than by sampling electrically. The work on time-lenses, however, may provide a new method for high time resolution, sensitive measurements without electrical sampling or pulsed lasers.

2.2.2 New optical sources

Summary: The work to produce new optical sources has been the most fruitful. The original work to develop new pulsed laser sources led to technology used to pioneer the field of temporal optical systems.

We pursued two ideas to find new pulsed laser sources. The first was to build a pulsed laser source by modelocking an erbium doped fiber (EDF) laser. These EDF lasers will serve as compact pulsed sources at 1.5 μm wavelength. We first characterized the pump absorption and gain of a heavily-doped EDF using a Ti-Sapphire laser and then assembled a 1m EDF with a 100 mW, 980 nm pump laser diode. We achieved a 35%

input coupling of pump light into the fiber, resulting in a CW output power of 2-3 mW for a simple, linear cavity laser design. We proceeded to investigate other configurations such as those incorporating a fiber loop reflector. For optimal performance and large bandwidth, we discovered that fusion splices and a ring laser design were needed to minimize reflections.

For our first efforts at modelocking, we designed and developed a bulk-crystal $LiNbO_3$ piezo-electric strain optic (PESO) optical modulator. The PESO modulator could be operated at an acoustic resonance ranging from 1 to about 100 MHz and gave a maximum modulation of 10% for 1.55 μm light. For higher-speed modelocked operation, we used a commercially available 3 GHz integrated optic Mach Zender fiber modulator. We generated 300 ps pulses at a 500 MHz repetition rate using a 14 m, all-fiber ring laser. The total average output power was 1 mW.

2.2.3 Temporal Optics

Summary: This was the most successful research effort conducted under this contract. The development of a high performance optical phase modulator gave us the capability to perform the fundamental and pioneering experiments in the field of temporal optics. This is a new experimental field which has a bright future in its ability to generate, measure and manipulate optical pulses. This effects most every field which uses pulsed lasers.

Temporal optics is a relatively new field which treats optical pulses just as spatial or conventional optical systems work on spatial objects. This field is based on the mathematical similarities between the effects of diffraction on spatially varying fields and temporal dispersion on time varying fields. The space-time analogy allows one to interchange spatial and temporal variables, diffraction and dispersion, and spatial and time-lenses. Since the effect of a spatial lens is to cause a spatially varying phase shift, a time-lens must impart a time-varying phase shift on an incident pulse. The enclosed thesis expands on these similarities and formally defines the space-time equivalents.

With the space-time analogy as a guide, temporal equivalents to spatial optical systems can be built. Figure 1 shows three spatial optical systems whose temporal equivalents have been demonstrated experimentally. They are: 1) temporal focusing; 2) temporal imaging; and 3) time-to-frequency conversion.

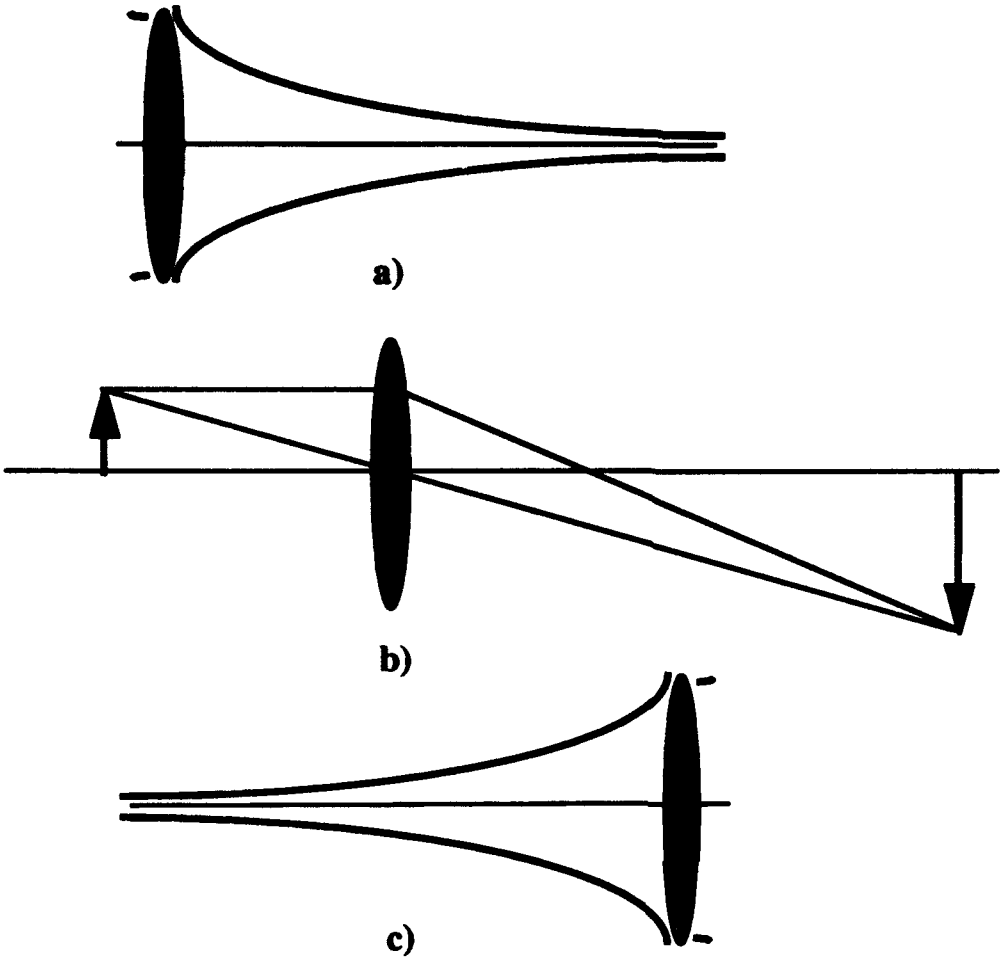

Figure 1. The spatial equivalents of the temporal optical systems demonstrated in this contract. a) shows focusing. b) shows imaging. and c) shows Fourier transform operation for time-to-frequency conversion.

A key element in these experiments is the time-lens. The time-lens is an extremely high performance electro-optic phase modulator which has been patented and commercially licensed. This device is capable of providing 13 radians of peak optical phase shift on a 1.064μm optical signal when driven with 1W of microwave power at a frequency of 5.2 GHz, and 52 radians with 16W. This modulator allows us to resolve optical pulses with pulse widths as small as 1.7 ps and formed the backbone for the temporal optical experiments.

Temporal focusing is another term for optical pulse compression. In this experiment, a long pulse enters the time-lens, is phase modulated, then travels through a dispersive delay line. The output is a compressed optical pulse. The spatial equivalent is focusing a large beam to a small spot. This work is different than previous optical pulse

compression demonstrations in that an active time-lens or electro-optic phase modulator is used in place of self phase modulation in an optical fiber. Experimental results have shown compression of 55 ps 1.064μm pulses down to 1.7 ps. Further work has shown the ability of such a system to reduce pulse-to-pulse timing fluctuations (time-jitter) when focusing pulses. Instead, the timing fluctuations are converted into frequency fluctuations which can be tolerated in many experiments. Short pulses with reduced timing jitter are required in high performance electro-optic sampling systems.

Figure 1b) shows a spatial imaging system analogous to the temporal imaging system explored in this work. This experiment uses dispersive elements before and after the time-lens to build a time microscope This is an experiment to demonstrate the ability to magnify or demagnify a portion of the time axis. An interesting property of such a system is time reversal. Just as the object and image in a spatial imaging system are inverted in space with respect to one another, the input and output pulses in a temporal imaging system are reversed in time. In these experiments, a pair of pulses separated by 20 ps at the input to the system was expanded to 80 ps at the output, and the pulse sequence was time-reversed. Such a system can be used for high time resolution pulse shape measurement when combined with various electrical receivers. This can be done by using the time-microscope to magnify a pulse before viewing with a fast photodiode. This can extend the resolution of fast photodiodes and sampling oscilloscopes down to the picosecond regime.

Figure 1c) shows the spatial equivalent to the latest temporal optical system. This system is a pulse shape measurement device which combines useful time resolution with excellent optical power sensitivity and system simplicity. The key to operation is the ability of a time-lens to perform a Fourier transform. The input signal is Fourier transformed by both the time-lens and an optical spectrum analyzer. The result of these successive Fourier transforms is a scaled replica of the original signal. This means that the optical spectrum analyzer trace is a direct measure of the input time-varying pulse intensity. This procedure is called time-to-frequency conversion and has demonstrated 3.0 ps system time resolution. This work is a significant contribution to optical pulse shape measurement and has inspired similar research by several groups.

3. Publication List

1. Weingarten, K. J., A. A. Godil, "FM mode-locking at 2.85 GHz using a microwave resonant optical modulator," IEEE Photonics Technology Letters, Oct. 1992. **4**: p. 1106-9.

2. Godil, A.A., B.A. Auld, and D.M. Bloom, "Time-lens producing 1.9 psec optical pulses," Applied Physics Letters, 1993. **62**: p. 1047-1049.

3. Kauffman, M.T., W. C. Banyai, A. A. Godil, and D. M. Bloom, "Applications of Time-Lens Optical Systems," Electronics Letters, 1993. **29**: p. 268.

4. Kauffman, M.T., W. C. Banyai, A. A. Godil, and D. M. Bloom, "Time-to-frequency converter for measuring picosecond optical pulses," Applied Physics Letters, 1994. **64**(3), pp. 270-2.

4. Personnel Involved

Principal Investigator: Prof. David M. Bloom
Research Associate: Dr. Bill Banyai
Research Assistants: Asif Godil, Mike Kauffman, Sam Hou.

Advanced Degrees Awarded:

12/92 Asif Godil, Ph. D., Electrical Engineering for Harmonic Mode-Locking of Diode-Pumped Lasers and Time-Lenses with Picosecond Resolution

6/94 Mike Kauffman, Ph. D., Electrical Engineering for Applications of Temporal Optical Systems.

5. Interactions

5.1 Papers presented

1. A. A. Godil, B. A. Auld, and D. M. Bloom, "Time-lens producing picosecond optical pulses," presented at 1992 Annual meeting of IEEE Lasers and Electro-Optics Society, paper OTA1.2, Nov. 16-19, 1992, Boston MA.

2. Kauffman, M.T., A. A. Godil, W. C. Banyai, and D. M. Bloom, "Applications of Time-Lens Optical Systems". in 1993 Ultrafast Electronics & Optoelectronics Topical Meeting. 1993. San Francisco, CA.

3. Kauffman, M. T., W. C. Banyai, and D. M. Bloom, "A Time-to-Frequency Converter for Measuring Picosecond Optical Pulses," 1993 Conference on Lasers and Electro-Optics, postdeadline paper PDP-35, May 2-7, 1993, Baltimore, MD.

5.2 Consultative Functions

The time-lens work has spurred interest by several other research groups. Discussions have been held with J. C. M. Diels from University of New Mexico about collaboration on pulse shape measurement techniques using the technologies developed under this and other contracts. Mike Kauffman met with Scott Diddams, a graduate student at UNM, on 1/28/94 to discuss the possibility of providing time-lens technology for a new optical pulse measurement system. Engineering drawings have been made available to any research group interested in pursuing temporal optics with the Stanford time-lens.

6. New Discoveries, Inventions, Patent disclosures

This grant cycle has been fruitful in the number of contributions the research has produced.

6.1 New Discoveries.

Fundamental discoveries include the development of several high performance optical modulators. This modulators have been used to modelock diode pumped solid state lasers and for the breakthrough research in temporal optics.

The optical modulator used as the time-lens in temporal optics has produced several new discoveries. It has been used for the first experimental demonstration of temporal imaging with time reversal and more importantly in a new optical pulse shape measurement technique, time-to-frequency conversion, which combines good time resolution with excellent power sensitivity.

6.2 Inventions filed

Title: "Partially Loaded Microwave Waveguide Standing Wave Electro-Optic Modulator"
U.S. Patent Application Number: 07/932,880
Filed: 8/19/92
Inventor: Asif A. Godil
This device is a very high performance optical phase modulator used as the time-lens in much of the work. Also called a resonant microwave optical modulator.
This device has been licensed to New Focus, Inc. Sunnyvale CA.

6.3 Patent Disclosures

Title: "High-Speed Photodiode Monolithically Integrated With a Microwave Detector"
Stanford Document Number: S92-115
Filed: 07/29/92
Govt. Sponsor: Capt. Helen R. Tyson, notified 11/06/92
Inventors: K. D. Li-Dessau, A. S. Hou, D. M. Bloom
This device is a solid state replacement to an optical correlator using both a fast photodiode and microwave detector diode.

Title: "Timelens"
Stanford Document Number: S92-104
Filed: 7/24/92
Govt. Sponsor: Capt. Helen R. Tyson
Inventor: A. A. Godil
This invention disclosure covers some of the time-lens experiments performed in this contract.

7. Appendix

Enclosed is a copy of the Ph.D. Thesis "Applications of Temporal Optical Systems" by M. T. Kauffman. In the interim report, A. A. Godil's Ph. D. thesis was enclosed. Together, the two cover the temporal optical system work performed under this contract.

APPLICATIONS OF TEMPORAL OPTICAL SYSTEMS

A DISSERTATION
SUBMITTED TO THE DEPARTMENT OF ELECTRICAL
ENGINEERING
AND THE COMMITTEE ON GRADUATE STUDIES
OF STANFORD UNIVERSITY
IN PARTIAL FULFILLMENT OF THE REQUIREMENTS
FOR THE DEGREE OF
DOCTOR OF PHILOSOPHY

Michael T. Kauffman
March 1994

I certify that I have read this dissertation and that in my opinion it is fully adequate, in scope and quality, as a dissertation for the degree of Doctor of Philosophy

David M. Bloom (Electrical Engineering)
(Principal Advisor)

I certify that I have read this dissertation and that in my opinion it is fully adequate, in scope and quality, as a dissertation for the degree of Doctor of Philosophy

Bertram A. Auld (Applied Physics)

I certify that I have read this dissertation and that in my opinion it is fully adequate, in scope and quality, as a dissertation for the degree of Doctor of Philosophy

Anthony Fraser-Smith (Electrical Engineering)

Approved for the University committee on Graduate Studies:

Abstract

Temporal optics is a relatively new experimental field with a promising future. This thesis discusses a number of applications of temporal optical systems for optical pulse measurement and manipulation. The space-time analogy is presented as a tool to understand the operation of temporal optical systems based on knowledge of spatial optical systems.

Temporal optical systems are comprised of dispersive delay lines and optical phase modulators or time-lenses. They operate on time varying fields just as spatial optical systems made of diffraction and spatial lenses operate on spatially varying fields. The space-time analogies are used to analyze and synthesize temporal optical systems for active optical pulse compression, temporal imaging and time-to-frequency conversion.

Pulse compression, or temporal focusing, is analogous to spatial beam focusing. Pulse compression with an active time-lens has the ability to suppress timing jitter in the pulses to be compressed. The system has been used to compress 55 ps pulses to 7 ps and reduce the timing fluctuations by more than a factor of 5. A theory to explain this ability agrees well with measured data.

Temporal imaging is used to distortionlessly magnify a portion of a time varying field distribution. Four times magnification has been demonstrated. Magnification can be used for pulse shape measurement by combing a time-microscope with a fast photodetector. An interesting and useful property of such a time magnifying system is time reversal. This property has applications to optical signal processing.

Time-to-frequency conversion is a fundamentally new pulse shape measurement technique. It utilizes a temporal optical system to perform a Fourier transform so that pulse shape can be measured directly with an optical spectrum analyzer. This technique combines 3.0 ps time resolution with high sensitivity in an experimental setup without any high speed components.

I dedicate this work to my wife Bonnie

Acknowledgments

- My dog Mickey.

- Prof. Dave Bloom for providing an atmosphere where interesting ideas are plentiful and can be pursued.

- Bill Banyai for all his guidance, advice and motivation.

- Asif Godil for his pioneering work developing a very useful time-lens and providing guidance for the early work in this thesis.

- Prof. Bert Auld for being my associate advisor and for his early, important contributions to the development of the time-lens.

- Prof. Tony Fraser-Smith for being on my reading committee and contributing more through his encouragement than was expected.

- Rory Van Tuyl for his advice during several summer jobs.

- Joe Vhrel and Chris Remen of the Crystal Shop.

- Ted Bradshaw and Dave Arnone of the Machine Shop.

- Alistair Black, Kathy Li, John Thackara for there early interactions and introductions to the group.

- Jeff Bostak and Sam Hou for their helpful discussions and general help.

- AFOSR for their financial support under contracts F49620-88-C-0103 and F49620-92-J-0099.

- And most of all, Bonnie

Table of Contents

List of Figures

Chapter 1 Introduction

A temporal optical system is a conceptual tool used to analyze and synthesize systems for measuring and manipulating optical pulses. The basis of temporal optics lies in the analogy between spatial objects and temporal pulses of light. Spatially and temporally varying fields behave similarly in response to analogous operations. The goal of temporal optics is to understand these analogous operations and use the analogy to apply knowledge of spatial systems to temporal systems. This thesis discusses the analogy and uses it to understand the operation of three different temporal optical systems.

The field of temporal optics has grown since the 1960's with the original analogy between the effect of diffraction on spatial objects and dispersion on pulses of light. The first application of temporal optical systems was for optical pulse compression, studied many years before the analogy was formalized. The term time-lens was coined in the late 1980's when the space time analogy was formalized and time-lens properties were defined.

With the development of the first practical time-lens by Asif Godil, the field of temporal optics has opened up. Active pulse compression or temporal focusing with this time-lens was quickly demonstrated.

The experiments described in Chapter 3 take the next step in further exploring the characteristics of temporal focusing and analyzing the ability to reduce fluctuations in pulse-

to-pulse arrival time, or timing jitter. The spatial equivalent to this experiment is shown in Figure 1.1a).

A more complicated temporal optical system whose spatial analogy is shown in Figure 1.1b) is used for temporal imaging. The ability to magnify the time axis over a finite time interval is demonstrated, along with the interesting property of time reversal.

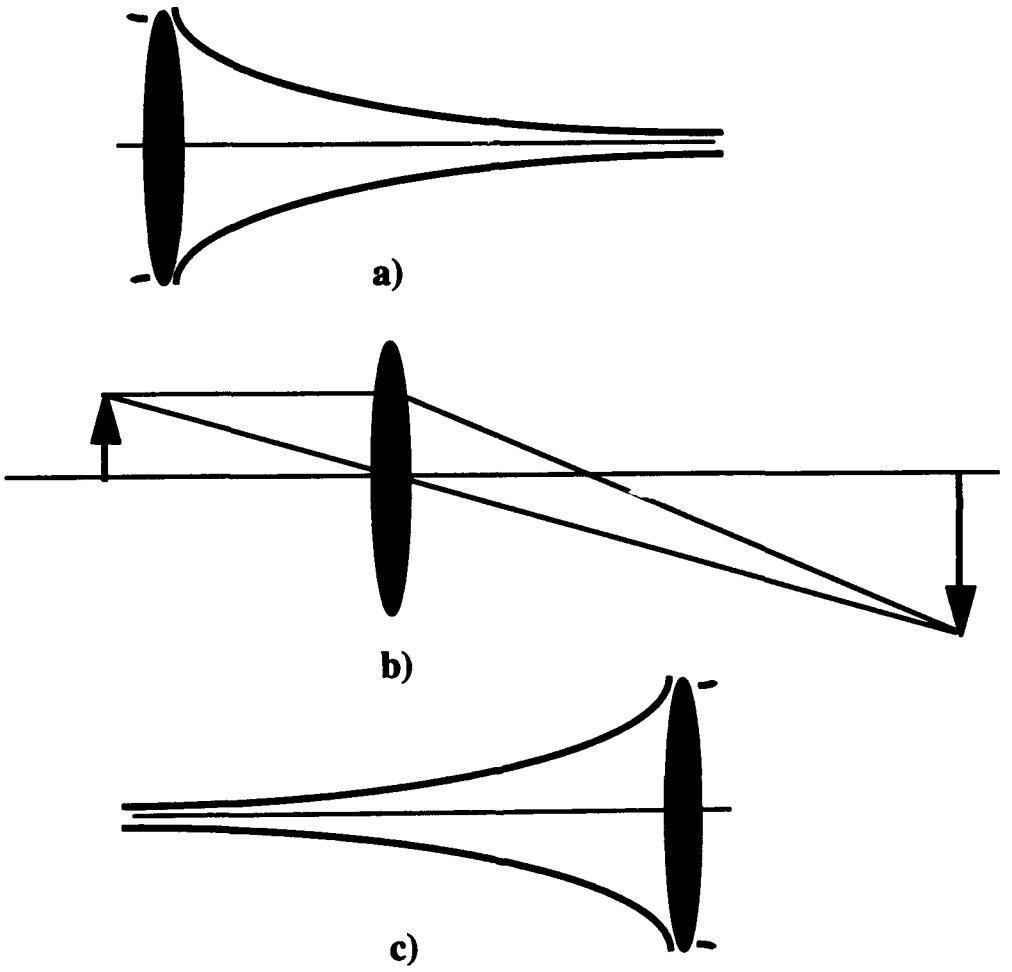

Figure 1.1. The spatial equivalents of the temporal optical systems demonstrated in this thesis. a) shows focusing. b) shows imaging. and c) shows Fourier transform operation for time-to-frequency conversion.

The final contribution this thesis makes is the development of a new method for optical pulse shape measurement called time-to-frequency conversion. The spatial equivalent is shown in Figure 1.1c). This measurement technique is shown to have the important properties of useful time resolution and excellent power sensitivity.

An interesting comment on optics noted that the field has come full circle in its development. In the 1960's, the traditional electrical engineering concepts of the Fourier transform and frequency domain filters were applied to spatial optics and diffraction of spatial objects. This was a powerful tool to understand the operation of spatial optical systems using electrical engineering tools and techniques. Temporal optics worked the other direction, applying the spatial optical concepts of images and lenses to the electrical engineering problem of pulse propagation.

Chapter 2 Introduction to Temporal Optics

The experiments in this thesis can be explained from a purely mathematical basis. The space-time analogy, however, allows them to be understood from a more intuitive level. By drawing on the analogy, knowledge of spatial optical systems can be applied directly to the time domain and temporal optical systems. The space-time analogy is rooted in the mathematical similarity between the paraxial approximation to the wave equation and the equation describing propagation of pulses in a dispersive medium. The analogy is extended to include spatial and temporal lenses. In this chapter, the space-time analogy will be presented both qualitatively and quantitatively. The goals of this chapter are to explain the entries of Table 2.1 and discuss the time-lens used in the experiments presented in the following chapters.

2.1 Qualitative description of the space-time analogy

Understanding the space-time analogy allows one to interchange spatial and temporal variables and directly apply knowledge of one system to the other. Figure 2.1 shows both spatial and temporal imaging systems. In either case, an imaging system requires dispersion from the object to the lens, a lens, and dispersion from the lens to the image. The analogy between spatial and temporal dispersion is subtle. In the spatial case,

dispersion results from free-space propagation of light, that is, diffraction. The phase relationship of light at a lens is determined by a single variable, for example, the object distance. In the temporal case, frequency dispersion is supplied by an dispersive element such as a diffraction grating pair or, as pictured, a length of optical fiber. From this, it is apparent that space and time are equivalent variables so that a spatially varying field is analogous to a time varying field. The effects of diffraction on the spatially varying field are analogous to the effects of dispersion on a time varying field. Likewise, a time-lens will work like a spatial lens.

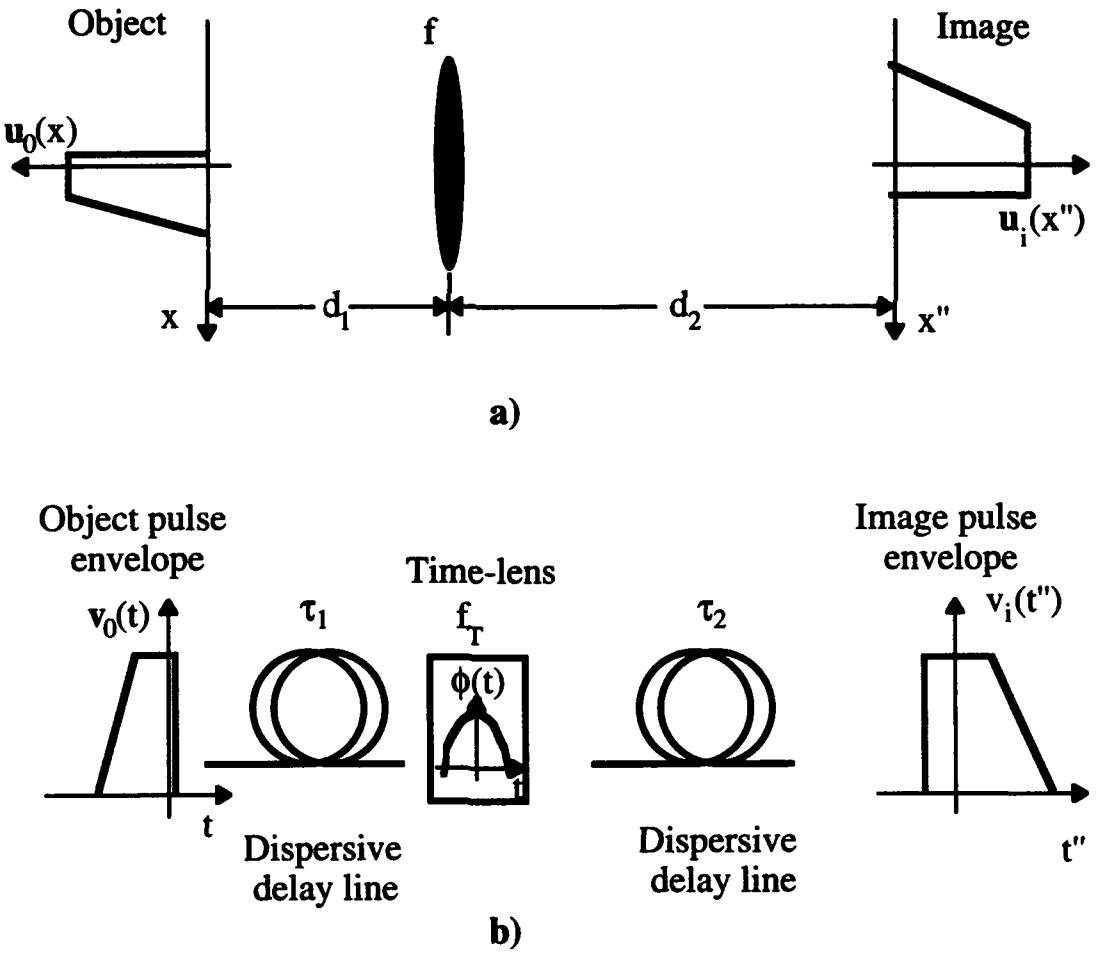

Figure 2.1 a) Spatial and b) Temporal optical imaging systems.

2.1.1 Spatial and temporal objects

A spatially varying field distribution is an object in a spatial optical system. This field distribution can be described in two Fourier transform related domains, space and spatial frequency. The spatial frequency content of a spatial object quantifies the amplitude and phase of each plane wave comprising the object. The spatial frequency indicates the angle with respect to the optic axis at which each plane waves travels. In a temporal optical system, an object is a time varying field which can also be described in the frequency domain through a Fourier transform. Space and time are analogous domains as are the spatial frequency and frequency domains. Since the optic axis of a spatial optical system is measured in distance units, the optic axis of a temporal optical system is measured in time units.

2.1.2 Diffraction and dispersion

In a spatial optical system, diffraction modifies the spatial object as it propagates through free space. In the Fresnel approximation[1], diffraction modifies the spatial frequency content of an object by multiplying by a transfer function which has quadratic phase versus spatial frequency. The phase curvature versus spatial frequency of this transfer function increases linearly with distance along the optic axis.

Similarly, a temporal object has its frequency content multiplied by a transfer function with quadratic phase versus frequency after traveling down a dispersive delay line. This is the definition of a first order dispersive system. The frequency rate of phase curvature also increases linearly with distance along the temporal optic axis.

So diffraction is analogous to dispersion and the effects of each on their respective objects can be characterized by a single parameter, the distance along the optic axis. This was originally noted by Akhmanov[2, 3].

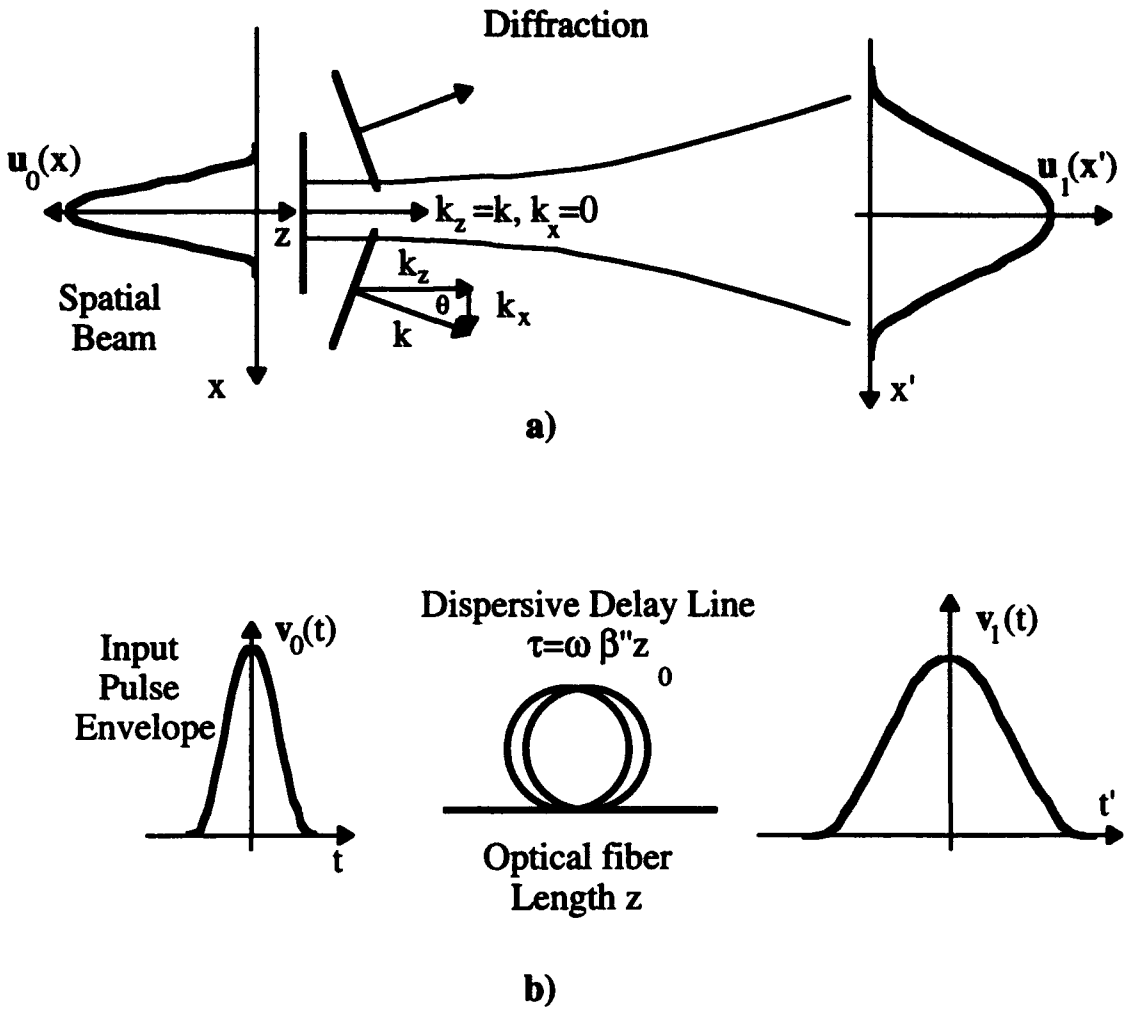

Figure 2.2 Effects of a) diffraction on a spatially varying field and b) dispersion on a time varying field.

A short optical pulse is the result of the constructive interference of a large number of frequencies just as a small optical beam results from the constructive interference of a large number of plane waves. When these (spatial) frequencies are in phase, the interference leads to a short pulse (small beam). After propagating through a dispersive medium (diffracting through free space), the nonlinear phase versus (spatial) frequency destroys the initial, constructive phase relationship so that the sinusoids no longer interfere

constructively. The result is a broad pulse (beam). This similarity between diffraction and dispersion is shown in Figure 2.2.

2.1.3 Lenses

Finally, the temporal analogy to spatial lenses must be developed. A spatial lens is simply a spatially varying phase modulator. Optical rays passing through the center of a convex lens propagate through more high index material than rays passing through the edges. This results in a spatially-varying phase profile which is, ideally, quadratic versus transverse distance from the optic axis. Since space and time are analogous domains, an ideal time-lens must therefore supply a time-varying phase which is quadratic in time. This analogy was formalized by Kolner[4]. While it is easy to build a spatial lens with many wavelengths of path length difference across the face of a spatial lens, it has been very difficult to produce a time-lens with many wavelengths of phase shift across the time aperture. The work in this thesis was made possible by the development of such a time-lens.

From this, we can see a large amount of symmetry in optics. Objects are described by field distributions in two Fourier transform related domains. Diffraction and dispersion modify these distributions by multiplying the frequency domain by a phase which varies quadratically versus frequency. Lenses modify the distributions by multiplying the space and time domains by a phase which varies quadratically versus space or time.

2.2 Quantitative explanation of the space-time analogy

The analogies outlined in Section 2.1 allow one to synthesize temporal optical systems to manipulate and measure optical pulses. In order to quantify the performance of these systems, the analogies must also be formally defined. Once the analogy between diffraction and dispersion is formalized, the remaining analogies can almost be written by

inspection. The casual reader can skip to Table 2.1 which summarizes the analogies, but will miss my best efforts to keep track of signs and unimportant constants. You can do it, but you'll be sorry.

2.2.1 Diffraction and dispersion

The effects of diffraction on spatial beams and dispersion on temporal pulses can be seen from solutions to the scalar wave equation

$$\nabla^2 E = \mu\varepsilon \frac{\partial^2 E}{\partial t^2} \quad . \tag{2.1}$$

Both solutions will be developed in parallel.

SPATIAL DIFFRACTION	TEMPORAL DISPERSION
Seek solutions of the form	Seek solutions of the form (2.2)
$E(x,z,t) = \Psi(x,z)e^{j\omega t}$	$E(t,z) = \Psi(z)e^{j\omega t}$
This is a monochromatic beam of light.	This is a plane wave.

When these trial solutions are inserted into the wave equations, the result is:

$\frac{\partial^2\Psi}{\partial x^2} + \frac{\partial^2\Psi}{\partial z^2} = -\omega^2\mu\varepsilon\Psi$	$\frac{\partial^2\Psi}{\partial z^2} = -\omega^2\mu\varepsilon\Psi$ (2.3)

The general solutions to this differential equation are

$\Psi(x,z) = e^{-j\beta_x x}e^{-j\beta_z z}$	$\Psi(z) = e^{-j\beta z}$ (2.4)
This is a plane wave traveling in a direction determined by the relative magnitudes of β_X and β_Z.	This is a plane wave traveling in the z-direction with propagation constant β.

Inserting these general solutions into Equation 2.3 gives the following eigenvalue relationship.

$$\beta_x^2 + \beta_z^2 = \omega^2\mu\varepsilon = \beta^2 \qquad \beta^2 = \omega^2\mu\varepsilon \tag{2.5}$$

Specific solutions to the wave equation are found as a summation of the general solutions given by Equation (2.4)

$$u_0(x,z) = \frac{1}{2\pi}\int d\beta_x U_0(\beta_x) e^{-j(\beta_x x + \beta_z z)} \qquad u_0(t,z) = \frac{1}{2\pi}\int d\omega\, U_0(\omega) e^{j\omega t} e^{-j\beta z} \tag{2.6}$$

A spaital object is a weighted sum of plane waves traveling at different angles with respect to the optic axis z.

A pulse is a weighted sum of sinusoids of different frequencies. $U_0(\omega)$ is the weighting function.

Adjust the z-axis so that u_0 is the solution when z=0. Equation (2.6) has the same form as an inverse Fourier transform, so that the following relations can be defined.

$$u_0(x,0) = u_0(x) = \frac{1}{2\pi}\int d\beta_x\, U_0(\beta_x) e^{-j\beta_x x} \qquad u_0(t,0) = u_0(t) = \frac{1}{2\pi}\int d\omega\, U_0(\omega) e^{j\omega t} \tag{2.7}$$

and

$$U_0(\beta_x) = \int dx\, u_0(x) e^{j\beta_x x} \qquad U_0(\omega) = \int dt\, u_0(t) e^{-j\omega t} \tag{2.8a}$$

Since this problem deals with the effect of dispersion on a pulse modulated optical carrier we can write the total field $u_0(t)$ in terms of a baseband pulse $v_0(t)$ and optical carrier $e^{j\omega_0 t}$

$$u_0(t) = v_0(t) e^{j\omega_0 t} \tag{2.8b}$$

So that using the Fourier shift theorem[5]

$$U_0(\omega) = V_0(\omega + \omega_0) \tag{2.8c}$$

Equation (2.8) points out one of the differences between spatial and temporal optics: temporal pulses ride on an optical carrier while spatial beams are "baseband" objects. To determine the effects of diffraction and dispersion, we need to find the response at the plane z, $u_1(x',z)$ and $u_1(t',z)$.

$$u_1(x',z) = \frac{1}{2\pi}\int d\beta_x U_0(\beta_x) e^{-j(\beta_x x' + \beta_z z)} \qquad u_1(t',z) = \frac{1}{2\pi}\int d\omega\, U_0(\omega) e^{j\omega t'} e^{-j\beta z} \tag{2.9}$$

This is the point where the paraxial approximation is applied to the case of diffraction, and first-order dispersion to the temporal case.

The paraxial approximation is that the beam in equation (2.7) can be adequately represented by plane waves propagating close to the optic axis so that from equation (2.5), β_z is approximated by

$$\beta_z = \sqrt{\beta^2 - \beta_x^2} \approx \beta - \frac{\beta_x^2}{2\beta} \tag{2.10}$$

A dispersive medium is one in which β is not a linear function of ω. This can occur when the dielectric constant is a function of the frequency, for example, or with a diffraction grating pair where the different wave groups travel with the same velocity along different paths[6]. The approximation made in this case assumes that the pulse is adequately represented by a band of frequencies around the carrier frequency ω_0. The function $\beta(\omega)$ can be expanded in a three term Taylor series about ω_0

$$\begin{aligned}\beta(\omega) &\approx \beta(\omega_0) + (\omega - \omega_0)\left.\frac{\partial\beta}{\partial\omega}\right|_{\omega_0} \\ &\quad + \frac{1}{2}(\omega - \omega_0)^2 \left.\frac{\partial^2\beta}{\partial\omega^2}\right|_{\omega_0} \\ &= \beta_0 + (\omega - \omega_0)\beta' \\ &\quad + \frac{1}{2}(\omega - \omega_0)^2\beta''\end{aligned}$$

Applying the Fourier transform relations of (2.8) and the approximations of (2.10) to equation (2.9), and after significant manipulation, the response at plane z is seen to be

$$u_1(x',z) = \frac{e^{-j\beta z}}{2\pi}\int dx\, u_0(x) \bullet \int d\beta_x\, e^{-j\beta_x(x'-x)} e^{j\frac{\beta_x^2}{2\beta}}$$

$$u_1(t',z) = e^{j\omega_0 t'}\frac{e^{-j\beta_0 z}}{2\pi}\int dt\, u_0(t)e^{-j\omega_0 t} \bullet \int d\omega\, e^{j(\omega-\omega_0)(t'-\beta' z-t)} e^{-j(\omega-\omega_0)^2\beta'' z} \quad (2.11a)$$

This can be simplified if this response is measured in a moving coordinate system by allowing $t'-\beta' z \rightarrow t'$. $\beta' z$ is the group delay that the midband frequencies incur while propagating through the dispersive medium. So in the moving coordinate system (2.11b)

$$u_1(t',z) = e^{j\omega_0(t'+\beta' z)}\frac{e^{-j\beta_0 z}}{2\pi} \bullet \int dt\, u_0(t)e^{-j\omega_0 t} \bullet \int d\omega\, e^{j(\omega-\omega_0)(t'-t)} e^{-j(\omega-\omega_0)^2\beta'' z}$$

The frequency domain integral in equation (2.11) can be evaluated[7] to yield

$$u_1(x',z) = \sqrt{\frac{j\beta}{2\pi z}} e^{-j\beta_0 z} \bullet \int dx\, u_0(x) e^{-j\frac{(x'-x)^2\beta}{2z}}$$

$$u_1(t',z) = e^{j\omega_0(t'+\beta' z)} \sqrt{\frac{-j}{2\pi\beta'' z}} e^{-j\beta_0 z} \bullet \int dt\, u_0(t) e^{-j\omega_0 t} e^{j\frac{(t'-t)^2}{2\beta'' z}} \quad (2.12a)$$

The quantity $u_0(t)e^{-j\omega_0 t}$ is seen by Equation (2.8b) to be the original pulse envelope $v_0(t)$. Following the same form as Equation (2.8), the output field $u_1(t')$ can be written in terms of a pulse modulated optical carrier so that the output pulse envelope $v_1(t')$ is

$$v_1(t',z) = \sqrt{\frac{-j}{2\pi\beta'' z}} e^{-j\beta_0 z} \bullet \int dt\, v_0(t) e^{j\frac{(t'-t)^2}{2\beta'' z}} \quad (2.12b)$$

Equation (2.12) shows that diffraction affects a spatial object in the same way that first order dispersion affects the temporal pulse envelope. In the spatial domain both the transverse axis variable x and the optic axis variable z have units of length. In the time domain, the transverse axis variable t has units of time while the optic axis variable z has units of length. To enhance the space-time parallelism, we can rewrite the temporal Equation (2.12) so that the temporal optic axis also has units of time. If τ is defined as the "distance" in time along the temporal optic axis, and make the substitution $\tau=\omega_0\beta''z$, then Equation (2.12b) becomes

$$u_1(t',z) = \sqrt{\frac{j\beta}{2\pi z}} e^{-j\beta_0 z} \bullet \int dx\, u_0(x) e^{-j\frac{(x'-x)^2\beta}{2z}}$$

$$v_1(t',\tau) = \sqrt{\frac{-j\omega_0}{2\pi\tau}} e^{-j\beta_0 \frac{\tau}{\omega_0\beta''}} \bullet \int dt\, v_0(t) e^{j\frac{(t'-t)^2\omega_0}{2\tau}} \quad (2.13a)$$

Since it will be used in later chapters, the entire output pulse consisting of envelope modulating the carrier is given by

$$u_1(t',\tau) = e^{j\omega_0(t'+\beta' z)} \sqrt{\frac{-j\omega_0}{2\pi\tau}} e^{-j\beta_0 \frac{\tau}{\omega_0\beta''}} \bullet \int dt\, v_0(t) e^{j\frac{(t'-t)^2\omega_0}{2\tau}} \quad (2.13b)$$

Equation (2.13) reveals most of the space-time equivalents listed in Table 2.1. The substitution

$$\tau = \omega_0 \beta'' z \quad (2.14)$$

leading to Equation (2.13) changes the space-time equivalents listed in Table 2.1 from those given by Harris[8] and Treacy[9] into a more parallel and pleasing form. This substitution has also been noted by Dijaili[10].

Table 2.1 Space-Time Equivalents

SPACE	TIME
x' Transverse axis variable.	t' Transverse axis variable. This is in the moving coordinate system in that the midband group delay was absorbed in the substitution $t'-\beta' z \rightarrow t'$.
z Distance along spatial optic axis.	τ 'Distance' along temporal optic axis. Measured physically with $\tau = \omega_0 \beta'' z$, where β'' is the group velocity dispersion parameter, and z is the distance traveled in the medium.
Objects are spatially varying fields described in the spatial $u_0(x)$ and spatial frequency $U_0(\beta_x)$ domains. $$u_0(x) = \frac{1}{2\pi}\int d\beta_x \, U_0(\beta_x) e^{-j\beta_x x}$$	Objects are time varying fields consisting of a baseband pulse envelope modulating an optical carrier. $u_0(t) = v_0(t) e^{j\omega_0 t}$. The time and frequency domains are related through the Fourier transform. $$u_0(t) = \frac{1}{2\pi}\int d\omega \, U_0(\omega) e^{j\omega t}$$ and $$U_0(\omega) = V_0(\omega + \omega_0)$$
Diffraction $$u_1(t',z) = \sqrt{\frac{j\beta}{2\pi z}} e^{-j\beta_0 z} \bullet \int dx \, u_0(x) e^{-j\frac{(x'-x)^2\beta}{2z}}$$	Dispersion $$v_1(t',\tau) = \sqrt{\frac{-j\omega_0}{2\pi\tau}} e^{-j\beta_0 \frac{\tau}{\omega_0 \beta''}} \bullet \int dt \, v_0(t) e^{j\frac{(t'-t)^2 \omega_0}{2\tau}}$$
$-\beta$ Propagation constant, $\beta = \frac{2\pi}{\lambda}$. (Note the negative sign preceding β.)	ω_0 Optical center frequency.
β_x Transverse propagation constant. Spatial frequency domain.	$(\omega-\omega_0)$ Frequency offset from optical carrier. Frequency domain.
$\theta = \frac{\beta_x}{\beta}$ Plane wave propagation angle. See Figure 2.2.	$\frac{\omega-\omega_0}{\omega_0}$ Fractional frequency offset.

f Focal length of spatial lens.	$f_T = -\frac{\omega_0}{A\omega_m^2}$ Focal time of time-lens. This expression gives the focal time for a time-lens with sinusoidal phase versus time $\phi(t) = A\cos(\omega_m t)$.
Spatial lens transfer function $h(x) = e^{-j\phi(x)} = e^{j\frac{\beta x^2}{2f}}$	Time-lens transfer function $h(t) = e^{-j\phi(t)} = e^{-j\frac{\omega_0 t^2}{2f_T}}$
$f^{\#}=f/D$ Spatial f-number D is the lens diameter	$f^{\#}=f_T/t_{aperture}$ Temporal f-number $t_{aperture}$ is the time-lens effective aperture.
Spatial resolution $\Delta x_{fwhm} \approx f^{\#}\lambda$	Time resolution of a gaussian pulse. $\Delta t_{fwhm} = \frac{2.8}{A\omega_m}$ For sinusoidal time-lens with $t_{aperture} = 1/\omega_m$.
Law of Spatial Imaging $\frac{1}{d_1}+\frac{1}{d_2}=\frac{1}{f}$	Law of Temporal Imaging $\frac{1}{\tau_1}+\frac{1}{\tau_2}=\frac{1}{f_T}$
Lateral Magnification $M = -\frac{d_2}{d_1}$	Temporal Magnification $M = -\frac{\tau_2}{\tau_1}$

Table 2.1 Space-Time equivalents, continued.

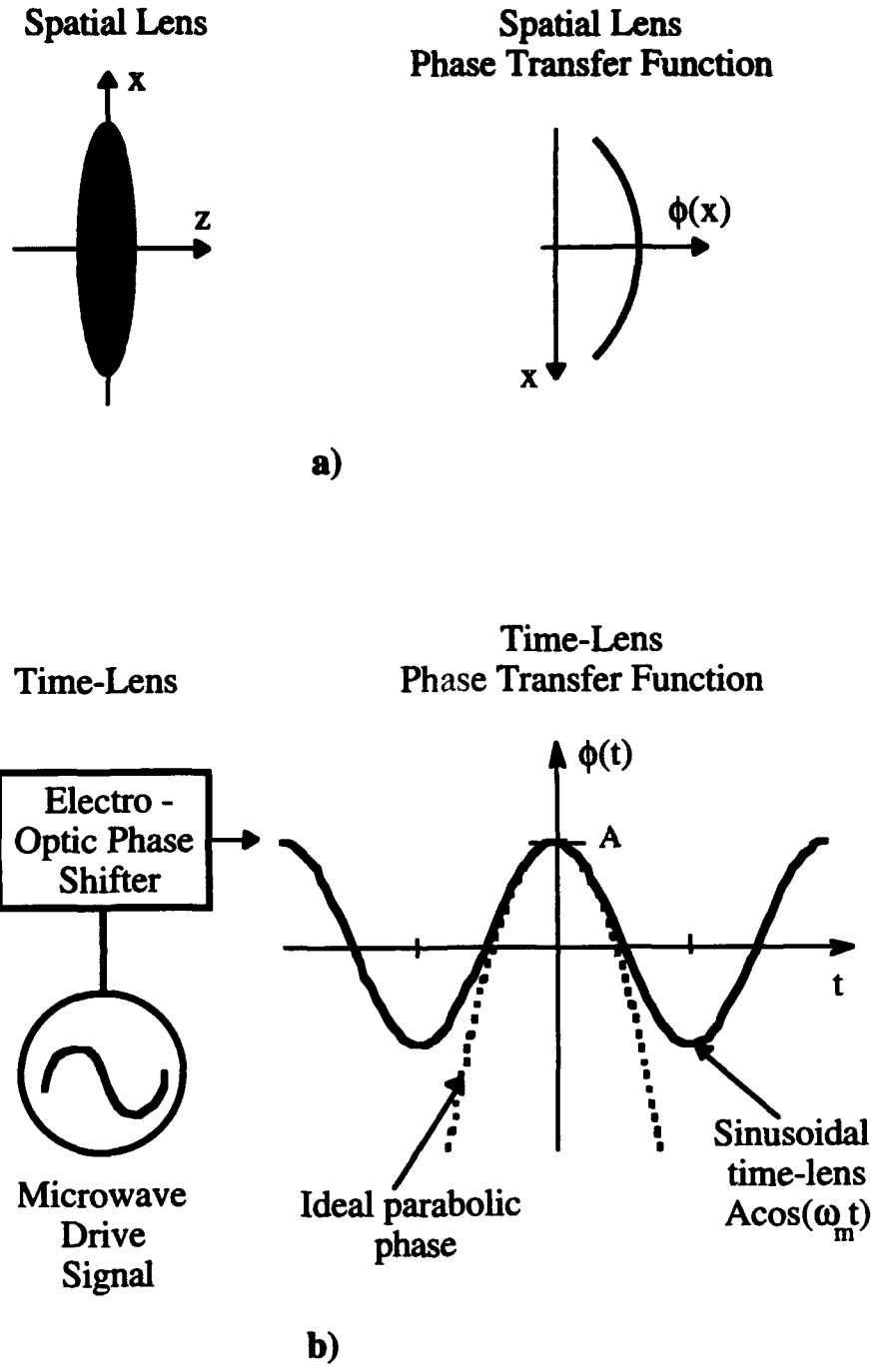

Figure 2.3 Phase characteristics of a) spatial and b) temporal lenses.

2.2.2 Spatial and Time-lenses

Diffraction and dispersion are just one of the space-time analogies. To build useful temporal optical systems, we need time-lenses. The space dependent phase characteristic of spatial lenses and time dependent phase characteristic of time-lenses is shown in Figure 2.3. It can be shown[1] that the position dependent phase transfer function $\mathbf{h}(x)$ of a thin spatial lens, ignoring a constant phase factor, is

$$\mathbf{h}(x) = e^{-j\phi(x)} = e^{j\frac{\beta x^2}{2f}} , \tag{2.15}$$

where x is the distance from the optic axis and f the focal length of the lens. The spatial rate of phase curvature is then

$$\frac{d^2\phi(x)}{dx^2} = -\frac{\beta}{f} . \tag{2.16}$$

This expression and the space-time analogies already developed can be used to define the focal time f_T of a time-lens as

$$f_T = \frac{\omega_0}{\frac{d^2\phi(t)}{dt^2}} . \tag{2.17}$$

Like a spatial lens, the ideal time-lens will have a quadratic phase versus time. Practical constraints have limited the use of sinusoidal phase versus time, which is the result of driving an electro-optic phase modulator with a microwave synthesizer. When attention is limited to the peaks and valleys of the sinusoid, the phase relation can be expanded in a two term Taylor series

$$\phi(t) = A\cos(\omega_m t) \approx A\left(1 - \frac{\omega_m^2}{2} t^2\right) . \tag{2.18}$$

Using Equation (2.17), the focal time for this sinusoidal time-lens with positive peak phase excursion A driven at angular frequency ω_m is

$$f_T = -\frac{\omega_0}{A\omega_m^2} , \tag{2.19}$$

so that the transfer function of a time-lens is

$$h(t) = e^{-j\phi(t)} = e^{-j\frac{\omega_0 t^2}{2f_T}} . \tag{2.20}$$

Equation (2.19) differs in sign from that given by Kolner[4] because that derivation absorbed the negative sign into the constant A. This shows one advantage of using a sinusoidal time-lens: both positive and negative time-lenses can be obtained by using the either the valley or peak of the sinusoid, respectively. The focal time defined by Equation (2.19) uses the positive phase peak which leads to a negative focal time.

Appropriately, the focal time of a time-lens has units of time. This underscores the utility of the substitution $\tau=\omega_0\beta''z$ leading to Equation (2.13). The focal plane of a spatial lens is located a distance f from that lens. Similarly the focal plane of a time-lens is located a time f_T from the time-lens. If, for example, a temporal optical system for focusing pulses is desired, the focal time is determined using Equation (2.19). This also determines the location of the focal plane so that for β'' corresponding to the particular dispersive medium placed after the time-lens, the length z of the dispersive medium is chosen to satisfy $\omega_0\beta''z=f_T$.

2.2.3 Time-lens resolution

Additional analogies can be drawn between spatial and temporal lenses. One measure of a spatial lens is its f-number, $f^{\#}$, given by the ratio of focal length to lens aperture. The f-number of a diffraction limited spatial optical system determines the spatial resolution. For a sinusoidally driven time-lens, the lens aperture is difficult to define, since there are no hard aperture limits. The effective quadratic portion of the sinusoidal phase was given by Kolner[4] as $t_{aperture}=1/\omega_m$ so that the temporal $f^{\#}$ is

$$f^{\#} = \frac{f_T}{t_{aperture}} = \frac{\omega_0}{A\omega_m} \quad . \tag{2.21}$$

We know from spatial optics[1] that the spatial resolution is approximately $\Delta x \sim f^{\#}\lambda$ so that by applying the space-time analogies, the temporal resolution $\Delta t \sim 2\pi f^{\#}\omega_0$. A more careful analysis of gaussian beams and pulses reveals the full width intensity half maximum time resolution to be

$$\Delta t_{fwhm} = \frac{2.8}{A\omega_m} \quad . \tag{2.22}$$

2.3 Time-lens characteristics

A time-lens is the key component in the experiments described in this thesis. It is a sinusoidally driven, electro-optic phase modulator, so its focal properties are determined by the expressions in Table 2.1. This modulator shown in Figure 2.4 was developed by Asif Godil and is well documented elsewhere[11, 12], so only the key points will be repeated here.

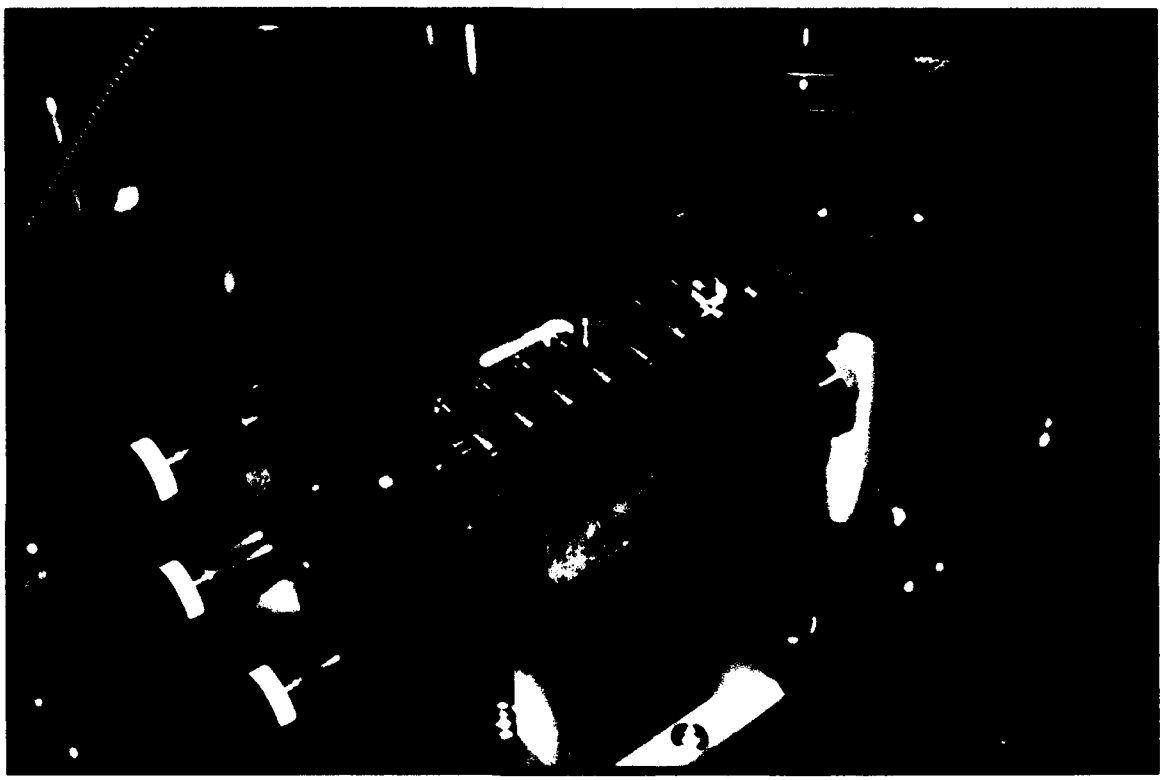

Figure 2.4 Photograph of optical phase modulator showing microwave resonator, coaxial feed line and optical resonator.

It is apparent from Equation (2.22) that to achieve short time resolution, the time-lens should be operated at a high frequency, ω_m, with as much phase modulation, A, as possible. Godil's time-lens operates at 5.2 GHz and produces A=13 radians for 1W of microwave power and 52 radians for 16W of microwave power. The FWHM time resolution given by Equation (2.22) is then 7 ps for 1W and 1.7 ps for 16W of microwave power. The optical frequency ω_0 corresponds to a wavelength of 1.064μm where all experiments in this thesis were performed.

2.3.1 Microwave resonator

To achieve this high performance, it was necessary to engineer a solution to the material shortcomings of lithium niobate, the electro-optic material used in this modulator. The microwave phase velocity is 2.5 times slower than the IR optical phase velocity so efficient, traveling wave phase modulation is not possible. By operating the microwave waveguide close to its microwave cutoff frequency, where the microwave phase velocity increases, the microwaves and optical waves can be phase matched.

Since a sinusoidal phase versus time is adequate for an effective time-lens, the phase modulator can be a narrowband device and resonated to increase the single-pass phase modulation. The end sections of the waveguide are not dielectrically loaded so that at the operating frequency, waveguide modes are cutoff. These cutoff sections of waveguide form microwave mirrors, and the resultant microwave cavity has Q = 1900. The microwave resonator is critically coupled to a 50Ω feed line by a probe inserted into the evanescent fields of the waveguide. The crystal dimensions are 2.25 x 11.5 x 68 mm, and the waveguide inside dimensions are 9.5 x 11.5 x 93 mm (XYZ).

2.3.2 Optical resonator

Even with this high Q resonator, the single pass phase modulation is only $A_{\text{single pass}} \sim 0.6$ rad, and is not enough for a useful time-lens. To increase the phase modulation, the microwave resonator is placed inside an optical resonator formed by a flat and curved mirror. This optical resonator is excited off-axis[13] so that the optical beam zig-zags its way down the crystal, back up, and out the way it entered. The optical multi-passing is shown schematically in Figure 2.5 in that only 6 passes are indicated. The light path in the actual modulator consists of 24 passes through the crystal. The mirror separation is adjusted so that the phase modulation is constructive in each of the 24 passes through the crystal. It is the combination of phase matching, high Q microwave resonator, and multi-pass optics that produce the extremely high performance of the modulator.

2.4 Time-lens improvements

Godil's phase modulator is a very nice work of engineering and was used for all experiments in this thesis. However, part of this thesis was to improve the performance by correcting one of the design flaws.

Figure 2.5 shows schematic cuts through the length and cross section of the modulator photographed in Figure 2.4. The desired electric field pattern in the modulator is included in this figure. Ideally, the electric field will form a standing wave with five maxima in the z-direction and one maximum in the x-direction. Since the optical beam multi-passes through the modulator in the y-direction, the electric field should be uniform in this direction. In the actual modulator, there are two waveguide modes with the same resonant frequencies. These degenerate modes form two hybrid modes with characteristics of both the unwanted TE^{x}_{110} and desired TE_{104} modes[14, 15]. The result is a non-uniform electric field in the y-direction. Since the multi-pass phase modulation is the sum of the

single pass modulation along the height of the crystal, the overall phase modulation will be reduced for a non-uniform field.

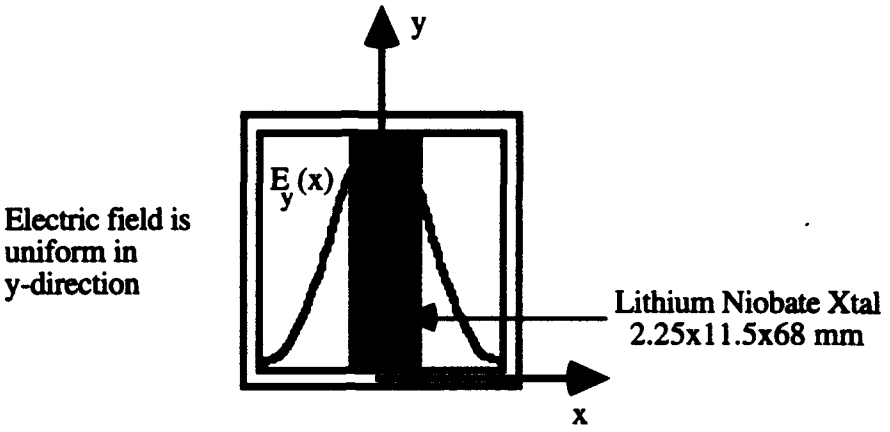

End View of Modulator

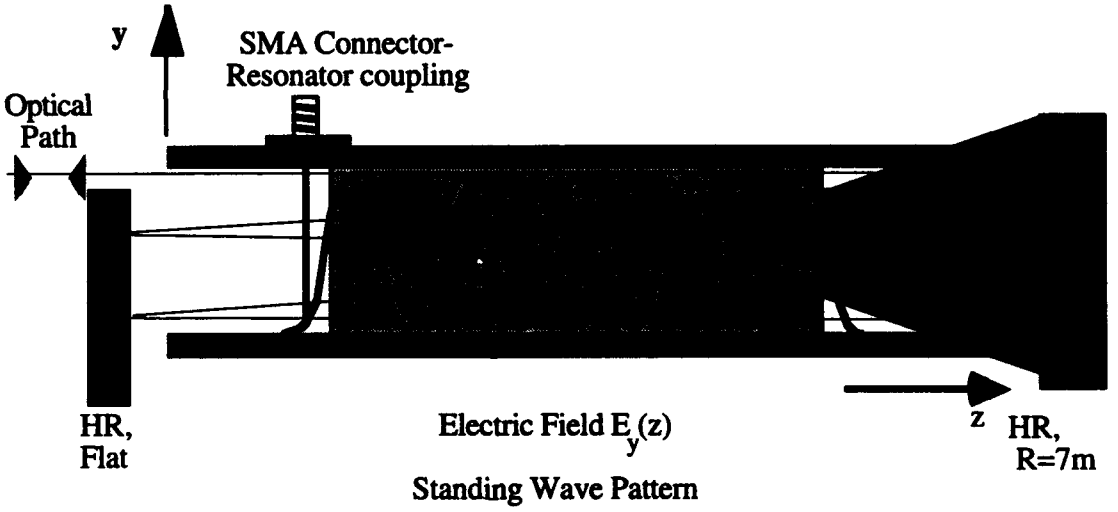

Cross Section Through Modulator

Figure 2.5 Cross-sectional and End views of the phase modulator.

A new modulator was constructed with the hope of achieving a uniform electric field. Two methods were tried. The first recognized the fact that the unwanted TE^x_{110}

mode has an electric field component in the x-z plane. Placing a fin inside the resonator, along the length of the crystal in the x-z plane and midway along the height of the crystal will suppress this mode. The mode suppression is achieved because the electric field boundary conditions forbid a tangential electric field at a perfect conductor. Even though 95% percent of the resonator energy is stored in the crystal, shorting out the unwanted field in the air is sufficient to suppress the undesired mode. Microwave return loss measurements confirm that only one mode is resonant at the appropriate frequency.

Inserting a metallic fin inside the cavity reduces resonator Q due to increased ohmic losses. The second method can achieve the desired results without lowering the Q. This approach is simply to lengthen the crystal to separate the resonance frequencies of the two modes so that they do not hybridize. Microwave return loss measurements and resonator field probing confirm that the modes have been separated enough to solve the problem. The real proof, however is seen by measuring the phase modulation along the height of the crystal as an indication of electric field strength.

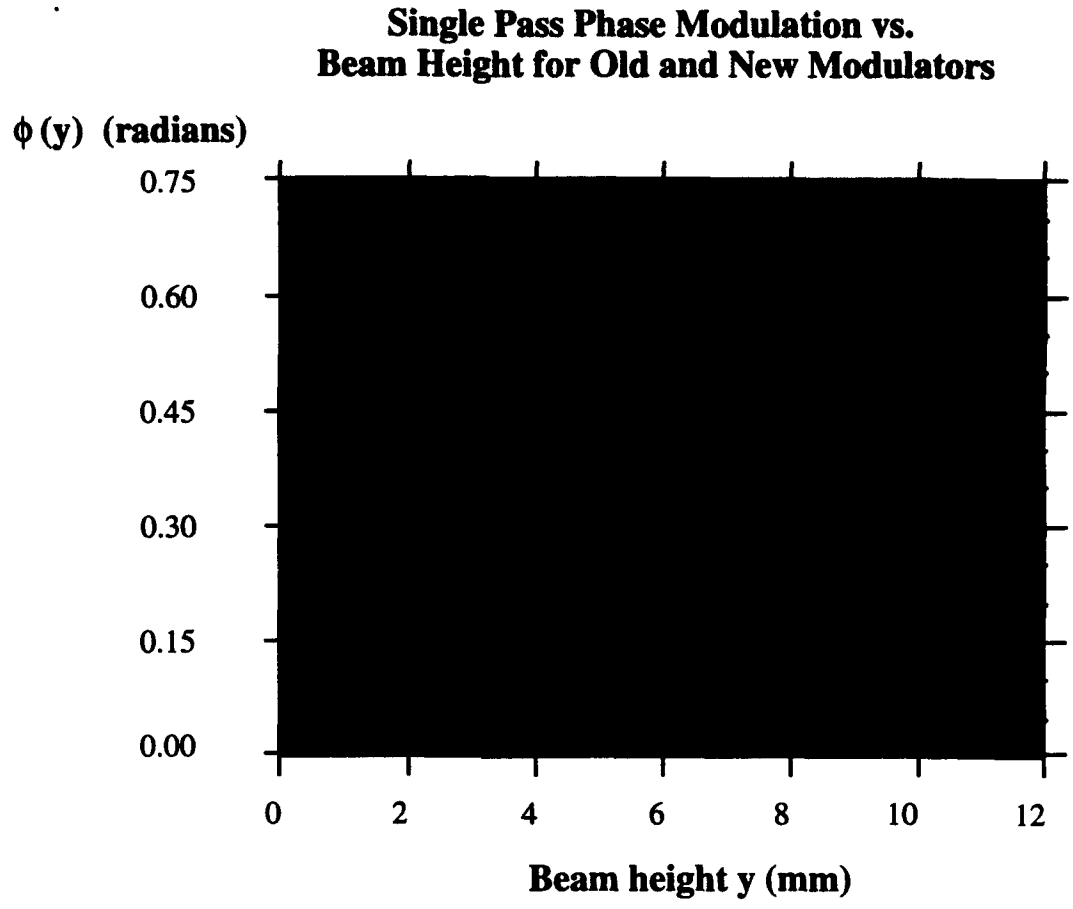

Figure 2.6 Measured single pass phase modulation versus beam height for the old and new resonators

Figure 2.6 shows the measured single pass phase modulation versus beam height in the y-direction for 1 W of microwave drive power. The data for old modulator was taken by Godil[12]. For the old modulator, the single pass phase modulation varies by 3:1 over the height of the crystal. In the new modulator, the phase modulation only varies by 10%. The result of this uniform field in the y-direction is an increase in the multi-pass phase modulation from 13 radians to 17 radians for 1W of microwave drive power. This is increase of 31% is significant because the phase modulation is proportional to the square-root of microwave power and it is difficult to increase the phase modulation by using more microwave power alone.

2.5 Conclusions

The space-time analogy will be useful in understanding the operation of the three temporal optical systems described in the following chapters. It will also prove helpful in understanding many other problems wherever optical pulses are used. The important points to remember are summarized in Table 2.1. Using the analogy, the performance of temporal optical systems can be analyzed almost immediately.

The Godil time-lens is a key element in performing the following experiments. It was a big improvement over previous optical phase modulators but the results in Section 2.4 show that more improvements can be made.

2.6 References

1. Goodman, J. W., Introduction to Fourier Optics (New York: McGraw-Hill, 1968) 287.

2. Akhmanov, S. A., et al., "Nonstationary nonlinear optical effects and ultrashort light pulse formation," IEEE Journal of Quantum Electronics QE-4 (1968): pp. 598-605.

3. Akhmanov, S. A., A. P. Sukhorukov, and A. S. Chirkin, "Nonstationary phenomena and space-time analogy in nonlinear optics," Soviet Physics JETP 28 (1969): pp. 748-757.

4. Kolner, B. H., and M. Nazarathy, "Temporal imaging with a time lens," Optics Letters 14.12 (1989): pp. 630-632.

5. McGillem, C. D., and G. R. Cooper, Continuous and Discrete Signal and System Analysis, Second ed. (New York: Holt, Rinehart and Winston, 1984) pp. 134.

6. Brorson, S. D., and H. A. Haus, "Diffraction gratings and geometrical optics," J. Opt. Soc. Am. B 5.2 (1988): pp. 247-248.

7. Siegman, A. E., Lasers, (Mill Valley, CA: University Science Books, 1986) pp. 337.

8. Harris, S. E., "EE 348 Class Notes," Stanford University, Chapter 4.

9. Treacy, E. B., "Optical Pulse Compression With Diffraction Gratings," IEEE Journal of Quantum Electronics QE-5.9 (1969): pp. 454-458.

10. Dijaili, S. P., A. Dienes, and J. S. Smith, "ABCD Matrices for Dispersive Pulse Propagation," IEEE Journal of Quantum Electronics 26.6 (1990): pp. 1158-1164.

11. Godil, A. A., B. A. Auld, and D. M. Bloom, "Time-lens producing 1.9 psec optical pulses," Applied Physics Letters 62 (1993): pp. 1047-1049.

12. Godil, A. A., "Harmonic Mode-Locking of Diode-Pumped Lasers and Time-Lenses with Picosecond Resolution," Ph. D. Thesis. Stanford University, 1992.

13. Trutna, W. R., and R. L. Byer, "Multiple-pass Raman gain cell," Applied Optics 19 (1980): pp. 301-312.

14. Bonek, E., and G. Magerl, "Propagation characteristics of dielectrially loaded rectangular waveguides for laser beam modulators," AEU 28 (1974): pp. 499-506.

15. Auld, B. A., "Personal Communication," Stanford University, 1992.

Chapter 3 Aspects of Temporal Focusing

Optical pulse compression has always been an important tool for experiments requiring short optical pulses. Experiments including many nonlinear optical investigations, optical material studies and electro-optic sampling use short pulses for their high peak optical power and useful time resolution. Before the invention of mode-locked lasers which can directly generate short optical pulses, pulse compression was the method used to obtain short pulses from a source of longer pulses. Pulse compression is typically performed by 'chirping' a long pulse so that the instantaneous frequency varies linearly across the pulse. The chirped pulse is then passed through a dispersive delay line which has a group delay which varies linearly with frequency so that the different frequency components of the input pulse are delayed in such a way that they exit the delay line at the same time. The result is a compressed pulse with increased peak power. This description of the compression process follows naturally from the techniques used to generated high peak power electrical pulses for chirp radar systems[1].

The compression process can also be described using the analogies developed in Chapter 2 to work backwards from the time to spatial domains. The linear frequency sweep imposed on the pulse is a result of a quadratic phase shift, since phase and instantaneous frequency are related by differentiation[2]. This quadratic phase is the same effect of a time-lens. Because the compressed pulse appears at the output dispersive delay

line, pulse compression has the form of a time-lens followed by a dispersive delay line. It will be shown below that the dispersive delay line must be adjusted to place the output at the back focal plane of the time-lens.

So pulse compression can be thought of as temporally focusing a long pulse into a short one. This analogy is seen in Figure 3.1 which shows a spatial optical system focusing a large beam into a small spot and a temporal optical system compressing a long pulse into a short one. The purpose of this chapter to demonstrate one of the properties of active pulse compression: the ability of an active time-lens to suppress timing jitter fluctuations.

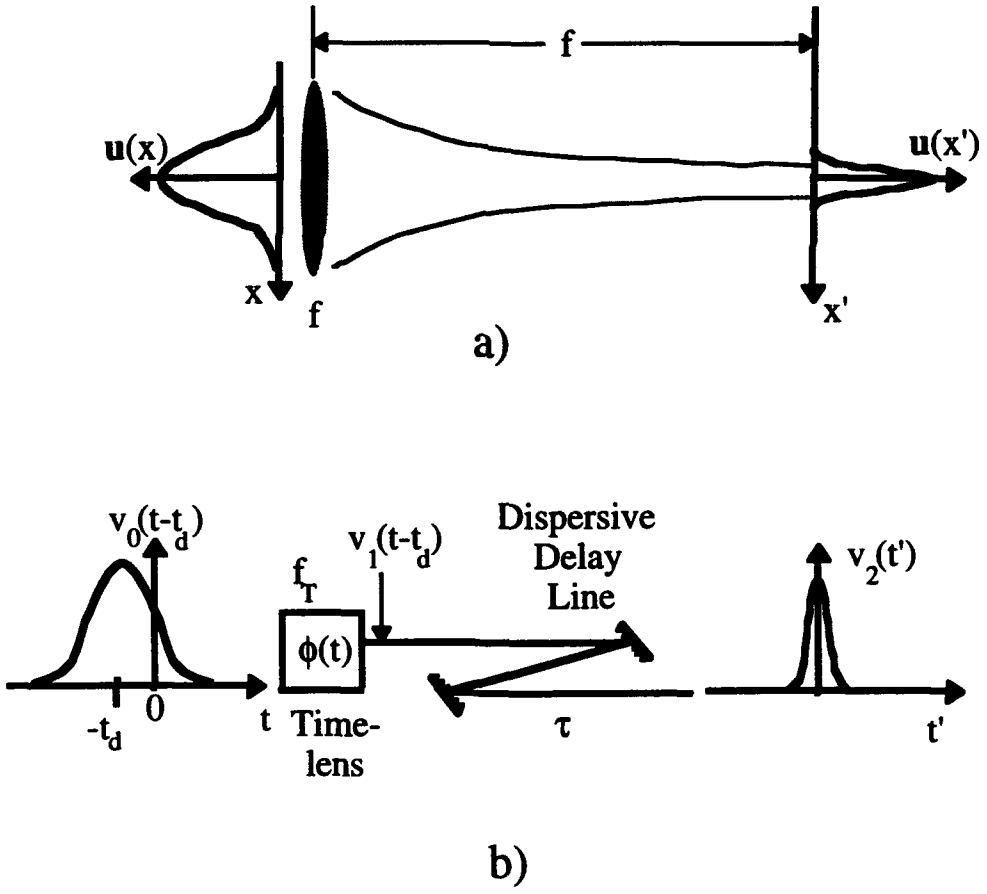

Figure 3.1. Systems for a) spatial and b) temporal focusing.

3.1 Time-lens parameters.

3.1.1 Kerr time-lens focusing.

Temporal focusing has been used for many years to produce[3] optical pulses as short as 6 fs. The time-lens used in most pulse compression experiments is different from the time-lens used in this thesis. The usual time-lens is a passive time-lens which generates a quadratic phase shift using self phase modulation generated via the Kerr effect in an optical fiber[4]. The Kerr effect describes how material index of refraction in many materials changes linearly with E^2 so that the time-dependent integrated phase accumulated by a pulse along the length of a Kerr medium has the same shape as the intensity of the pulse. For many pulses, the shape near the pulse maximum is approximately quadratic so that a Kerr material can act upon a pulse to produce a time-varying quadratic phase shift[5].

This properties of the Kerr time-lens depend on the pulse which generates the lens. The time rate of phase curvature which determines the focal time of the time-lens through Equation (2.17) is a function of the peak intensity and width of the pulse. Conversely, the focal time of the active time-lens described in Chapter 2 is independent of the optical pulse. The focal time is set by adjusting the microwave power and modulator mirror adjustments. This has many experimental advantages in that the lens properties can be easily adjusted electronically.

3.1.2 Active time-lens focusing.

A more important advantage of this active time-lens over the Kerr time-lens is the fact that the phase modulation is independent of the pulse it modulates. In a Kerr lens, the time at which peak phase shift occurs at the same time relative to the pulse generating the phase shift. In an active time-lens, the time at which the peak phase shift occurs depends only on the microwave synthesizer driving the phase modulator and is completely

independent of the optical pulse. In other words, the optic axis of a Kerr lens optical system shifts in time as the pulse shifts. In an active time-lens, the peak phase time or optic axis is fixed by the microwave synthesizer.

This timing relationship between pulse and time-lens is important when considering fluctuations in pulse-to-pulse spacing. In a mode-locked laser, pulses leave the laser cavity at some nominal rate so that there is a definite period between them. Real systems experience fluctuations in the pulse-to-pulse spacing due to cavity perturbations and other noise sources. When compressing pulses with a Kerr lens, the timing fluctuations remain since the lens moves in time with the input pulse. These variations in pulse arrival time can degrade the time resolution in experiments such as electro-optic sampling which use pulses for measurement[6].

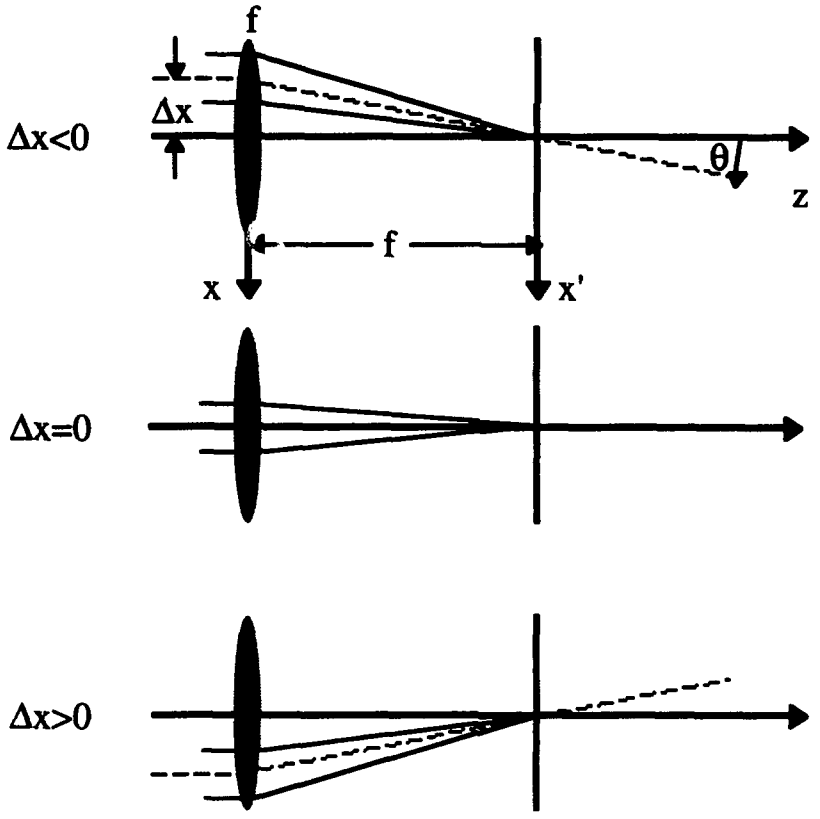

Figure 3.2. Spatial focusing with spatial jitter at the input.

Pulse compression with an active time-lens can reduce timing jitter precisely because the lens is independent of the input pulses. The timing jitter suppression can be seen by analogy to a spatial focusing system shown in Figure 3.2. Here, timing jitter corresponds to uncertainty in locating the beam to be focused with respect to the optic axis. From optics we know that all incident rays parallel to, but displaced from, the optic axis will be focused to the same point in the focal plane. If the whole input beam is displaced a distance Δx from the optic axis of a lens with focal length f, the focused spot will still appear at the same location in the focal plane, but will travel at an angle $\Delta\theta=-\Delta x / f$ with respect to the optic axis.

When focusing with an active time-lens, the temporal optic axis is determined by the microwave synthesizer, so the pulse to be focused is positioned with respect to the optic axis by the time delay $t_d = \Delta t$. This is the time interval between the peak phase time of the time-lens and the pulse peak. Drawing on the space time analogy, the compressed pulse will emerge from the dispersive delay line at the same time it would have given $t_d=0$. Following the analogies formalized in Chapter 2, the compressed pulse will have its center frequency shifted by an amount $\Delta\omega = -\Delta t\, \omega_0 / f_T$. It will be shown below that the total delay through the temporal optical system is, to first order, independent of the arrival time of the input pulses at the time-lens aperture. Because of this, pulse-to-pulse timing jitter in the pulse arrival time will be removed. This means that the system clock is the microwave signal source driving the time-lens. The phase noise of the microwave signal source determines the timing jitter of the system, not the timing jitter of the mode-locked laser. Timing fluctuations at the input of the time-lens are transferred to wavelength fluctuations at the output of the temporal optical system, but for many experiments, reduction of timing jitter is more important that the creation of wavelength jitter.

Pulse compression with an active time-lens has been demonstrated by Kolner[7] and by Godil[8]. The timing jitter reduction properties were suggested by Godil[9] and experimentally demonstrated by Kauffman[10, 11].

The timing jitter suppression property of focusing with an active time-lens will be formally proven below. The jitter suppression property has been shown by equating an electrical phenomena, chirp radar, to spatial focusing. Next a property of the spatial optical system was noted and referred back to the time domain as timing jitter suppression. It is the ability to apply knowledge and intuition of one domain to the other that makes the space-time analogy a powerful tool.

3.2 Analysis of timing jitter suppression by perfect time-lens

3.2.1 Formal Theory

The analysis of temporal focusing relies on the derivations given in Chapter 2. The pulse to be focused is the input field $\mathbf{u}_0(t)$, which is a pulse modulated optical carrier.

$$\mathbf{u}_0(t) = \mathbf{v}_0(t)e^{j\omega_0 t} \quad . \tag{3.1}$$

The pulse envelopes are shown in Figure 3.1b. In this focusing experiment, the time origin of this signal is determined by the zero phase time of the modulator. The phase modulator is the system clock so it is important to refer the input pulse to this temporal reference point. This is accounted for by the delay time t_d. The output $\mathbf{u}_1(t)$ from the time-lens for an input field $\mathbf{u}_0(t\text{-}t_d)$ delayed by time t_d with respect to the time-lens is phase modulated according to Equation (2.20)

$$\mathbf{u}_1(t) = \mathbf{v}_0(t-t_d)e^{j\omega_0(t-t_d)}e^{-j\frac{\omega_0 t^2}{2f_T}} \quad . \tag{3.2}$$

The pulse envelope $v_1(t)$ after the lens is therefore

$$v_1(t) = v_0(t - t_d)e^{-j\omega_0 t_d} e^{-j\frac{\omega_0 t^2}{2f_T}} \quad . \tag{3.3}$$

After the time-lens, the pulse $u_1(t)$ propagates down a dispersive delay line and the signal $u_2(t')$ emerges. Referring to Equation (2.14), $u_2(t')$ is related to the pulse $u_1(t)$ emerging from the time-lens by

$$u_2(t') = e^{j\omega_0(t'-\beta' z)} \sqrt{\frac{-j\omega_0}{2\pi\tau}} e^{j\beta_0 \frac{\tau}{\omega_0 \beta''}} \int dt\, v_1(t) e^{\frac{j\omega_0(t'-t)^2}{2\tau}} \quad . \tag{3.4}$$

Inserting Equation (3.3) in (3.4), and ignoring unimportant constant phase factors, the output pulse becomes

$$u_2(t') = e^{j\omega_0 t'} \sqrt{\frac{-j\omega_0}{2\pi\tau}} \int dt\, v_0(t - t_d) e^{\frac{-j\omega_0 t^2}{2f_T}} e^{\frac{j\omega_0(t'-t)^2}{2\tau}} \quad . \tag{3.5}$$

Which can be rearranged to yield

$$u_2(t') = e^{j\omega_0 t'} \sqrt{\frac{-j\omega_0}{2\pi\tau}} e^{\frac{-j\omega_0 t'^2}{2\tau}} \bullet \int dt\, v_0(t - t_d) e^{\frac{-j\omega_0 t^2}{2}\left(\frac{1}{f_T} - \frac{1}{\tau}\right)} e^{\frac{-j\omega_0 t' t}{\tau}} \quad . \tag{3.6}$$

If the dispersive delay line is adjusted such that the output is at the focal plane of the time lens so that $\tau = f_T$, then the quadratic phase term inside the integral disappears. Using

Equation (2.14), the length L and dispersion parameter β" of the dispersive delay line are set so that

$$f_T = \tau = \omega_0 \beta'' L \tag{3.7}$$

This simplifies Equation (3.6) to

$$u_2(t') = e^{j\omega_0 t'} \sqrt{\frac{-j\omega_0}{2\pi f_T}} e^{\frac{-j\omega_0 t'^2}{2f_T}} \cdot \bullet \int dt\, v_0(t - t_d) e^{\frac{-j\omega_0 t' t}{f_T}} \tag{3.8}$$

Making the substitution $t \rightarrow t - t_d$, Equation (3.8) can be rewritten as

$$u_2(t') = e^{j\omega_0 t'} e^{\frac{-j\omega_0 t' t_d}{f_T}} \sqrt{\frac{-j\omega_0}{2\pi f_T}} e^{\frac{-j\omega_0 t'^2}{2f_T}} \int dt\, v_0(t) e^{\frac{-j\omega_0 t' t}{f_T}} . \tag{3.9}$$

The linear phase term outside the integral, $\exp(-j\omega_0 t' t_d / f_T)$, is equivalent to a constant frequency shift $\Delta\omega$

$$\Delta\omega = -\frac{t_d}{f_T}\omega_0 . \tag{3.10}$$

Equation (3.9) can be written in the form of an envelope modulating an optical carrier not at ω_0, but at the new frequency $\omega_0 + \Delta\omega$

$$u_2(t') = v_2(t') e^{j(\omega_0 + \Delta\omega)t'} . \tag{3.11}$$

Then the new envelope is found to be

$$v_2(t') = \sqrt{\frac{-j\omega_0}{2\pi f_T}} e^{\frac{-j\omega_0 t'^2}{2f_T}} \int dt\, v_0(t) e^{\frac{-j\omega_0 t' t}{f_T}} \quad . \qquad (3.12)$$

The output pulse envelope is of the form of a Fourier transform of the input pulse envelope. Except for unimportant phase factors, the output envelope is independent of the delay of the input pulse with respect to the phase modulator. The input pulse time delay has been converted to a frequency shift in the output pulse carrier given by Equations (3.11) and (3.10).

3.2.2 Qualitative Theory

This mathematical analysis masks the simple explanation of timing jitter suppression in a temporal focusing system. Jitter suppression is achieved by the cooperative action of the time-lens and dispersive delay line. Figure 3.3 shows the characteristics of both components in the temporal focusing system The dispersive delay line following the time-lens is characterized by a group delay $t_0=\beta' L$ at the optical center frequency ω_0, and group delay dispersion $dt/d\omega=\beta'' L$ which describes how the group delay changes with center frequency. The group delay through the dispersive delay line is

$$t(\omega) = t_0 + \beta'' L(\omega - \omega_0) = t_0 + \omega_0 \beta'' L \frac{\Delta\omega}{\omega_0} = t_0 + \tau \frac{\Delta\omega}{\omega_0} \quad . \qquad (3.13)$$

According to Equation (2.18), the time-lens imposes a quadratic phase shift $\phi(t) = \omega_0 t^2 / 2f_T$ on the input pulse. Since instantaneous frequency is the time derivative of the total phase, the quadratic phase shift causes a linear frequency shift. Equation (3.10) shows how this quadratic phase shift causes a time delay dependent phase shift $\Delta\omega(t_d)$. Input pulse time delay shifts the pulse center frequency by an amount

proportional to the time delay. For a negative time-lens where the time origin is at the positive peak of the phase $A\cos\omega_m t$, if the pulse is delayed with respect to the phase modulator, the center frequency is upshifted. Since the system "clock" is determined by the time-lens, the total pulse delay time through the system, t_{out}, is the sum of the input time delay and the group delay through the dispersive delay line.

$$t_{out} = t_d + t(\omega) = t_d + t_0 + \tau\frac{\Delta\omega}{\omega_0} \quad . \tag{3.14}$$

Applying Equation (3.10) to (3.14), the total pulse delay time is

$$t_{out} = t_0 + t_d + \tau\frac{\Delta\omega}{\omega_0} = t_0 + t_d - \frac{\tau}{f_T}t_d \quad , \tag{3.15}$$

so that applying the definition of focal plane given by Equation (3.7), $\tau=f_T$, the total pulse delay time is independent of input delay time: input pulse timing jitter is removed.

The definition of focal plane given by Equation (3.7) means that for a given time delay t_d, the frequency is upshifted by just the correct amount that the group delay through the dispersive delay line decreases by an amount t_d. Therefore, the total propagation time in Equation (3.15) under the constraint of Equation (3.7) is $t_{out}=t_0$, independent of input delay time t_d.

Only active time-lenses like the one used in this thesis have the ability to suppress timing jitter. A Kerr time-lens cannot because the time-lens depends on the pulse itself, so regardless of time delay, the zero phase time of the time-lens occurs at the same time relative to the pulse to be focused.

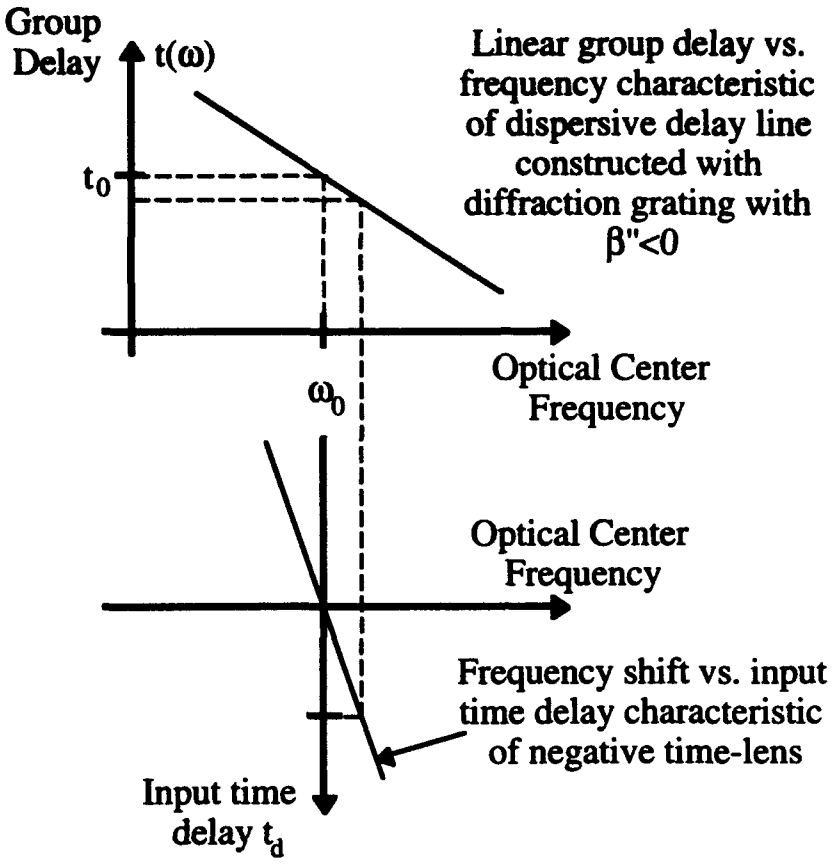

Figure 3.3. Group delay and frequency shift characteristics of temporal focusing components which lead to jitter suppresion with an active time-lens. When the two slopes are equal magnitude, timing jitter is removed.

3.3. Analysis of jitter reduction by imperfect time-lens

The simplified explanation presented at the end of the last section can be extended to analyze temporal focusing with an imperfect time-lens like the one used for these experiments. This time-lens has sinusoidal phase versus time rather than the ideal quadratic phase variation. The focal time definition in Chapter 2 was based on a two term Taylor series expansion of the phase. If the next term in the series is considered, the phase is seen to be

$$\phi(t) = A\cos(\omega_m t) \approx A\left(1 - \frac{(\omega_m t)^2}{2} + \frac{(\omega_m t)^4}{24}\right) . \quad (3.16)$$

The instantaneous frequency shift is

$$\omega(t) - \omega_0 = -\frac{\partial\phi}{\partial t} = A\omega_m^2 t - \frac{A\omega_m^4 t^3}{6} , \quad (3.17)$$

so that the total propagation time t_{out}, given by Equation (3.15), is now a function of the input delay time t_d.

$$t_{out} = t_d + t(\omega) = t_0 - \frac{\omega_m^2}{6} t_d^3 . \quad (3.18)$$

Equation (3.18) shows that non-quadratic phase leads to time-lens aberrations which prevent timing jitter suppression.

3.4 Measured Jitter Suppression

3.4.1 Experimental Setup

The jitter suppression property when focusing with an active time-lens was investigated using the timing-stabilized, mode-locked laser system described by Rodwell[12]. The setup used to perform these experiments is shown in Figure 3.4. The mode-locked laser directly produces 55 ps pulses. A portion of the pulse train is sampled and fed to a photodiode. In normal operation, the phase of this laser output signal is compared to the phase of a reference synthesizer. The error signal is used to drive a voltage controlled phase shifter whose input is the reference synthesizer and whose output is fed to the laser

mode-locker. In normal operation, the phase noise of the mode-locked pulse train is reduced to close to that of the reference synthesizer. The measured 0.25 Hz - 25 kHz timing jitter of this system is 300 fs.

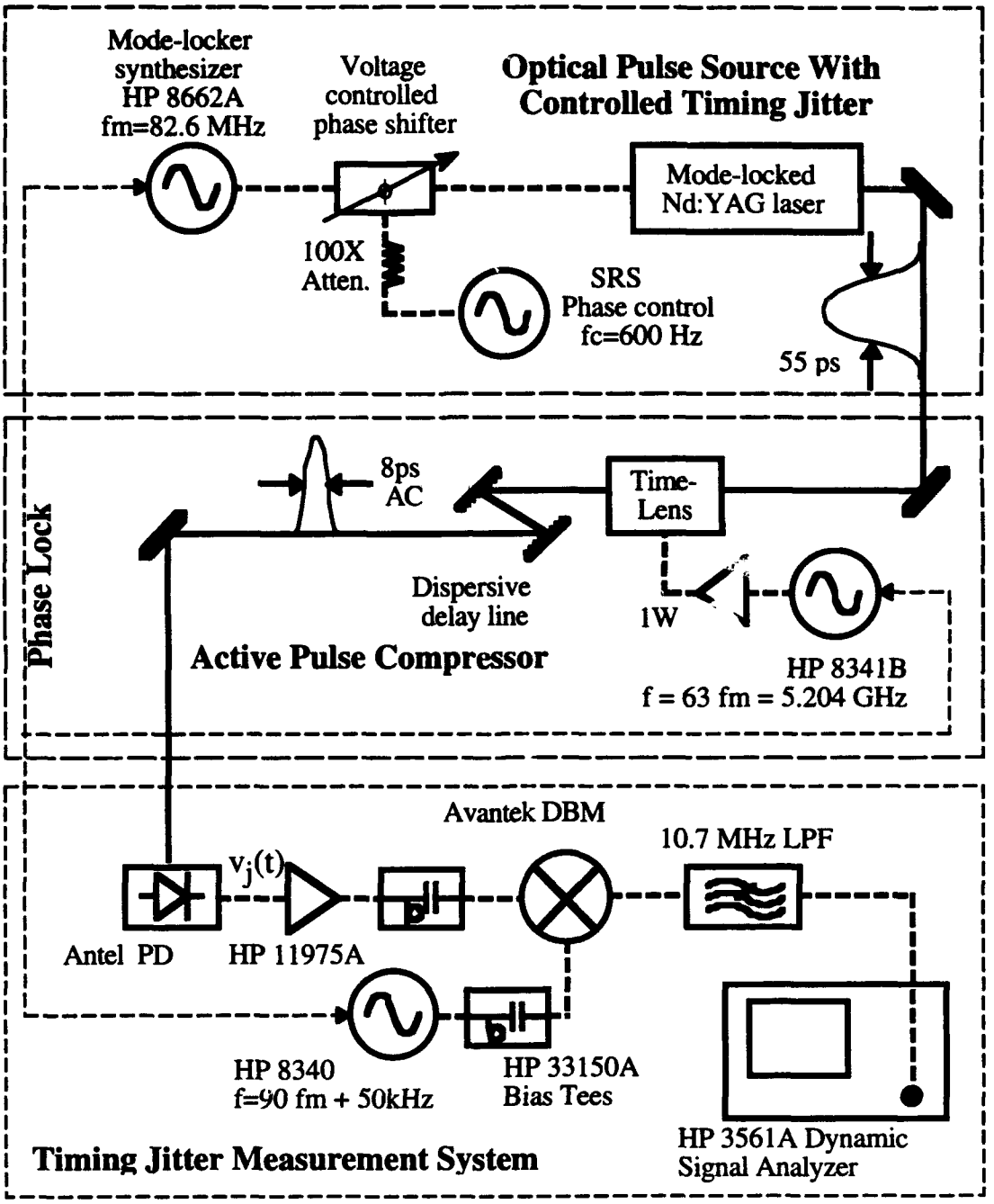

Figure 3.4 Experimental setup used to investigate timing jitter suppression

In these experiments, however, the timing stabilization loop is broken and an external error signal is injected into the voltage controlled phase shifter. By varying the amplitude of this error signal, the timing jitter of the laser pulses can be externally controlled.

The controlled jitter laser pulses are fed into the time-lens driven by a 5.204 GHz, 1W microwave source phase locked to the mode-locker synthesizer. The time-lens has a peak phase modulation of A=12 rad so that the focal time f_T = 138 ns. The dispersive delay line is constructed with a four-pass, 1700 lines / mm diffraction grating. The output pulses are monitored by an autocorrelator and the delay line length is adjusted to produce the shortest pulses with approximately 7 ps FWHM.

To measure laser timing jitter, the laser pulses are monitored with a 10 GHz photodiode and amplified. Rodwell shows that for a pulse train with both amplitude noise and timing jitter, the phase noise power increases with the square of harmonic number. At low harmonics, the amplitude noise dominates, but at high harmonics the phase noise dominates. To isolate the phase noise, the 90th harmonic of the laser repetition rate is mixed down to a 50 kHz center frequency by a third synthesizer, and the noise spectrum is measured with a low frequency, FFT spectrum analyzer.

3.4.2 Experimental Theory

If the signal driving the laser pulse jitter generator is sinusoidal, and amplitude noise is ignored, the photodiode signal $v_j(t)$ varies as

$$v_j(t) = \sqrt{2C}\sin\left(\omega_s t + \theta_0 \sin(\omega_x t)\right) \quad . \tag{3.18}$$

where C is the average carrier power, ω_s is 90th harmonic of the laser repetition frequency of 82.6 MHz, and θ_0 is the peak phase modulation. The peak timing jitter is related to the peak phase modulation by

$$t_{peak} = \frac{\theta_0}{\omega_s} \quad . \tag{3.19}$$

Equation (3.18) can be expanded[13, 14] in terms of Bessel functions

$$v_j(t) = \sqrt{2C}\begin{bmatrix} J_0(\theta_0)\sin\omega_s t + \\ J_1(\theta_0)\sin(\omega_s+\omega_x)t - J_1(\theta_0)\sin(\omega_s-\omega_x)t + \\ J_2(\theta_0)\sin(\omega_s+2\omega_x)t + J_2(\theta_0)\sin(\omega_s-2\omega_x)t \\ +\cdots \end{bmatrix} \quad . \tag{3.20}$$

For small phase modulation θ_0, only the first order sidebands are significant, and the average upper and lower sideband power varies as

$$P_{usb} = P_{lsb} = CJ_1^2(\theta_0) \approx C\frac{\theta_0^2}{4} \quad . \tag{3.21}$$

Measuring the sideband power gives θ_0, and applying Equation (3.19), the RMS timing jitter is

$$t_{RMS} = \frac{T_c}{2\pi}\sqrt{\frac{P_{lsb}+P_{usb}}{P_{carrier}}} \quad . \tag{3.22}$$

T_c is the period of the microwave carrier signal.

3.4.3 Experimental Results

The noise sidebands are measured before temporal focusing for several control voltages. The measurement is also made on the compressed, focused pulses. Figure 3.5 shows the measured phase noise versus frequency offset from carrier for the control voltage peak amplitude of 100 mV. Noise data taken before and after the lens is displayed, and displaced vertically for clarity. The spectrum analyzer resolution bandwidth 38.2 Hz for this measurement. The phase noise consists of a noise floor along with individual noise spikes at offsets corresponding to multiples of the control signal frequency, 600 Hz. The individual harmonic noise spikes are suppressed after focusing as well as much of the close in phase noise.

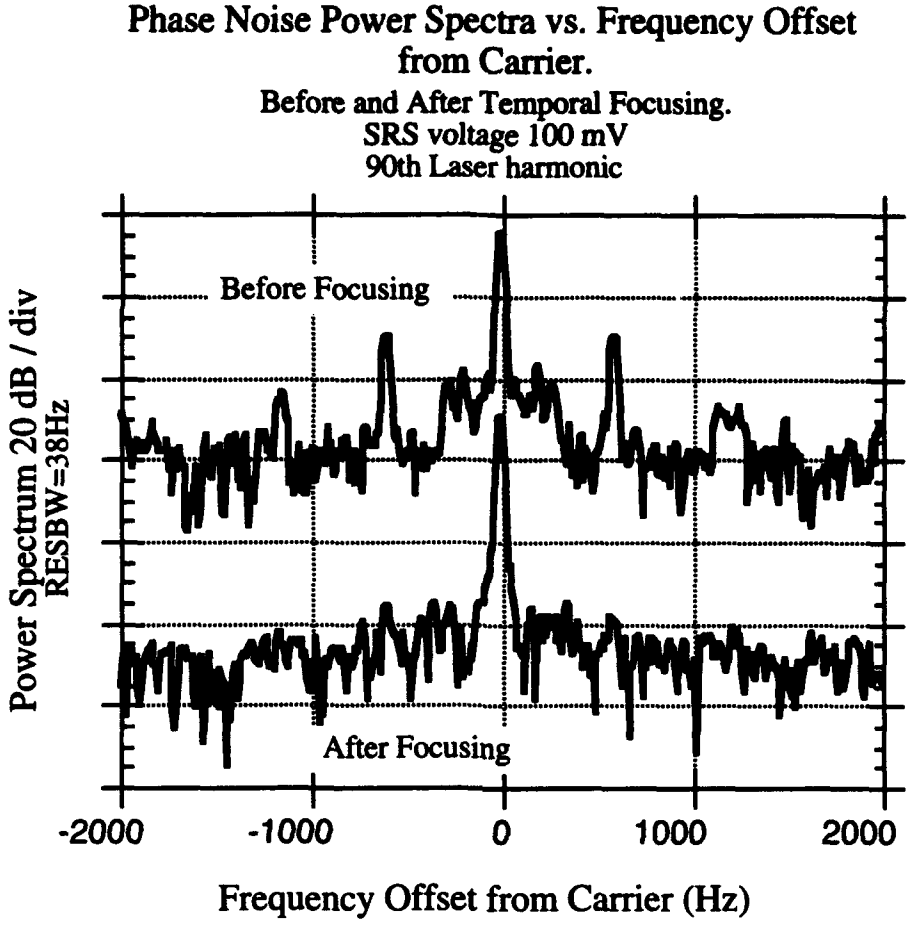

Figure 3.5. Measured noise spectrum around 90th laser harmonic before and after time-lens for control voltage 100 mV.

The noise to carrier at the harmonics of the control signal frequency ratios before and after the time-lens are tabulated below at various values of error voltage amplitudes.

Jitter Control Voltage (SRS) (mV)	Phase Noise Sidebands Offset +600 Hz -600 Hz		Offset +1200 Hz -1200 Hz		Offset +1800 Hz -1800 Hz	
	Before Lens (dBc)	After Lens (dBc)	Before Lens (dBc)	After Lens (dBc)	Before Lens (dBc)	After Lens (dBc)
50	-32.33 -31.78	-49.38 N/A	-43.25 -43.40	N/A	N/A	N/A
100	-25.51 -25.42	-47.27 -48.24	Broad -38.95	-47.27 -48.24	N/A	N/A
200	-19.75 -19.39	-39.75 -39.91	-33.58 -34.36	-52.23 -51.96	N/A	N/A
300	-17.88 -17.86	-36.30 -36.11	-30.52 -31.99	-52.65 -52.47	N/A	N/A
400	-14.09 -13.90	-33.99 -34.17	-28.80 -30.81	-43.22 -44.06	-36.48 -36.82	-49.70 -47.85
500	-12.95 -12.92	-30.23 -30.81	-25.62 -27.57	-37.96 -38.88	-36.18 -36.95	-48.10 -47.80
600	-11.56 -11.47	-28.39 -28.22	-24.07 -23.80	-33.98 -34.64	-34.86 -34.75	-42.23 -43.26

Table 3.1 Measured noise / carrier ratios at 600, 1200, & 1800 Hz offset from carrier

The integrated phase noise from 400 Hz to 2 kHz offset determines the total timing jitter in this frequency range and the output vs. input RMS timing jitter shown in Figure

3.6. The timing jitter is reduced by a factor 5 over the entire input timing jitter range and by a factor of 10 over part of the range.

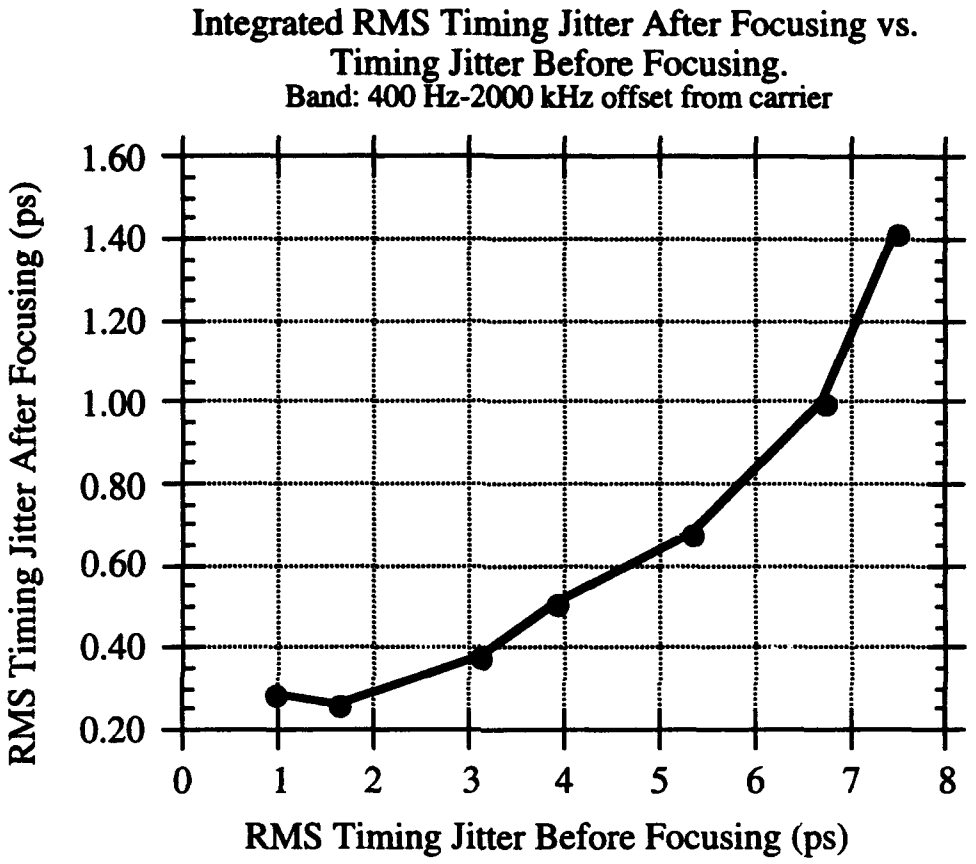

Figure 3.6. Integrated RMS timing jitter after focusing vs. RMS timing jitter before focusing.

The output timing jitter seems to have a noise floor of about 250 fs. This can be attributed to the fact that there are three synthesizers involved in this measurement: one driving the laser mode-locker, one driving the time-lens, and one mixing the 7.435 GHz photodiode signal down to 50 kHz. Rodwell has measured the single-sided phase noise / carrier power of an HP8341B microwave synthesizer to be approximately -89dBc for the band 400 Hz to 2 kHz offset from carrier. The integrated timing jitter corresponding to

this phase noise is 43 fs, so assuming the phase noise is the same for all three synthesizers, the minimum observable timing jitter will be 129 fs.

3.4.4 Analysis of measured data

The analysis of Section 3.3 explains why the laser timing jitter is not completely suppressed, and helps to explain the shape of the curve in Figure 3.6. If the laser jitter before the lens $t_d(t)$ is sinusoidal with RMS jitter t_{d1}, and static delay t_{d0},

$$t_d(t) = t_{d0} + \sqrt{2}t_{d1}\sin(\omega_x t) \quad , \tag{3.23}$$

Equation (3.17) predicts that the pulse group delay varies as

$$\begin{aligned} t_{out}(t) &= \tau_0 - \frac{\omega_m^2}{6}\left(t_{d0} + \sqrt{2}t_{d1}\sin(\omega_x t)\right)^3 \\ &= \tau_0 - \frac{\omega_m^2}{6}\begin{pmatrix} t_{do}^3 + 3\sqrt{2}t_{do}^2 t_{d1}\sin(\omega_x t) + \\ 6t_{d0}t_{d1}^2\sin^2(\omega_x t) + 2\sqrt{2}t_{d1}^3\sin^3(\omega_x t) \end{pmatrix} . \end{aligned} \tag{3.24}$$

This experiment cannot measure static delays, so expanding (3.24) and ignoring static delays, the time varying output group delay with sinusoidal input jitter becomes

$$t_{out}(t) = -\frac{\omega_m^2}{6}\begin{pmatrix} 3\sqrt{2}t_{d1}\left(t_{d0}^2 + t_{d1}^2/2\right)\sin(\omega_x t) - \\ 3t_{d0}t_{d1}^2\cos(2\omega_x t) + \sqrt{2}/2\, t_{d1}^3\sin(3\omega_x t) \end{pmatrix} . \tag{3.25}$$

It is clear from Equation (3.25) and from the presence of a second harmonic term in the data in Table 3.1 that there is a static delay t_{d0} between the input pulses and the time-lens phase. This is not unexpected because the normal operation of the timing-stabilizer loop has been turned off in order to manually inject an error signal. Because the static delay is

unknown, the curve in Figure 3.6 cannot be fit to Equation (3.17). However, the third harmonic term of Equation (3.25) does not depend on the static delay, only on the dynamic, controlled delay t_{d1}. The RMS third harmonic output timing jitter is related to the RMS input jitter by

$$\left(t_{out3}\right)_{RMS} = \frac{\omega_m^2}{12} t_{d1}^3 \quad . \tag{3.26}$$

The magnitude of the measured third harmonic sidebands is greater than what would be expected simply from a Bessel function expansion of the fundamental, 600 Hz harmonic according to Equation (3.20), so it is expected that the third harmonic sideband power should follow Equation (3.26). There are not enough third harmonic data points in Table 3.1 to fit Equation (3.26) to the data, but the equation can be evaluated on a point-by-point basis. The input jitter is only that due to the 600 Hz sideband, not the integrated phase noise. The results are tabulated in Table 3.2. The measured and predicted third order delays agree well.

Jitter Control Voltage (SRS) (mV)	Phase Noise Sidebands		RMS Jitter		
	Before Lens +600 Hz -600 Hz (dBc)	After Lens +1800 Hz -1800 Hz (dBc)	Before Lens t_{do} (ps)	After Lens $(tout3)_{rms}$ Predicted (fs)	Measured (fs)
400	-14.09 -13.90	-49.70 -47.85	1.71	.45	.58
500	-12.95 -12.92	-48.10 -47.80	2.18	.92	.69
600	-11.56 -11.47	-42.23 -43.26	3.02	2.45	2.29

Table 3.2. Comparison of measured 3rd harmonic jitter to predicted.

3.5 Conclusions

Temporal focusing with an active time-lens suppresses timing jitter on input pulses. Unlike a conventional Kerr effect time-lens used in many pulse compression experiments, the active time-lens is decoupled from the pulse so that the temporal optic axis is independent from the input pulse. With a perfect time-lens having quadratic phase versus time, timing jitter is completely canceled. For an imperfect, sinusoidal time-lens, the timing jitter is not completely eliminated because of the lens aberrations.

A simple theory has been developed to explain why complete suppression is not possible with imperfect time-lenses. The active time-lens has been shown to suppress timing jitter by more than a factor of five. The timing jitter before and after focusing has been measured agrees well with theory.

3.6 References

1. Klauder, J. R., et. al., "The theory and design of chirp radars," Bell System Technical Journal (1960): pp. 745-808.

2. Siegman, A. E., Lasers, (Mill Valley, CA: University Science Books, 1986) pp. 332.

3. Fork, R. L., C. H. B. Cruz, P. C. Becker, and C. V. Shank, "Compression of optical pulses to six femtoseconds by using cubic phase compensation," Optics Letters 12 (1987): pp. 483-485.

4. Siegman, A. E., Lasers, (Mill Valley, CA: University Science Books, 1986) pp. 376-386.

5. Tomlinson, W. J., R. H. Stolen, and C. V. Shank, "Compression of optical pulses chirped by self-phase modulation in fibers," J. Opt. Soc. Am. B 1.2 (1984): pp. 139-149.

6. Weingarten, K. J., "Gallium Arsenide Integrated Circuit Testing Using Electrooptic Sampling," Ph. D. Thesis. Stanford University, 1987.

7. Kolner, B. H., "Active pulse compression using an integrated electro-optic phase modulator," Applied Physics Letters 52 (1988): pp. 1122-1124.

8. Godil, A. A., B. A. Auld, and D. M. Bloom, "Time-lens producing 1.9 psec optical pulses," Applied Physics Letters 62 (1993): pp. 1047-1049.

9. Godil, A. A., "Harmonic Mode-Locking of Diode-Pumped Lasers and Time-Lenses with Picosecond Resolution," Ph. D. Thesis. Stanford University, 1992.

10. Kauffman, M. T., A. A. Godil, W. C. Banyai, and D. M. Bloom, "Applications of Time-Lens Optical Systems," Electronics Letters 29 (1993): pp. 268.

11. Kauffman, M. T., A. A. Godil, W. C. Banyai, and D. M. Bloom, "Applications of Time-Lens Optical Systems," in *1993 Ultrafast Electronics & Optoelectronics Topical Meeting* (San Francisco, CA: 1993).

12. Rodwell, M. J. W., D. M. Bloom, and K. J. Weingarten, "Subpicosecond Laser Timing Stabilization," IEEE Journal of Quantum Electronics 24 (1989): pp. 817-827.

13. Robins, W. P., Phase Noise in Signal Sources (Theory and Applications), (London: Peter Peregrinus Ltd., 1982) pp. 10-13.

14. Goldman, S. J., Phase Noise Analysis in Radar Systems Using Personal Computers, (New York: John Wiley & Sons, Inc., 1989) pp. 5-7.

Chapter 4 Temporal Imaging

The temporal optical system in the previous chapter consisted of a time-lens followed by a dispersive element. The space time analogy can be followed to see the effects of adding an additional dispersive element before the time-lens. When the dispersive elements are properly adjusted, the temporal equivalent of spatial imaging is possible. Figure 4.1 shows a spatial imaging and the equivalent temporal imaging system. In such a system, an optical pulse can be magnified or demagnified without distortion. This time magnifier or time microscope can be used with various electrical receivers to perform high resolution pulse shape measurement or for optical signal processing.

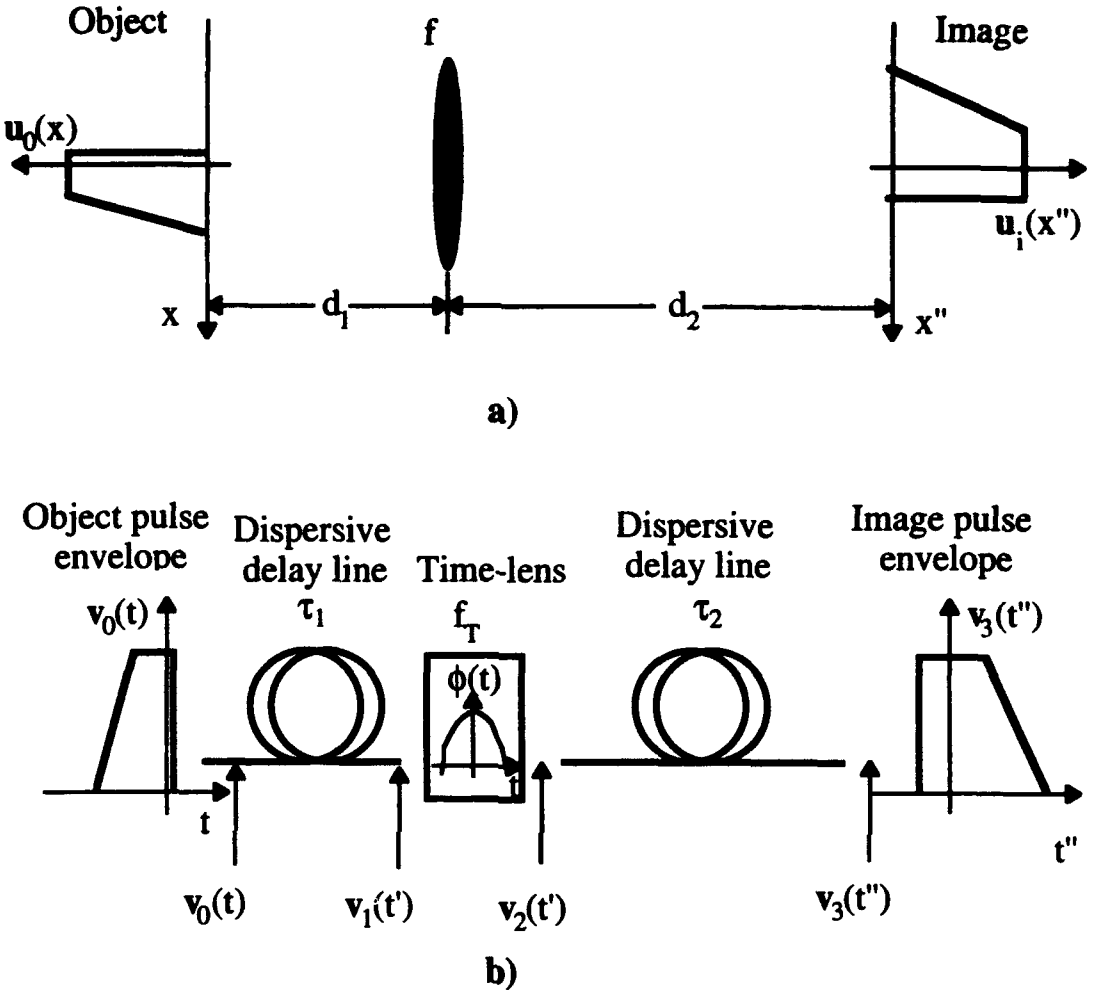

Figure 4.1. a) Spatial and b) Temporal imaging systems

The idea of temporal imaging was actually conceived and demonstrated by Caputi[1] in 1964, but not reported until 1971. This work demonstrated imaging with magnification and time reversal of electrical pulses with carrier frequencies in the 10 MHz range. Caputi refers to the concept of data rate matching. Just as impedance matching is used to obtain maximum power transfer in an electrical, data rate matching is used to maximize the performance of time domain test equipment. The problem of viewing a short pulse with a slow oscilloscope is remedied by data rate matching the short pulse through a time magnifier which slows the pulse down enough to use the slow oscilloscope. Caputi's

analysis and operational explanation does not refer to the similarities of spatial optical systems, but rather the concepts of chirp radar[2].

Temporal imaging of optical pulses was proposed by Kolner[3, 4]. The strength of Kolner's explanation was that it made analogy to spatial imaging. A temporal imaging law analogous to spatial imaging was developed and magnification and time-reversal predicted. Christov[5] discusses a 'time-telescope' which uses a time-lens based on self phase modulation in optical fiber and mixing in a nonlinear optical crystal. The space-time analogies given in this paper are not correct, however, as a dispersive element is called a time-lens and the configuration he describes is analogous to Kolner's time-microscope rather than a telescope.

Using the analogy developed in Chapter 2, this chapter will analyze the operation of and show experimental results from a temporal imaging system[6, 7].

4.1 Analysis of Temporal Imaging System

4.1.1 Quantitative Analysis

Figure 4.1 shows a spatial imaging system and its temporal equivalent. Using the results of Table 2.1, the object pulse envelope $v_0(t)$ will be followed through the temporal imaging system. After propagating through the first dispersive element with dispersion τ_1, the object is distorted into

$$v_1(t') = \sqrt{\frac{\omega_0}{2\pi\tau_1}} e^{j\phi_1} \int dt\, v_0(t) e^{j\frac{(t'-t)^2 \omega_0}{2\tau_1}}, \qquad (4.1)$$

where ϕ_1 is an unimportant constant phase factor and τ_1 is given by Equation 2.14.

The time-lens phase modulates $v_1(t')$ so the output from the lens $v_2(t')$, is

$$v_2(t') = e^{-j\frac{\omega_0 t'^2}{2f_T}} v_1(t') \quad . \tag{4.2}$$

After the second dispersive delay line with dispersive parameter τ_2, the final pulse envelope $v_3(t')$ is

$$\begin{aligned} v_3(t'') &= \sqrt{\frac{\omega_0}{2\pi\tau_1}} e^{j\phi_2} \int dt' \, v_2(t') e^{j\frac{\omega_0 (t''-t')^2}{2\tau_2}} \\ &= \frac{\omega_0}{2\pi\sqrt{\tau_1\tau_2}} e^{j\phi_1} e^{j\phi_2} e^{j\frac{\omega_0 t''^2}{2\tau_2}} \\ &\bullet \int dt \, v_0(t) e^{j\frac{\omega_0 t^2}{2\tau_1}} \int dt' \, e^{j\frac{\omega_0 t'^2}{2}\left(\frac{1}{\tau_1}+\frac{1}{\tau_2}-\frac{1}{f_T}\right)} e^{-j\frac{\omega_0 t'}{\tau_1}\left(t+t''\frac{\tau_1}{\tau_2}\right)} \end{aligned} \quad . \tag{4.3}$$

If the dispersion relationship

$$\frac{1}{\tau_1} + \frac{1}{\tau_2} = \frac{1}{f_T} \tag{4.4}$$

is satisfied, then Equation (4.3) becomes

$$\begin{aligned} v_3(t'') &= \frac{\omega_0}{2\pi\sqrt{\tau_1\tau_2}} e^{j\phi_1} e^{j\phi_2} e^{j\frac{\omega_0 t''^2}{2\tau_2}} \\ &\bullet \int dt \, v_0(t) e^{j\frac{\omega_0 t^2}{2\tau_1}} \int dt' \, e^{-j\frac{\omega_0 t'}{\tau_1}\left(t+t''\frac{\tau_1}{\tau_2}\right)} \end{aligned} \quad . \tag{4.5}$$

The second integral can be performed, yielding

$$v_3(t'') = \sqrt{\frac{\tau_1}{\tau_2}} e^{j\frac{\omega_0 t''^2}{2\tau_2}} \int dt\, v_0(t) e^{j\frac{\omega_0 t^2}{2\tau_1}} \delta\left(t + \frac{\tau_1}{\tau_2} t''\right) , \tag{4.6}$$

which also can be evaluated, with the following result

$$v_3(t'') = \sqrt{\frac{\tau_1}{\tau_2}} e^{j\frac{\omega_0 t''^2}{2f_T}\frac{\tau_1}{\tau_2}} v_0\left(-\frac{\tau_1}{\tau_2} t''\right) . \tag{4.7}$$

Constant phase factors have been ignored.

4.1.2 Law of temporal imaging

The dispersion relationship of Equation (4.4) could also have been derived by applying the space-time analogy to the spatial imaging equation

$$\frac{1}{d_1} + \frac{1}{d_2} = \frac{1}{f} , \tag{4.8}$$

where d_1 and d_2 are the object and image distances, respectively, from the spatial lens with focal length f. Temporal imaging requires that the object and image dispersion times given by Equation (2.14) and the focal time satisfy an analogous relationship.

A magnification factor can be defined for both spatial and temporal imaging systems

$$M = -\frac{d_2}{d_1} = -\frac{\tau_2}{\tau_1} . \tag{4.9}$$

Applying this definition to Equation (4.7), the image pulse intensity $I_3=|v_3|^2$ becomes

$$I_3(t'') = \frac{1}{|M|} I_0\left(\frac{t''}{M}\right) . \qquad (4.10)$$

The output pulse is a magnified image of the input pulse in that the time axis is stretched by a factor of M. In order to conserve energy, the peak power is reduced by the same factor. Note that if the same type of dispersive medium is used before and after the lens, τ_1 and τ_2 will have the same sign, so that the magnification will be negative. The output pulse is then a time-reversed, magnified image of the input. This time reversal is equivalent to image inversion in a spatial optical system. Because this is time reversal in a moving coordinate system, as discussed in Chapter 2, causality is not violated.

4.1.3 Virtual temporal images

It was shown before that the law of temporal imaging given by Equation (4.4) is analogous to the law of spatial imaging given by Equation (4.8). One of the differences, however is that to form a real spatial image, the values d_1 and d_2 in Equation (4.8) must be positive values. In a temporal optical system, however, the dispersive delay line can provide dispersion of either sign so that τ_1 and τ_2 can be positive or negative. According to Equation (4.9), if τ_1 and τ_2 have opposite sign, the magnification will be positive. The closest spatial analogy to this is the formation of a virtual image. The difference in a spatial imaging system is that this image can be viewed directly with a photodiode. Unlike a spatial system, an additional lens is not needed to view a virtual temporal image.

4.1.4 Qualitative operation

Temporal imaging was explained by Caputi in terms of how the input pulse is 'chirped' by the three components in an imaging system. If the object is an impulse, then it will be dispersively broadened by the input delay line and acquire a quadratic phase shift whose time rate of phase curvature is $-\omega_0/\tau_1$. This can be seen from Equation (2.13a)

when $v_0(t)=\delta(t)$. The quadratic phase of the time lens has a time rate of phase curvature ω_0/f_T. Finally, the output dispersion causes a quadratic phase with time rate of phase curvature $-\omega_0/\tau_2$ so that the total phase curvature is $-\omega_0/\tau_1 + -\omega_0/\tau_2 + \omega_0/f_T$. The image of this pulse appears at the output plane where the phase curvature is zero. This location is the same as that given by the law of temporal imaging in Equation (4.4).

4.2 Experimental demonstration of temporal imaging

The experimental setup used to demonstrate temporal imaging is shown in Figure 4.2. It consists of a mode-locked Nd:YAG laser operating at 1.064 μm and fiber-grating pulse compressor producing 1.7 ps pulses at a repetition rate of 82.6 MHz. The time-lens is driven with 1W at the 63rd harmonic of the laser repetition rate. This produces A=13 rad of peak phase shift so that the focal time is f_T=128 ns and the resolution given by Equation 2.22 is 7 ps. Both the input and output dispersion are provided by 4-pass grating dispersive delay lines so that the dispersion times τ_1 and τ_2 are negative[8]. The grating angles and retro-reflector distances are set to provide dispersion times τ_1= 5/4 f_T and τ_2= 5 f_T so that the magnification is M=-4.

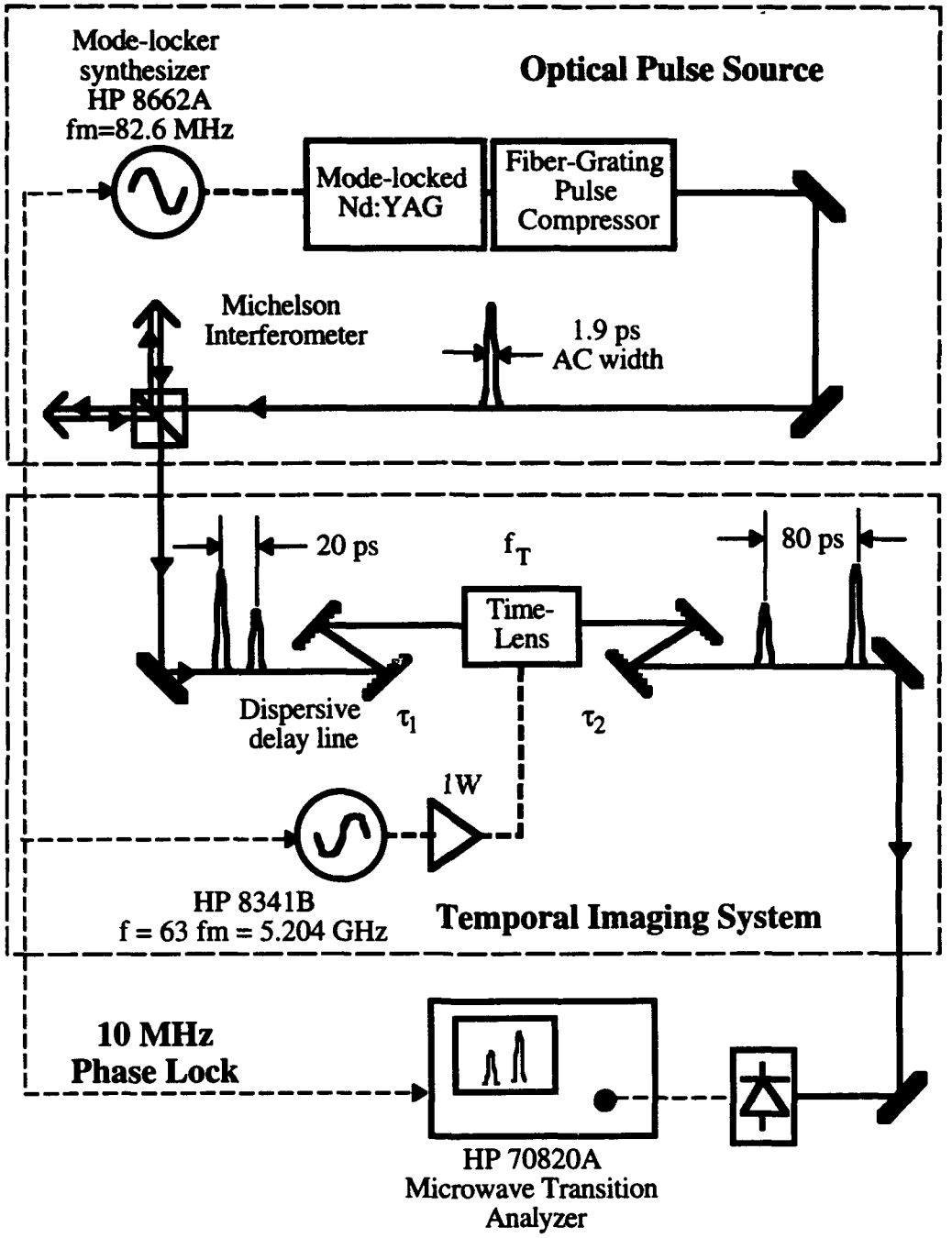

Figure 4.2 Experimental setup used to demonstrate temporal imaging.

Because the input pulses are longer than the resolution of the time-lens, they will overfill the effective aperture and be aberrated. Time reversal and time magnification will still be demonstrated, however. To do this, a sequence of two pulses is created using a

Michelson interferometer whose mirror spacing is adjusted to produce pulse separation of 20 ps. To demonstrate time reversal, the input pulses are coded as a tall pulse followed by a short pulse. An output pulse sequence of short pulse followed by the tall pulse with peak separation of 80 ps is what is expected to demonstrated time reversed magnification.

The input and output pulses are viewed with a fast photodetector (New Focus Inc. model 1404) and sampling oscilloscope (Hewlett-Packard model 70820A) with system time resolution 20 ps. This does not allow the pulse shape to be measured, but the peaks can be distinguished and peak separation measured.

The timing relationship between the pulses and the phase modulator is established by viewing the output pulses on the same photodetector and adjusting a microwave delay line between the phase modulator and its driving synthesizer.

The input and output pulse sequences are shown in Figure 4.3. As expected, the peak-to-peak separation is increased by a factor of 4, and the pulse sequence is reversed.

The decrease in signal-to-noise ratio from the input to output is a result of the many lossy elements in the magnification system and the fact that the high speed photodiode / sampling oscilloscope receiver used to measure the pulses does not have good sensitivity.

To achieve much higher magnification ratios requires very long dispersive delay lines. While delay lines built with diffraction gratings are convenient because of the ability to adjust the dispersion, there are limits to the amount of first order dispersion which can be supplied. The dispersion from diffraction gratings can be easily adjusted but the amount of first order dispersion τ, is limited because of the effects of higher order group delay variations with frequency[9]. Some sort of higher order compensation is required to use diffraction gratings as dispersion sources. Two methods will be discussed in Section 4.3 and in Chapter 5 which eliminate the need for large amounts of dispersion.

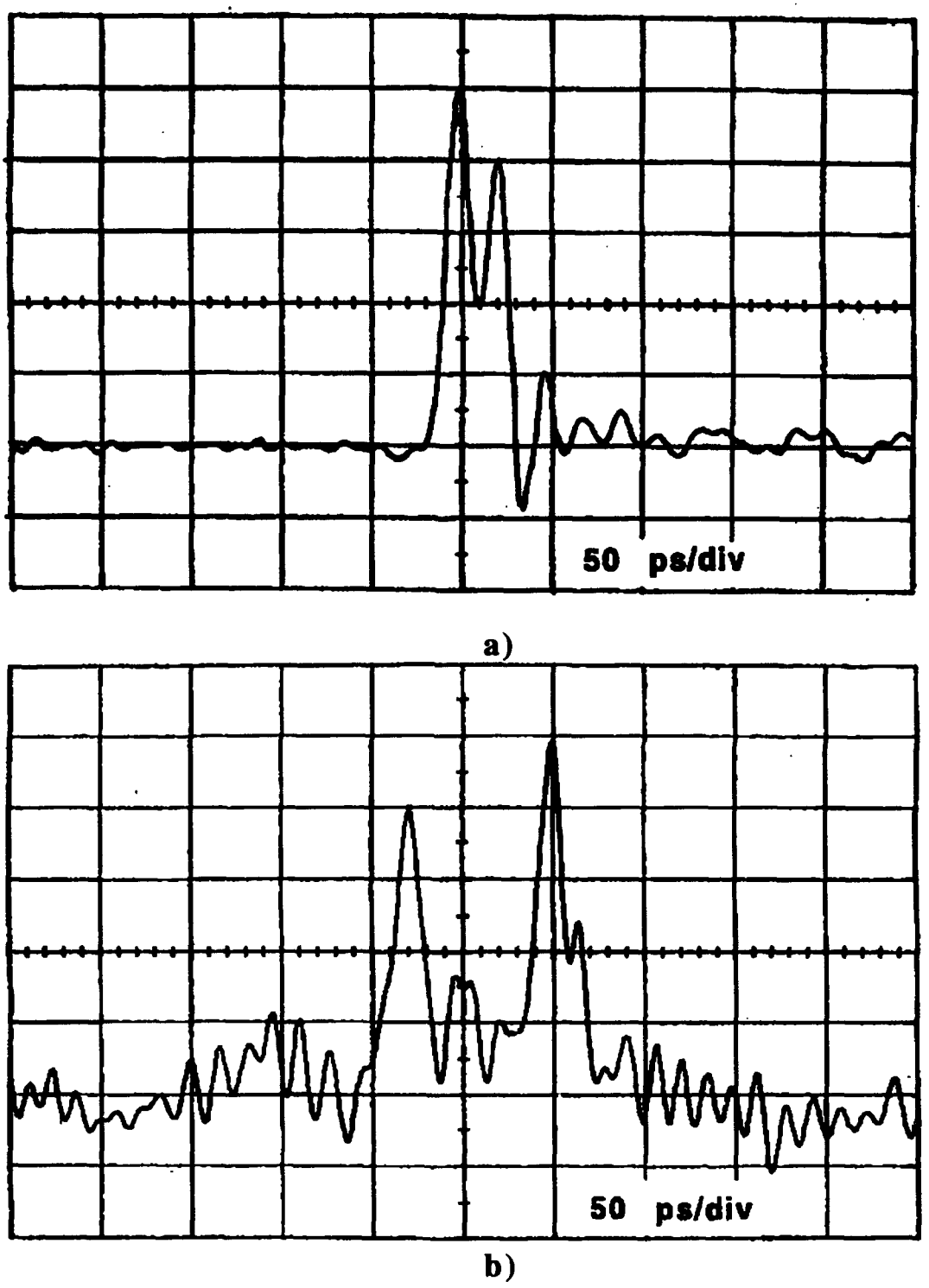

Figure 4.3 Experimental demonstration of temporal imaging showing a) pulse pair at the input to and b) output from temporal imaging system Time reversal is apparent by the change in pulse order from tall-short to short-tall. Magnification is demonstrated by the increased separation between pulse peaks.

4.3 Pulse shape measurement using time-reversal and correlation

Temporal imaging and time reversal are interesting applications of temporal optical systems. The ability to time reverse a pulse sequence should have applications in optical signal processing. One example is the ability to measure pulse shape using an optical correlator. An optical correlator measures the intensity correlation of two signals by delaying one with respect to the other with a scanning optical delay line and passing the two signals through an optical second harmonic generation crystal. The second harmonic signal is the detected signal. For two electric fields $\mathbf{E}_1(t)$ and $\mathbf{E}_2(t)$ present at the input of a background free optical correlator, the output signal $v(\tau)$ is proportional to the time averaged intensity cross correlation

$$v(\tau) \propto \int dt\, I_1(t) I_2(t-\tau) \quad , \tag{4.11}$$

where $I_1(t)=|\mathbf{E}_1(t)|^2$. This can be seen by extending the analysis in Haus[10] to two independent inputs.

4.3.1 Pulse autocorrelation

In its traditional mode of operation as an intensity autocorrelator $\mathbf{E}_1=\mathbf{E}_2$, so that $v(\tau)=\Gamma(\tau)$, the autocorrelation function

$$\Gamma(\tau) = \int dt\, I(t) I(t-\tau) \quad . \tag{4.12}$$

This is shown in Figure 4.4a. Because the phase is lost in this process, there is not enough information in $\Gamma(\tau)$ to uniquely determine $I(t)$. So the major drawback of intensity

autocorrelation is that it only allows estimates of pulse width. A pulse shape I(t) must be assumed based on knowledge of the process producing the pulse and an estimated pulse width backed out from the measured autocorrelation.

4.3.2 Pulse autoconvolution

It is more interesting if one of the inputs to the optical correlator is a time reversed replica of the other. This is achieved by splitting a pulse into two and feeding one of the pulses into a temporal 1:1 imaging system with magnification M=-1. This is shown in Figure 4.4b. The two pulses at input to the optical correlator are $\mathbf{E}_1(t)$ and $\mathbf{E}_2(t)=\mathbf{E}_1(-t)=\mathbf{E}(-t)$. Now $I_2(t-\tau)=I(\tau-t)$ so that $v(\tau)=r(\tau)$ and

$$r(\tau) = \int dt\, I(t)I(\tau - t) = I(t)*I(t) \quad . \tag{4.13}$$

This instrument measures the autoconvolution of the signal. Unlike autocorrelation, autoconvolution is a unique process. The pulse shape can be retrieved from this measurement by noting that the Fourier transform of the measured signal is

$$\mathrm{F}\{r(\tau)\} = \mathbf{R}(\omega) = \mathbf{I}(\omega)\cdot\mathbf{I}(\omega) \quad , \tag{4.14}$$

and $\mathbf{I}(\omega)$ is the intensity spectrum. The time varying input pulse intensity is then given by

$$I(t) = \mathrm{F}^{-1}\left\{\sqrt{\mathbf{R}(\omega)}\right\} \quad . \tag{4.15}$$

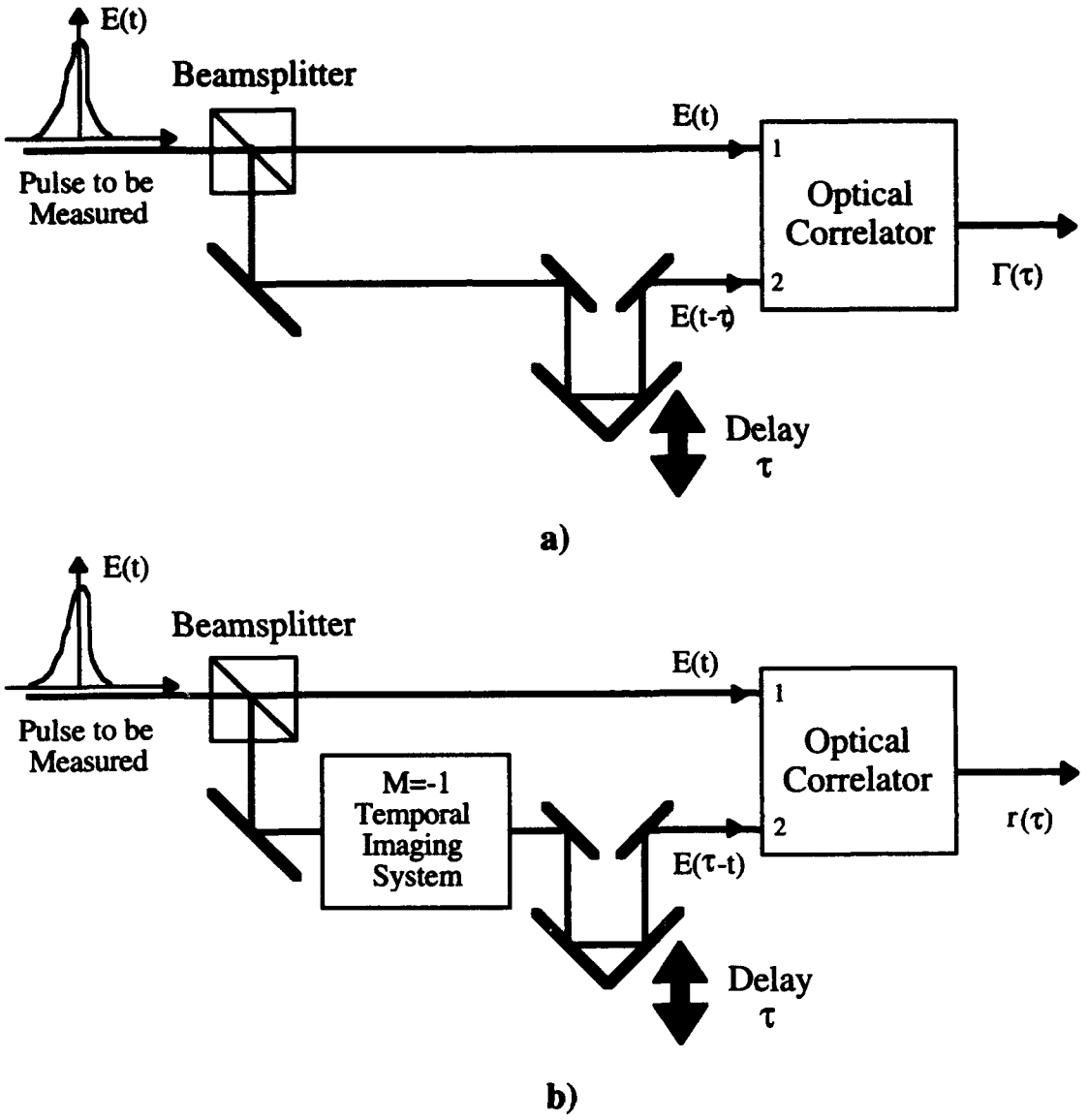

Figure 4.4. Additional pulse measurement techniques. a) Conventional pulse width estimation using autocorrelation. b) Pulse shape measurement using a temporal optical system to perform an autoconvolution.

The advantage of this configuration for pulse shape measurement over the configuration experimentally demonstrated in 4.2 is the simple electrical receiver. A temporal imaging system with moderate magnification still requires a relatively fast electrical receiver following the temporal optical system. This approach, however, uses a

very simple detection scheme involving an optical correlator. A low bandwidth, high sensitivity optical detector such as a photomultiplier tube follows the SHG crystal. The magnification method requires a high speed photodetector. A simple mechanical delay line comprises the timebase of the convolution method rather than a complex sampling oscilloscope.

4.4 Conclusions

This chapter demonstrated the operation of a temporal imaging system which is constructed with dispersive delay lines on either side of a time-lens. The operation is analogous to a spatial imaging system, with an equivalent lens law relating object and image dispersion time to the time-lens focal time. The lateral magnification is also given by the negative ratio of the object and image times as well. In the time domain, negative magnification means that the image is a time reversed replica of the object. An interesting difference between spatial and temporal imaging systems is the ability to view a virtual temporal image. This is possible because of the ability to have dispersion of either sign.

The application of temporal imaging for pulse shape measurement has been demonstrated by magnifying a pulse pair by -4X. To achieve the higher magnifications needed for very high magnifications requires very long dispersive delay lines. This limits the application for direct pulse shape measurement using temporal magnification. Another application for pulse shape measurement using a -1 time magnifier and an optical correlator has been proposed.

While these are interesting applications of temporal imaging systems for pulse shape measurement, Chapter 5 will demonstrate that they are not optimum. Temporal magnification and time reversal, however, should have applications in optical communications and other optics experiments.

4.5 References

1. Caputi, W. J., "Stretch: A Time-Transformation Technique," IEEE Transactions on Aerospace and Electronic Systems AES-7.No. 2 (1971): pp. 269-178.

2. Klauder, J. R., et. al., "The theory and design of chirp radars," Bell System Technical Journal (1960): pp. 745-808.

3. Kolner, B. H., and M. Nazarathy, "Temporal imaging with a time lens," Optics Letters 14.12 (1989): pp. 630-632.

4. Kolner, B. H., and M. Nazarathy, "Temporal imaging with a time-lens: erratum," Optics Letters 15.11 (1990): pp. 655.

5. Christov, I. P., "Theory of a 'time telescope'," Optical and Quantum Electronics 22.5 (1990): pp. 473-80.

6. Kauffman, M. T., A. A. Godil, W. C. Banyai, and D. M. Bloom, "Applications of Time-Lens Optical Systems," in *1993 Ultrafast Electronics & Optoelectronics Topical Meeting* (San Francisco, CA: 1993).

7. Kauffman, M. T., A. A. Godil, W. C. Banyai, and D. M. Bloom, "Applications of Time-Lens Optical Systems," Electronics Letters 29 (1993): pp. 268.

8. Treacy, E. B., "Optical Pulse Compression With Diffraction Gratings," IEEE Journal of Quantum Electronics QE-5.9 (1969): pp. 454-458.

9. Brorson, S. D., and H. A. Haus, "Geometrical limitations in grating pair pulse compression," Applied Optics 27.1 (1988): pp. 23-25.

10. Haus, H. A., Waves and Field in Optoelectronics, (Englewood Cliffs, New Jersey: Prentice Hall, 1984) pp. 356-357.

Chapter 5 Time-to-Frequency Conversion

The experiments in this chapter demonstrate a new method for pulse shape measurement based on a temporal optical system performing time-to-frequency conversion. This pulse shape measurement technique has significant performance advantages over the techniques discussed in Chapter 4 and other measurement methods.

The technique is based on the fact that if two successive Fourier transforms are applied to a signal, the result is a scaled version of the original signal. It will be shown below that with this technique the frequency domain of the output signal has the same shape as the time domain of the input pulse. This transformation is therefore called time-to-frequency conversion. A scale factor relates how the time axis of the original signal is related to the frequency axis of the output signal.

The first of the two Fourier transforms producing this time-to-frequency conversion is supplied by a temporal optical system and the second by an optical spectrum analyzer (OSA) measuring the output of the temporal optical system. The power of the time-to-frequency conversion method is that the output signal is a direct measure of the pulse shape: the OSA trace directly shows pulse intensity. That a temporal optical system can perform a Fourier transform should not be surprising given the knowledge of the Fourier relationships of a spatial optical system[1]. Chapter 3 showed that, except for a quadratic phase factor, the front entrance plane and back focal plane of a time-lens are related by a

Fourier transform. This chapter will show that the front focal plane and back exit plane are also related through a similar Fourier transform. This relationship will be used to perform the pulse shape measurement.

Figure 5.1a) shows the temporal optical system used for time-to-frequency conversion. The equivalent spatial optical system is shown in Figure 5.1c). The pulse spectrum and analogous spatial frequency domains are shown in Figure 5.1b). As will be shown below, the output spectrum has the same shape as the input time domain. This system is a logical extension of the previously demonstrated temporal optical systems which had dispersion only after the lens (focusing) to a system which had dispersion on both sides of the lens (imaging) to a system having dispersion before the lens only.

Like temporal imaging, the time-to-frequency conversion method allows direct measurement of pulse shape but it has substantial advantages over temporal imaging. Time-to-frequency conversion will be shown to be qualitatively similar to streak cameras[2], and can have equivalent sensitivity. Other pulse shape measurement methods using nonlinear optical techniques such as higher order correlation[3], chronocyclic tomography[4] and frequency resolved optical gating[5-7] (FROG) can be used to measure both pulse intensity and phase but are not direct methods. They require substantial, iterative numerical processing of the measured data to arrive at the actual pulse shape. These methods also require the use of optical nonlinearities which impose sensitivity penalties on the measurement.

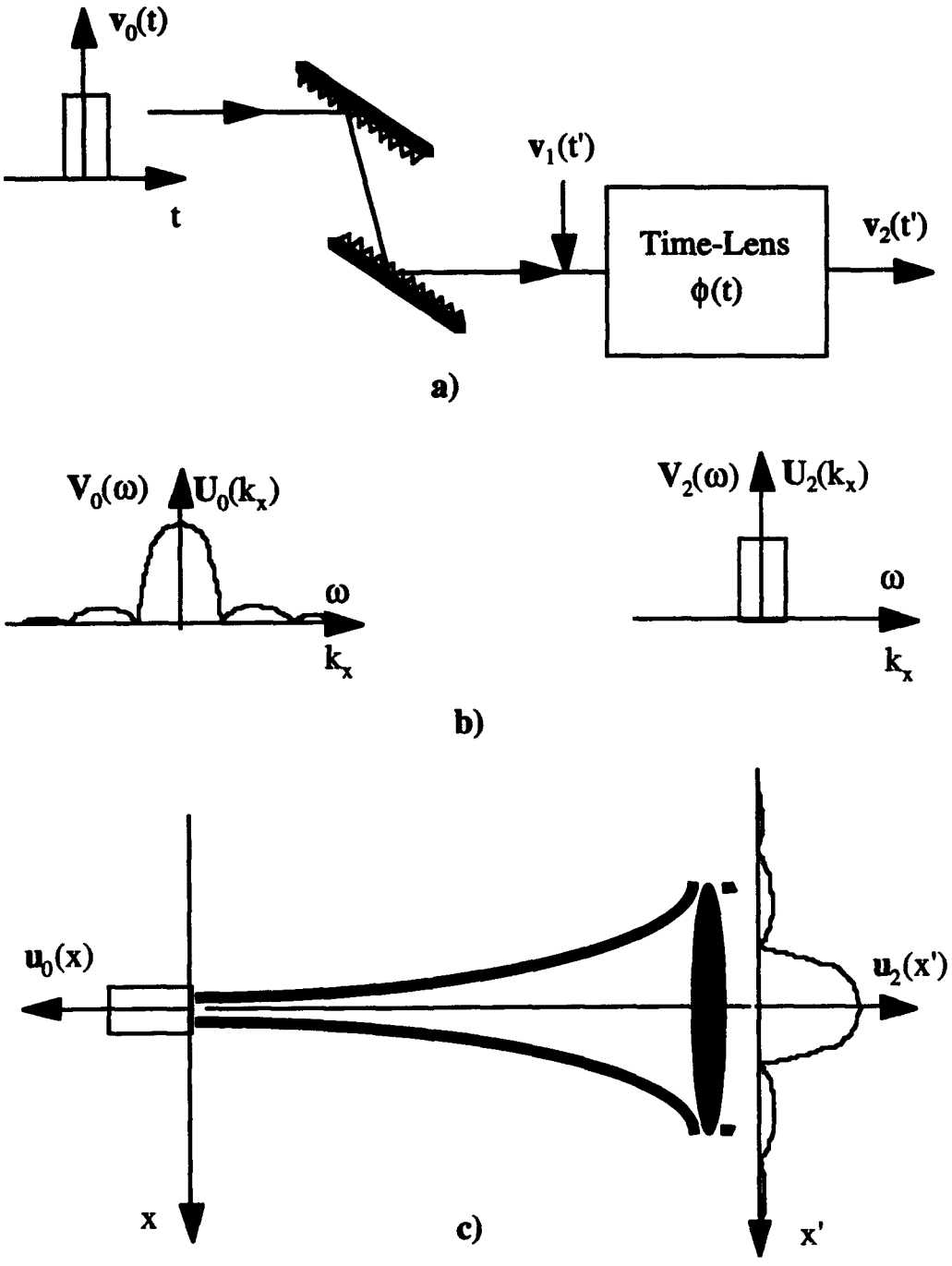

Figure 5.1. a) Temporal optical system for performing time-to-frequency conversion. b) Frequency domain of input and output signals. c) Equivalent spatial optical system.

5.1 Quantitative analysis of time-to-frequency conversion

Referring to Figure 5.1, the pulse envelope modulating the optical carrier $e^{j\omega_0 t}$ at the input to the system is $v_0(t)$. From Equation (2.13) and ignoring the unimportant constant phase factors, after the input dispersive element, this pulse envelope is distorted into

$$v_1(t') = \sqrt{\frac{\omega_0}{2\pi\tau}} \int dt\, v_0(t) e^{j\frac{\omega_0 (t'-t)^2}{2\tau}} , \tag{5.1}$$

where τ quantifies the amount of dispersion according to Equation (2.14), and unimportant constant phase factors have been ignored. This envelope is phase modulated by the time-lens into $v_2(t')$

$$\begin{aligned} v_2(t') &= v_1(t') e^{-j\frac{\omega_0 t'^2}{2f_T}} \\ &= e^{-j\frac{\omega_0 t'^2}{2f_T}} \sqrt{\frac{\omega_0}{2\pi\tau}} \int dt\, v_0(t) e^{j\frac{\omega_0 (t'-t)^2}{2\tau}} \end{aligned} . \tag{5.2}$$

The frequency domain of this envelope $V_2(\omega)$ is seen through a Fourier transform

$$V_2(\omega) = \int dt'\, v_2(t') e^{-j\omega t'} . \tag{5.3}$$

Inserting Equation (5.2) into (5.3) and rearranging, $V_2(\omega)$ is seen to be

$$V_2(\omega)=\sqrt{\frac{\omega_0}{2\pi\tau}}\int dt\, v_0(t)e^{j\frac{\omega_0 t^2}{2\tau}} \cdot \int dt' e^{-j\frac{\omega_0 t'^2}{2}\left(\frac{1}{f_T}-\frac{1}{\tau}\right)}e^{-j\omega_0 t'\left(\frac{t}{\tau}+\frac{\omega}{\omega_0}\right)} \tag{5.4}$$

If the dispersion is adjusted to that $\tau=f_T$, that is, the input plane is located one focal time from the time-lens then the quadratic phase term in the second integral disappears. The second integral then has the form of a delta function[8] so that the output spectrum becomes

$$V_2(\omega)=\sqrt{\frac{2\pi}{\omega_0\tau}}\int dt\, v_0(t)e^{j\frac{\omega_0 t^2}{2\tau}}\delta\left(\frac{t}{\tau}+\frac{\omega}{\omega_0}\right), \tag{5.5}$$

which can be evaluated to yield

$$V_2(\omega)=\sqrt{\frac{2\pi\tau}{\omega_0}}v_0\left(-\frac{\tau\omega}{\omega_0}\right)e^{j\frac{\omega^2\tau}{2\omega_0}}, \tag{5.6}$$

Equation (5.6) shows that the output spectrum has the same shape as the input pulse: the temporal optical system in Figure 5.1 maps the time axis onto a frequency axis. The leading constants in Equation (5.6) simply ensure that the pulse energy is conserved.

The optical spectrum analyzer after the time-lens measures the power spectral density of the output field $|U_2(\omega)|^2=|V_2(\omega-\omega_0)|^2$. The measured data are

$$|U_2(\omega)|^2=\frac{2\pi|\tau|}{\omega_0}\left|v_0\left(-\frac{\tau(\omega-\omega_0)}{\omega_0}\right)\right|^2. \tag{5.7}$$

Applying the dispersion requirement $\tau=f_T$ and noting that

$$\frac{\omega-\omega_0}{\omega_0}=\frac{\Delta\omega}{\omega_0}=-\frac{\Delta\lambda}{\lambda_0}\ , \tag{5.8}$$

the optical spectrum analyzer measures

$$|U_2(\lambda)|^2=\frac{2\pi|f_T|}{\omega_0}\left|v_0\left(\frac{f_T\Delta\lambda}{\lambda_0}\right)\right|^2\ . \tag{5.9}$$

The OSA trace has the same shape as the input intensity with the pulse time axis mapped to the OSA wavelength axis. In this experiment, the dispersion was supplied by a diffraction grating[9] with $\beta''<0$, so that $\tau<0$, and therefore $f_T<0$. According to Equation (5.9) $f_T<0$ means that increasing wavelength difference $\Delta\lambda$ corresponds to decreasing time. Equation (5.9) means that by measuring the power spectral density at wavelength λ is equivalent to measuring the intensity at time

$$t=f_T\frac{\lambda-\lambda_0}{\lambda_0}=f_T\frac{\Delta\lambda}{\lambda_0}\ . \tag{5.10}$$

This is the time to frequency or time-to-wavelength conversion factor.

Equation (5.9) also shows an important property of this measurement method: the intensity of a chirped pulse is measured correctly. Since the power spectral density is measured, the intensity of a chirped pulse will be measured correctly. Ideally, this measurement technique ignores the time-varying phase of the pulse it is measuring.

5.2 Qualitative explanation of system operation

The space-time analogy can intuitively explain the operation of the time-to-frequency converter. Figure 5.2 shows an object placed at the front focal plane of the

spatial lens. This object is the sum of an infinite number of point sources with amplitude and phase corresponding to the particular location in the object. Each point source diffracts as a spherical wave to fill the time-lens aperture, and for a perfect time-lens, is collimated into a plane wave. This collimated plane wave travels at an angle with respect to the optic axis which depends on the source location. The point source on axis travels parallel to the optic axis while points above the axis are collimated into plane waves with positive angles. For small angles, the angle is linearly related to point source position. For this optical system each location on the input plane is mapped uniquely to a plane wave traveling at a specific angle with respect to the optic axis so that by measuring the magnitude of each exiting plane wave, the input object can be measured.

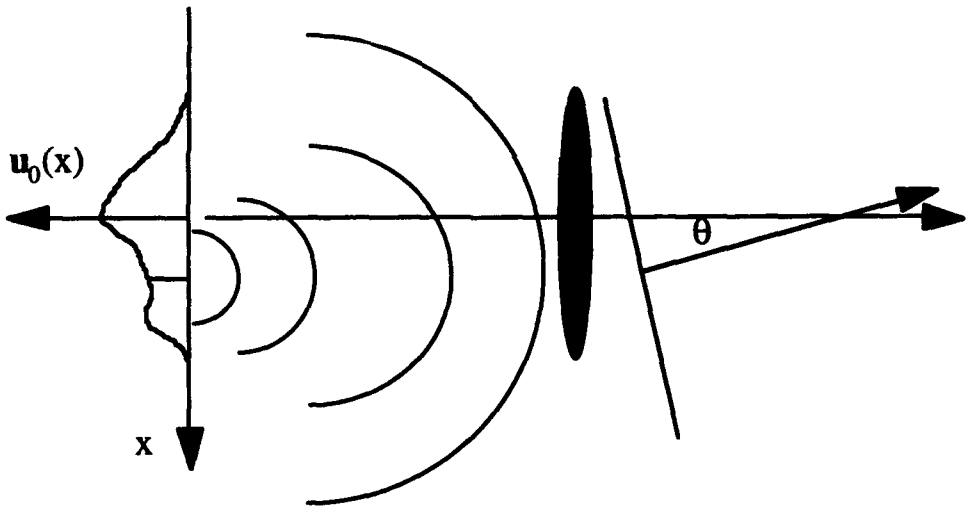

Figure 5.2 Equivalent spatial optical system collimating input beam and showing qualitative operation of the time-to-frequency converter.

Now the space-time analogies can be directly applied. Point sources in space are analogous to delta functions in time so that the object pulse is represented by a number of weighted delta functions. These delta functions have infinite frequency content so that they are dispersively broadened by the input dispersive delay line from impulses to completely fill the aperture of the time-lens. The quadratic phase front they acquire because of the

dispersion is exactly canceled by the quadratic phase modulation from the time-lens and the original high frequency content signal is transformed into a single frequency. Since the frequency shift properties of the time-lens depend on when the impulse arrives as shown in Chapter 3, the output frequency is linearly related to source time. Each point of time of the input pulse is uniquely mapped to a single frequency at the output of the time-lens. This frequency is linearly related to the input time so that the input pulse is determined by measuring the output spectrum.

This analogy can be used to find the resolution of the system. Since the time-lens has a finite time aperture, it cannot map a single point into a single output frequency but rather a finite pulse width is mapped into a finite bunch of output frequencies. The time-resolution of the system is the pulse of a given width, which when placed at the front focal plane of the time-lens, expands to just fill the quadratic portion of the time-lens aperture. This is the same resolution that was shown in Chapter 2 so that the time resolution of the time-to-frequency conversion method is

$$\Delta t_{fwhm} = \frac{2.8}{A\omega_m} \quad . \tag{5.11}$$

The analysis shows that this temporal optical system is not a linear operation since the frequency content of the original signal is not preserved. When transforming the input pulse, frequencies are destroyed and the energy at a particular input frequency is shifted to another frequency. This is not the characteristic of a linear system. However, this system is said to be bilinear since the amplitude and phase of each output frequency component is linearly related to the amplitude and phase of the original impulse.

5.3 Experimental demonstration of time-to-frequency conversion

The experimental setup used to perform the pulse shape measurement is shown in Figure 5.3. The time-lens in these experiments is driven with a custom designed and hand-constructed, limited edition 16W microwave amplifier. The peak phase modulation with this amount of microwave power ranges from 48 to 52 radians, depending on minor adjustments to the modulator. For each experiment, the peak phase modulation is measured so that the time-to-frequency conversion factor in Equation (5.10) can be determined. The increased phase modulation shortens the focal time and increases the resolution given by Equation (2.22) to 1.7 ps.

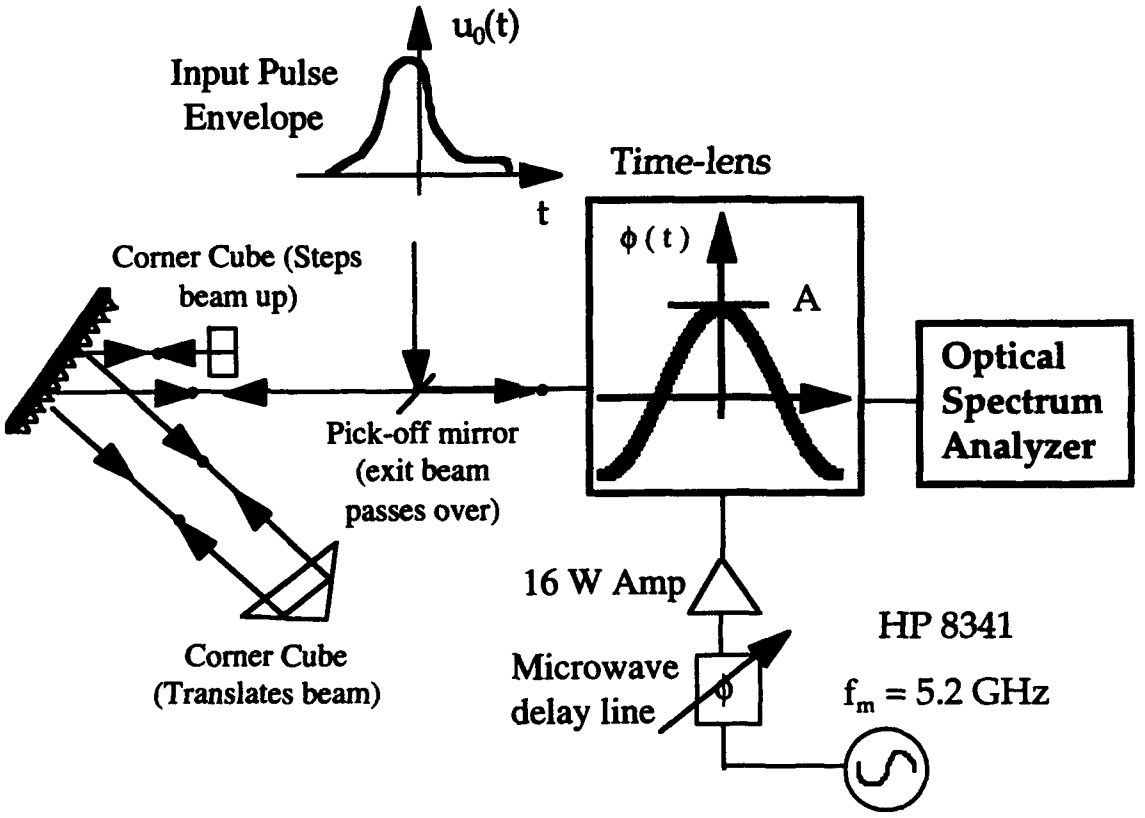

Figure 5.3 Experimental setup for performing time-to-frequency conversion.

Godil[10] describes how the increased microwave power affects the optical multipassing described in Chapter 2 due to thermal lensing in the lithium niobate. The effects of a 1W thermal lens was included in the original time-lens design. To accommodate the stronger thermal lens effects caused by the increased microwave power in these experiments, the synthesizer driving the time-lens was pulse modulated at 55 kHz rate with a 7.7% duty cycle to keep the average power close to 1W. This way, the thermal effects will be the same as when driving the time-lens with 1W of power and the same optical multipassing scheme can be used. Since the microwave resonator has a Q=1900, the resonator bandwidth is 2.7 MHz and can easily respond to microwave drive power changes at the 55 kHz rate.

Pulse modulating the time-lens drive power means that the time-lens is performing a time-to-frequency conversion only when the microwave power is on. Light travels through the system continuously, however, so that most of the pulses are not properly encoded. To solve this problem, an acousto-optic modulator (AOM) follows the time-lens. The output is taken from the first order diffracted beam which contains about 20% of the total power. The AOM driver is also pulse modulated synchronous to the synthesizer with a 5% duty cycle so that the light is blocked from reaching the OSA until the microwave power activates the time-lens. The first order diffracted beam is taken from AOM output because good on/off extinction ratio is achieved. In this configuration with pulse modulation, only about 1% of the average optical power is transmitted through the AOM. A highly sensitive optical spectrum analyzer can still measure this attenuated signal. This is proof of the sensitivity of this approach.

The dispersive delay line was constructed with a diffraction grating in a four-pass configuration. This is shown in Figure 5.3. The grating angle was chosen to minimize the effects of second order dispersion[11].

A microwave phase shifter placed between the time-lens synthesizer and power amplifier is used to select the correct portion of the sinusoidal phase modulator. As shown

in Chapter 3, if the pulse is not synchronized to pass through the peak sinusoidal phase shift, the pulse is either frequency upshifted or downshifted depending on whether the pulse is late or early, respectively. By monitoring the center wavelength of the output pulse on the OSA, the correct phase relationship between the time-lens and pulse train can be established. First, the microwave delay line in Figure 5.3 is set so that the pulse is frequency upshifted (wavelength downshifted). Then the microwave delay is increased until the center frequency returns to its nominal value. At this point, the phase relationship is set correctly and the input pulse is traveling through the positive phase peak.

To demonstrate the time-to frequency conversion, a fiber-grating pulse compressor[12] was built to transform the 55 ps pulses from the laser into 12 ps pulses. These pulses are passed through the input dispersive delay line and into the time-lens. The output spectrum of this pulse train is shown in Figure 5.4a with the wavelength axis converted to time using the relation -30.3ps/nm. As noted in 5.1, this time-to-frequency conversion factor is negative; increasing wavelength corresponds to decreasing time. These results show a pulse with a FWHM of 11.8 ps and an asymmetric trailing tail. The autocorrelation of the input pulse was measured with an Inrad model 5-14B autocorrelator. Figure 5.4b compares this measured autocorrelation to the autocorrelation computed from the measured pulse intensity. The directly measured and computed autocorrelations agree well, and the computed autocorrelation points out experimental error in the measured data which is not symmetric as it must be by definition. It is important to note from this figure that this technique measures pulse shape and therefore reveals more information than the traditional autocorrelation which cannot show asymmetric features of a pulse. The direct measurement ability of this technique is revealed in the fact that the trace in Figure 5.4a is taken directly from the OSA, and only the abscissa must be scaled from wavelength to time. Unlike indirect techniques like FROG, no other calculations are necessary.

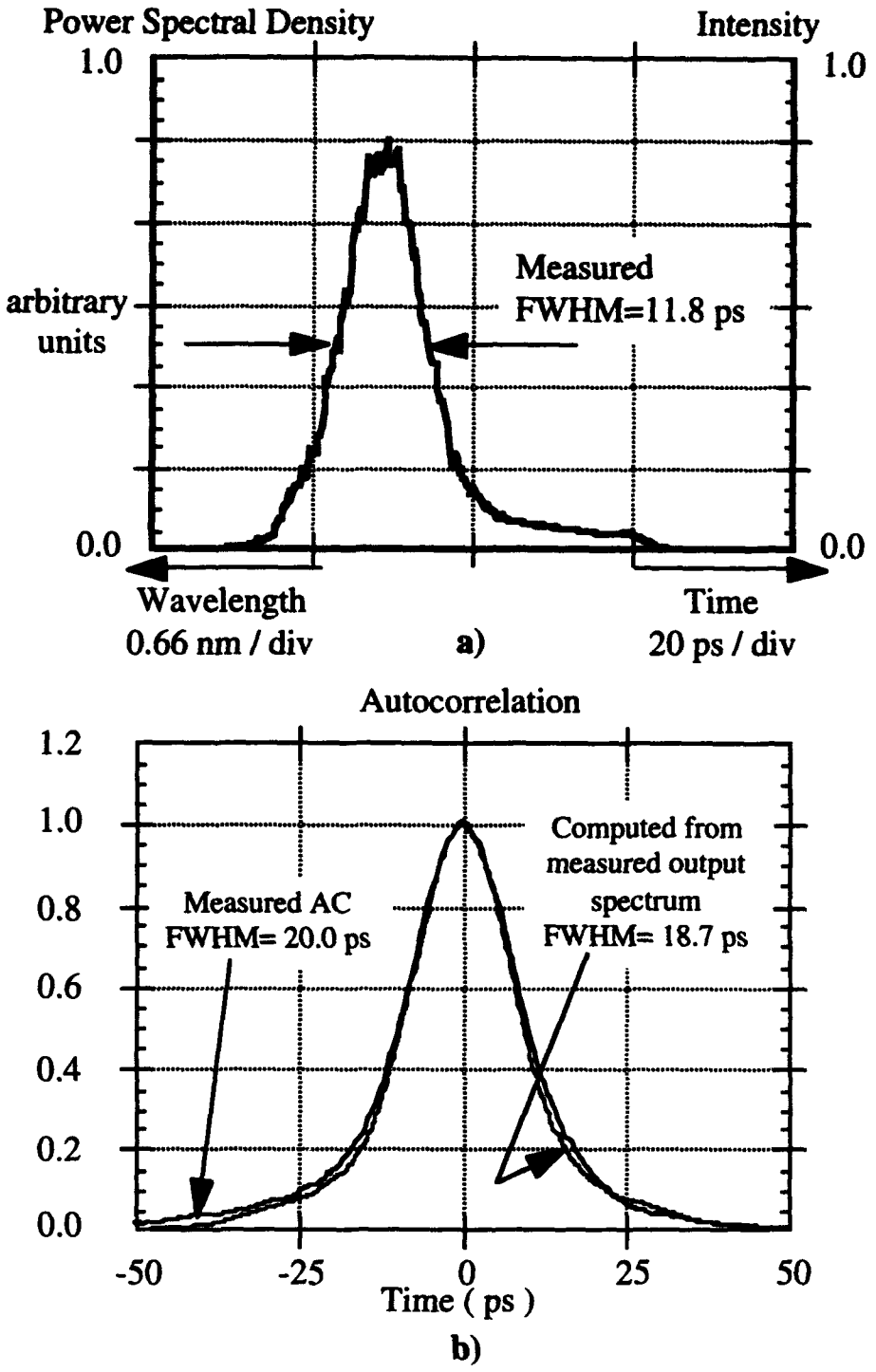

Figure 5.4 Example measurement showing operation of the time-to-frequency converter. a) shows the measured output spectrum and equivalently the input pulse intensity with the wavelength axis scaled to time. b) compares the measured autocorrelation of the input pulse to the computed autocorrelation of intensity measured in a).

5.4 Time-to-frequency limits of operation

The important operational limitations in a practical system are time-resolution, temporal field of view, and sensitivity. These limitations to the time-to-frequency conversion method arise mainly from the use of a non-ideal time-lens. As discussed in Chapter 2, the sinusoidal time-lens limits the time resolution and temporal field of view because of the limited time aperture over which the ideal quadratic phase versus time is approximated. The time aperture and peak phase modulation determine the resolution of this time-lens to be 1.7 ps according to Equation (2.22). The definition of a resolution limited pulse is one that expands through dispersion to fill the quadratic region of the sinusoidal time-lens. Pulses shorter than the resolution limit will dispersively expand to overfill the quadratic region, and the non-quadratic phase will introduce aberrations. Another situation which results in overfilling the time-lens effective aperture is when the input pulse is so long that even before dispersively broadening, it is longer than the time aperture. This long pulse limit determines the temporal field of view of the time-lens, much as a spatial lens in a microscope has a limited spatial field of view. Both limits are shown schematically in Figure 5.5.

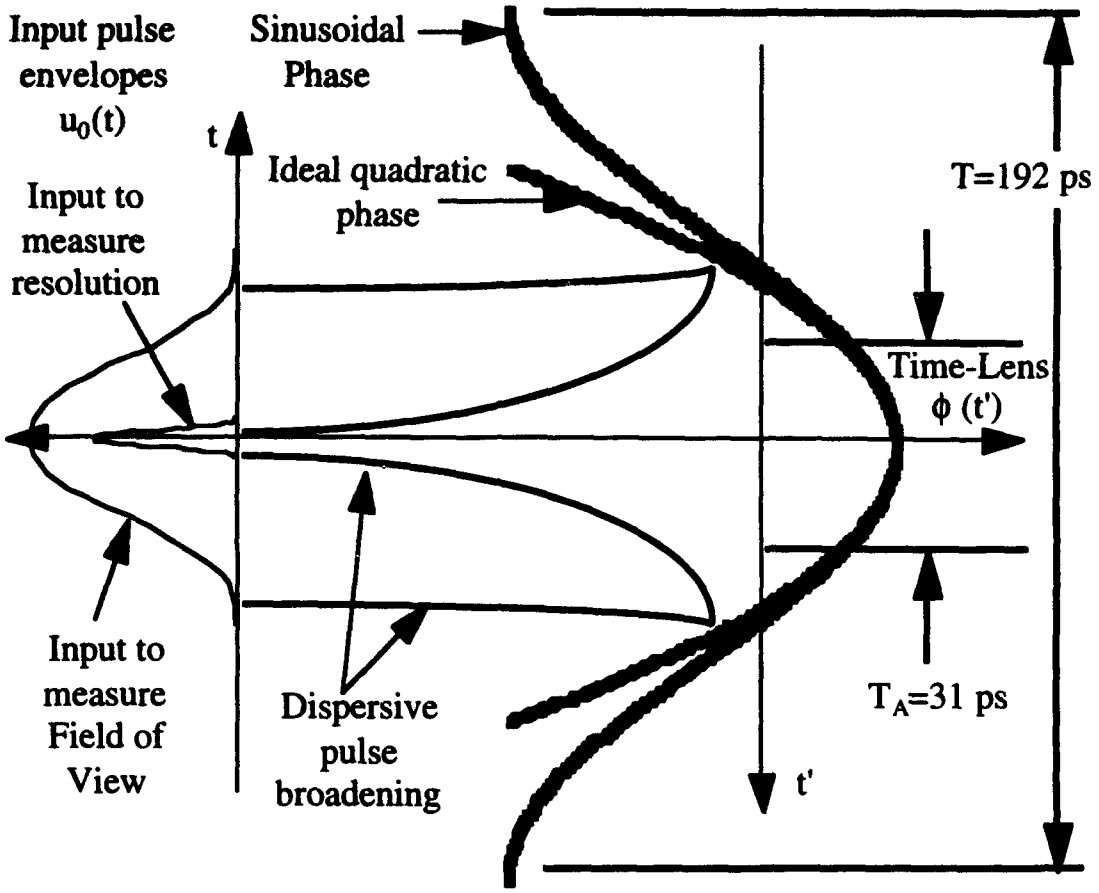

Figure 5.5 Schematic demonstration of time-lens time resolution and field of view limits.

5.4.1 Resolution limit

The resolution limit is demonstrated experimentally by using the system to measure the pulse train whose autocorrelation is shown in Figure 5.6a. These pulses are formed with the fiber-grating pulse compressor described by Weingarten[13]. The autocorrelation FWHM is 1.9 ps so that assuming a hyperbolic secant pulse, the actual pulse width is 1.2 ps[14]. The pulse spectrum is shown in Figure 5.6b. The sharp drop-off on the high wavelength edge is due to knife edge filtering in the fiber grating pulse compressor. This pulse is shorter than the theoretical resolution of the measurement system, and so provides

a method to determine the resolution similar to the way an electrical impulse is used to determine the response of an electrical network. The output pulse spectrum is shown in Figure 5.6c with the wavelength axis scaled to time. The measured pulse width is 3.0 ps which is greater than expected. In this measurement, the pulse width is limited by the 0.08 nm resolution of the optical spectrum analyzer, which corresponds to a time resolution of 2.7 ps. This result shows that the temporal optical system resolution is less than 3 ps. In these experiments, the optical spectrum analyzer limits the system resolution as much as the time-lens. Because the time-lens and OSA resolution are similar, however, there is not much improvement to be gained by using a higher resolution OSA.

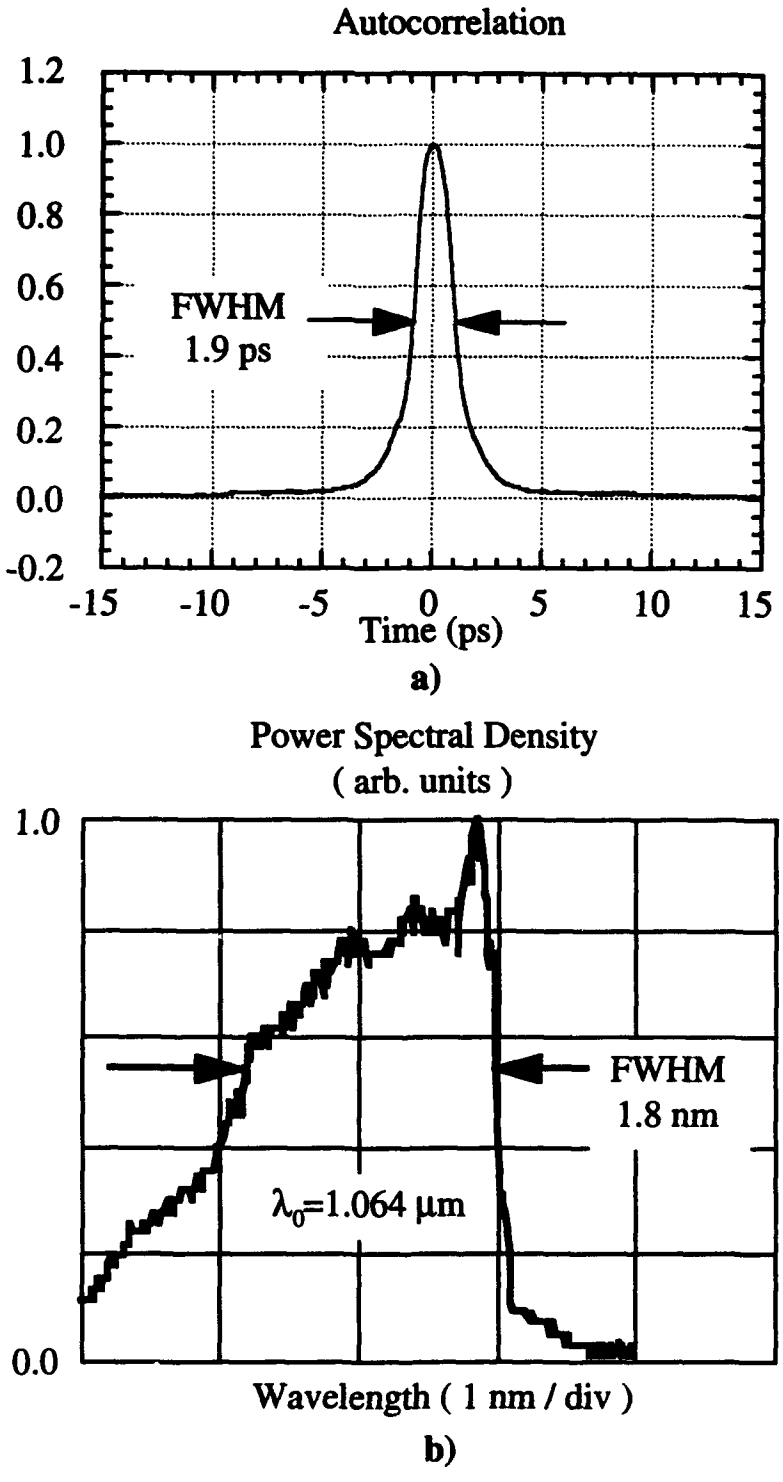

Figure 5.6 Measured time resolution of time-to-frequency converter. a) shows the measured input pulse autocorrelation. b) shows the input pulse spectrum.

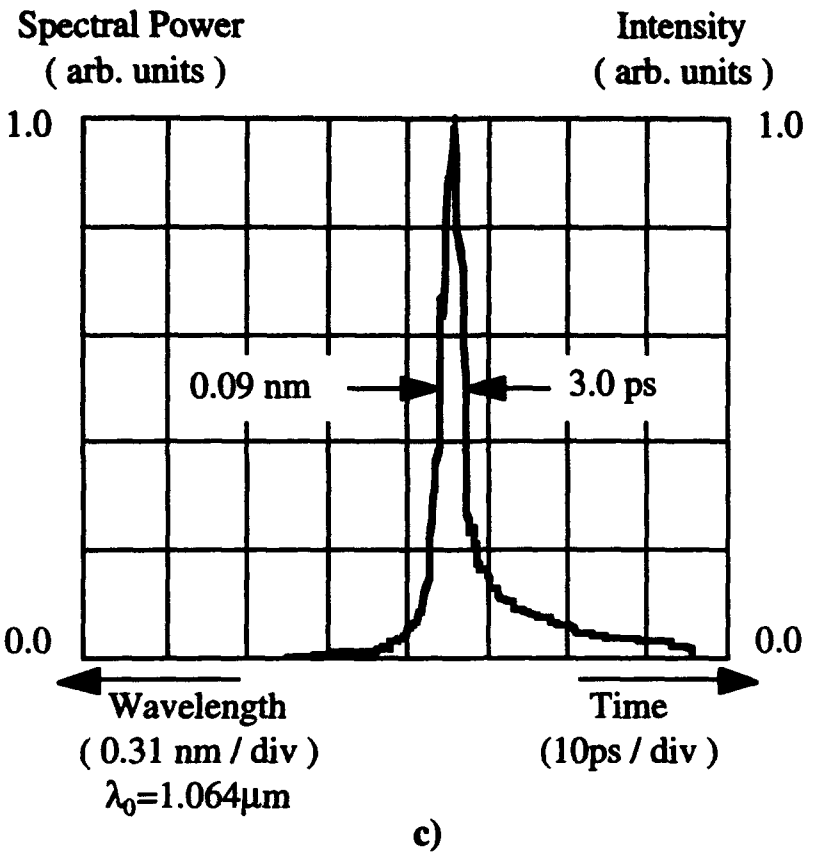

Figure 5.6(cont'd) Measured time resolution of time-to-frequency converter. c) shows the measured output pulse spectrum with wavelength axis converted to time.

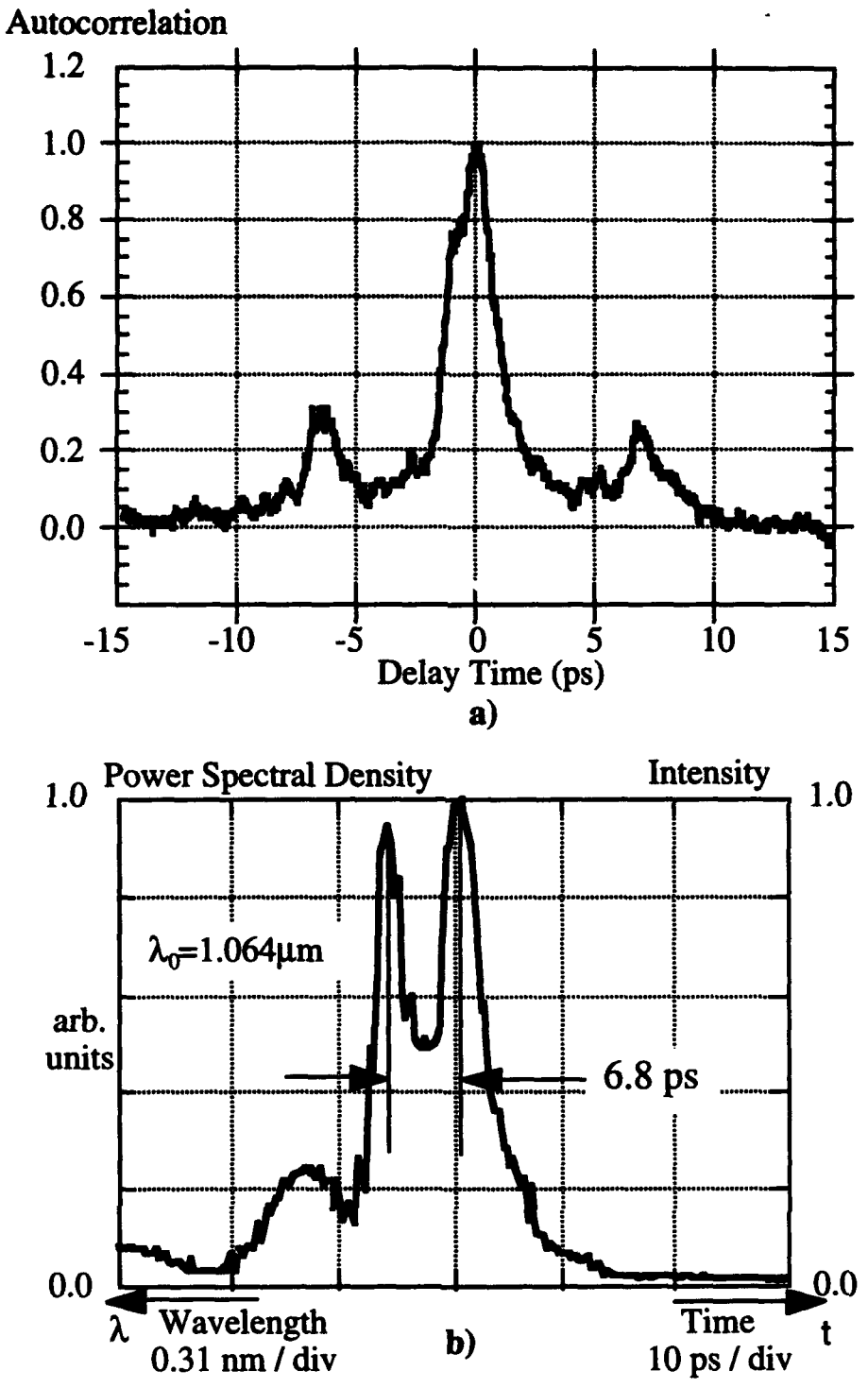

Figure 5.7 Result showing measurement of two closely separated pulses. a) shows the measured autocorrelation of the two input pulses. The separation is 6.8ps. b) shows the output spectrum and equivalently input pulse intensity. The wavelength axis is scaled to time.

To further demonstrate the resolution of the system, a Michelson interferometer is used to create a sequence of two pulses separated by 6.8 ps. The pulse separation is easily adjusted by moving one arm in the Michelson interferometer and is measured with an autocorrelator. The input pulse autocorrelation is shown in Figure 5.7a. The time-lens output spectrum is shown in Figure 5.7b with wavelength axis scaled to time as well. The pulse separation is also seen to be 6.8 ps in this measurement as well. The measurement shows the ability to resolve two pulses separated by 6.8 ps.

The resolution given by Equation (2.22) corresponds to a chirp free gaussian pulse. If the pulse at the input to the time-to-frequency converter has the same temporal width but is not time-bandwidth-limited, it will dispersively broaden more than the chirp free pulse and overfill the quadratic region of the time-lens. It is under these conditions that the time-varying phase of the pulse to be measured can corrupt the measurement process.

5.4.2 Temporal field of view

While the time-to-frequency conversion method has the ability to measure pulses as short as 3.0 ps, the current experimental setup does have problems measuring long pulses. This limitation arises because the phase shift generated by the sinusoidal time-lens is not quadratic. A long pulse will automatically overfill the quadratic phase region of the time-lens and be aberrated as shown in Figure 5.5. This is shown by using the time-to-frequency conversion method to measure the pulse shown in Figure 5.8a. This input pulse was measured with a fast photodetector (New Focus Inc. model 1404) and Microwave Transition Analyzer (Hewlett-Packard model 70820A) with system time resolution 20 ps. The input pulse FWHM is 63 ps. The output spectrum with wavelength axis scaled to time is shown in Figure 5.8b. That it shows no relation to the actual pulse indicates the severity of phase errors on the measurement process.

5.4.3 Time-lens stops

This limitation is not a fundamental flaw of the time-to-frequency measurement. A time-lens stop is needed to prevent this type of error. A spatial lens has a finite extent, and lens stops are used to block light from reaching non-ideal portions of the lens. The sinusoidal time-lens, however, has infinite extent: the phase goes on indefinitely. Nothing prevents the input pulse from being phase modulated by the negative phase peak which has the exact opposite phase needed to perform the correct operation. A time-lens stop will act to block the light from the non quadratic phase regions are allow operation over larger temporal fields of view. In this case, a time-lens stop is an intensity modulator operating synchronously with the phase modulator. Both modulators can be scanned in time to look at larger pulses in the same way that the microscope stage is moved under the objective lens to view a larger object.

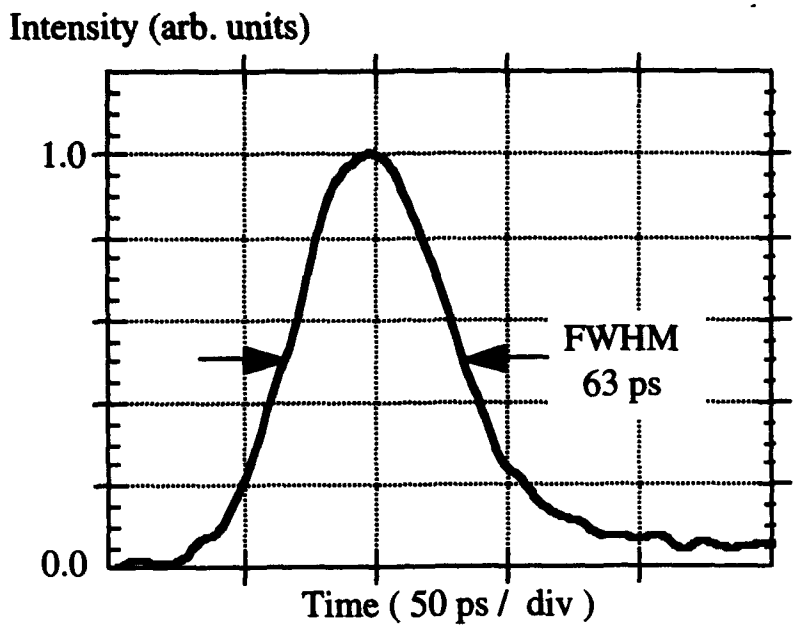

a)

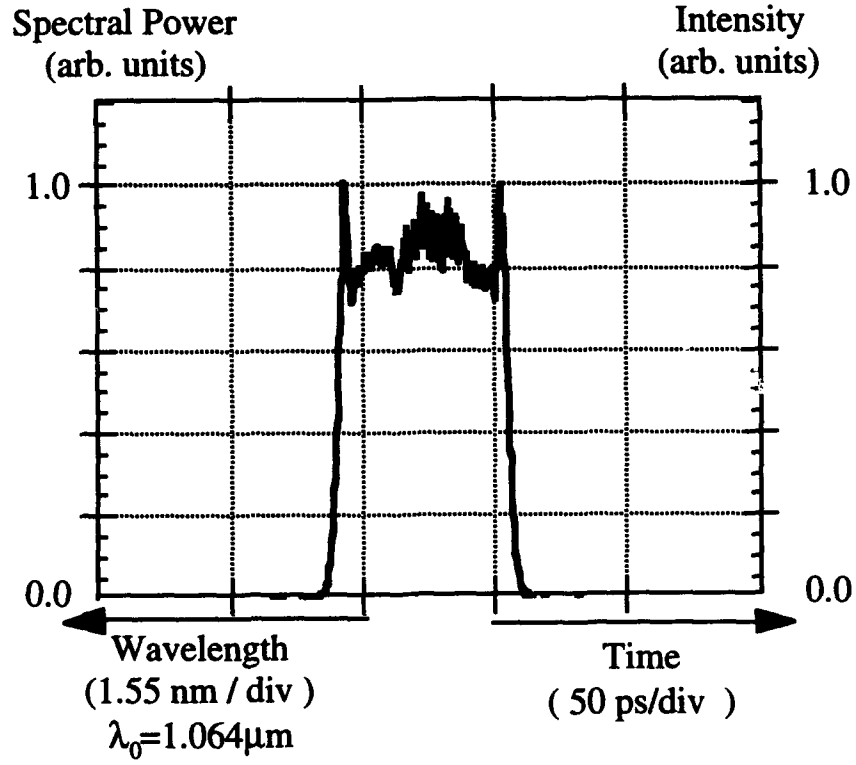

b)

Figure 5.8 Temporal field of view limitations. a) shows the input pulse measured with a fast photodetector / oscilloscope. b) shows the measured output spectrum and consequently the estimated input intensity with the wavelength axis converted to time.

5.4.3 Sensitivity considerations

One of the real advantages of this pulse shape measurement method over temporal imaging and other optical correlation methods is the sensitivity. Because this method does not rely on nonlinear optics (except for the electro-optic time-lens), there is no pulse energy threshold that methods like FROG face. The sensitivity requirements of optical correlation techniques is apparent in the fact that photomultiplier tubes are required to measure the weak second harmonic signal. The time-to-frequency conversion experiments used a sensitive photodiode based optical spectrum analyzer to measure the output signal. The OSA is sensitive because it only has to measure optical power and therefore can have a low bandwidth, high transimpedance measurement circuit. It is possible to increase the sensitivity of this measurement by using a single shot spectrum analyzer which has an array of photodetectors to simultaneously measure the power spectrum over a range of wavelengths. The sensitivity improves because the entire output pulse is continuously used, and for the same measurement time, the value at each frequency can be integrated longer than for a scanning OSA. This is not the case with temporal imaging of Chapter 4 where a sampling oscilloscope is used to view only a selected time interval of the magnified pulse at each instant. It is a fundamental property of the sampling process to ignore most of the energy in the signal being measured[15].

Even more sensitivity is possible with this technique if desired. Figure 5.9 shows both a schematic streak camera for measuring pulse shape and the time-to-frequency conversion method. The similarities between the two are obvious. The real sensitivity of the streak camera comes in the multi-channel plate (MCP) image intensifier at the end. If the same expensive MCP is applied to the time-to-frequency method, few photon pulse sensitivity is possible.

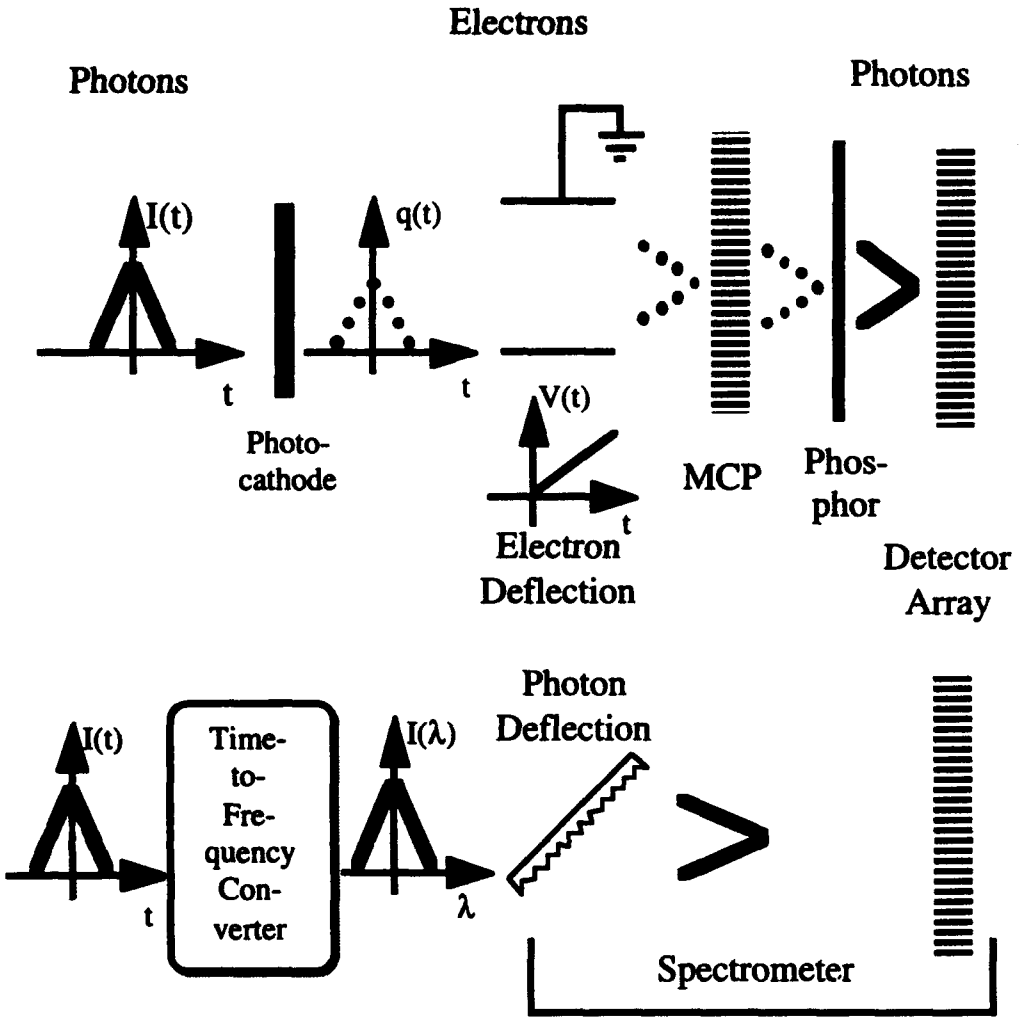

Figure 5.9 Schematic comparison of a) streak camera operation to b) time-to-frequency conversion method.

5.5 Additional characteristics

Techniques such as FROG have demonstrated the ability to measure both the amplitude and phase of optical pulses. To date, the time-to-frequency conversion method has only been used to measure the intensity of the pulse. Several research groups have shown that it is possible to measure phase as well. Beck[16] has shown that by placing the input pulse a fixed dispersive distance from the time lens, adjusting the focal time of the time-lens over a range of values and measuring the output spectrum for each value, pulse

amplitude and phase can be retrieved. This retrieval method, called chronocyclic tomography does not require iterative numerical calculations.

Another method[17] involves using the linear phase versus time portion of the sinusoidal phase modulator to frequency shift the pulse. This frequency shifted pulse is interfered with an unshifted replica to measure the pulse's phase curvature. Combined with the time-to-frequency method technique, amplitude and phase can be measured.

5.6 Conclusions

A new pulse shape measurement technique has been introduced. Time-to-frequency conversion is seen to be the temporal analog of a spatial beam collimator. This system performs a Fourier transform on an input pulse so that the time axis is mapped to the frequency axis with a known scale factor. The output from the system can be measured with an optical spectrum analyzer so that the trace is an exact replica of the input intensity.

This temporal optical system represents a real improvement in pulse shape measurement technology. This chapter has shown its ability to measure pulse shape with picosecond time resolution and excellent power sensitivity . From a practical point of view, the system required to implement this technique is much less complicated than temporal imaging as no high speed electronics are needed to make the measurement.

5.7 References

1. Goodman, J. W., Introduction to Fourier Optics, (New York: McGraw-Hill, 1968) pp. 77-90.

2. Tsuchiya, Y., "Advances in Streak Camera Instrumentation for the Study of Biological and Physical Processes," IEEE Journal of Quantum Electronics 20.12 (1984): pp. 1516-28.

3. Diels, J. C. M., J. J. Fontaine, I. C. McMichael, and F. Simoni, "Control and measurement of ultrashort pulse shapes (in amplitude and phase) with femtosecond accuracy," Applied Optics 24.9 (1985): pp. 1270-82.

4. Paye, J., "The Chronocyclic Representation of Ultrashort Light Pulses," IEEE Journal of Quantum Electronics 28.10 (1992): pp. 2262-73.

5. Trebino, R., "Using phase retrieval to measure the intensity and phase of ultrashort pulses: frequency-resolved optical gating," JOSA A 10.5 (1993): pp. 1101-11.

6. Kane, D. J., and R. Trebino, "Single-shot measurement of the intensity and phase of an arbitrary ultrashort pulse by using frequency-resolved optical gating," Optics Letters 18.10 (1993): pp. 823-5.

7. Kane, D. J., "Characterization of arbitrary femtosecond pulses using frequency-resolved optical gating," IEEE Journal of Quantum Electronics 29.2 (1993): pp. 571-9.

8. Shanmugam, K. S., Digital and Analog Communication Systems, (New York: John Wiley & Sons, 1979) pp. 30.

9. Treacy, E. B., "Optical Pulse Compression With Diffraction Gratings," IEEE Journal of Quantum Electronics QE-5.9 (1969): pp. 454-458.

10. Godil, A. A., "Harmonic Mode-Locking of Diode-Pumped Lasers and Time-Lenses with Picosecond Resolution," Ph. D. Thesis. Stanford University, 1992.

11. Brorson, S. D., and H. A. Haus, "Geometrical limitations in grating pair pulse compression," Applied Optics 27.1 (1988): pp. 23-25.

12. Tomlinson, W. J., R. H. Stolen, and C. V. Shank, "Compression of optical pulses chirped by self-phase modulation in fibers," J. Opt. Soc. Am. B 1.2 (1984): pp. 139-149.

13. Weingarten, K. J., "Gallium Arsenide Integrated Circuit Testing Using Electrooptic Sampling," Ph. D. Thesis. Stanford University, 1987.

14. Sala, K. L., G. A. Kenney-Wallace, and G. E. Hall, "CW Autocorrelation measurements of Picosecond Laser Pulses," IEEE Journal of Quantum Electronics 16.9 (1980): pp. 990-996.

15. Grove, W. M., "Sampling for Oscilloscopes and other RF Systems: DC through X-band.," IEEE Transactions on Microwave Theory and Techniques MTT-14.12 (1966): pp. 269.

16. Beck, M., M. G. Raymer, I. A. Walmsley, and V. Wong, "Chronocyclic tomography for measuring the amplitude and phase structure of optical pulses.," Optics Letters 18.23 (1993): pp. 2041-43.

17. Diddams, S., "Personal communication," University of New Mexico, 1994.

Chapter 6 Summary and Future Directions

6.1 Summary

This thesis has demonstrated both the synthesis and analysis powers of the space-time analogy in understanding the operation of temporal optical systems. Qualitative understanding led to the construction and demonstration of temporal equivalents of imaging and time-to-frequency conversion, as well as an interesting property of temporal focusing. Quantitative understanding allowed the prediction of performance limits.

The emphasis of this thesis has been to build temporal optical systems which have useful applications in optical pulse measurement and manipulation. Specifically, three systems have been demonstrated. The ability of a temporal focusing system to reduce fluctuations in pulse-to-pulse arrival time has been shown. This property allows one to produce a train of short optical pulses whose phase noise characteristics are dominated mainly by low phase noise microwave synthesizers. Timing jitter plays an important role in optical communications and electro-optic sampling experiments and reduction of timing jitter is important to build higher bit-rate communications systems.

Temporal imaging with magnification and time reversal of an optical pulse pair has also been demonstrated. The ability to reverse the time axis over a limited time window is an interesting and attention grabbing characteristic of temporal optical systems and has

important applications as well. Temporal imaging highlights some of the differences between spatial and temporal optical systems, with one being the ability to view a 'virtual' image with a temporal optical system. The application of temporal imaging to pulse shape measurement was the theme in this thesis with two techniques presented. There are, I am sure, other important applications, probably in the field of signal processing.

My main contribution to the field has been the development of the time-to-frequency method of pulse shape measurement and exploration of the important limits of operation. This technique combines the important features of good time-resolution and excellent power sensitivity in an approach which yields a direct measure of the pulse shape. This combination is not present in any other technique that I am aware of.

6.2 Future directions

By far the most important direction this work should take is the development of a time-lens step. The imperfections of the sinusoidal time-lens are well documented and the aberrations leading from the non-ideal phase transfer characteristics have been demonstrated. This is the greatest limitation to making accurate pulse shape measurements using either temporal imaging or time-to-frequency conversion.

The ability to measure pulse phase as well as amplitude has been predicted but not experimentally demonstrated. This ability could be valuable to those using solitons for optical communication to study the evolution of the soliton pulse. Timing jitter is also a problem in high bit rate soliton communication systems. Temporal focusing to reduce timing jitter could be an important substitute to the current techniques to reduce jitter in soliton systems.

Improving the resolution of the time-lens is another important area of future study. The time-lens developed by Asif Godil represents a fine piece of engineering and the experiments in this thesis have proven it to be a valuable tool. This basic design is a good

fit to the requirements of the problem: since the modulator is driven at a single frequency, the microwave circuit can be resonated to increase the microwave-optical interaction. The improvements made to the original design have increased the phase modulation and correspondingly the time-resolution significantly, but there is much room left for improvement. Increasing the number of optical passes through the crystal and engineering a solution for the thermal lens effects caused by high microwave power are two avenues to follow in order to improve the current design. This should push the time resolution to hundreds of femtoseconds when driven with practical high power microwave sources.

To reach the femtosecond regime, a new time-lens architecture is probably needed. A likely candidate is the same vehicle used to compress pulses to femtosecond width: self and cross phase modulation in optical fibers. The real intelligence here will be finding ways to separate the time-lens from the pulse being modulated and do deal with the effects of dispersion in the fiber. Perhaps this is when the concept of a thick lens will be applied to temporal optics.

Regardless of the lens technology, there are still many interesting temporal optical systems to explore. The combination of several time-lenses to form a true time-microscope, and time-lens aberration correction are just two. For the community who actually care about picosecond and femtosecond phenomena, the concepts of temporal optical systems will provide a powerful tool to understand a wide range of pulse phenomena.